UNIVERSITAT DE BARCELONA

Role of ZEB factors in macrophages in atherosclerosis and ovarian cancer

Maria del Carmen Martinez Campanario

Memoria presentada por María del Carmen Martínez Campanario para optar al grado de Doctora en Biomedicina por la Universidad de Barcelona

ROLE OF ZEB FACTORS IN MACROPHAGES IN ATHEROSCLEROSIS AND OVARIAN CANCER

Tesis doctoral
Universitat de Barcelona
Programa de Doctorado en Biomedicina
Marzo 2021

Esta tesis se ha realizado en el grupo de Regulación Transcripcional de la Expresión Génica en las instalaciones del Instituto de Investigaciones Biomédicas August Pi i Sunyer (IDIBAPS) en Barcelona.

María del Carmen Martínez Campanario	**Dr. Antonio Postigo**	**Dr. Marlies Cortes**	**Dr. Carles Enrich**
Doctoranda	Director de tesis	Directora de tesis	Tutor

PREFACE

The experimental study presented in this doctoral thesis was performed at the Institut d'Investigacions Biomèdiques August Pi i Sunyer (IDIBAPS) and the University of Barcelona School Medicine (Barcelona), in the laboratory of Transcriptional Regulation of Gene Expression, under the supervision of Dr. Antonio Postigo and Dra. Marlies Cortes and Dr. Carles Enrich as tutor. The work was supported by an FPI scholarship from the Spanish Government (Ministerio de Educación, Cultura y Deporte).

ABSTRACT

Macrophages polarization from an inflammatory to a tolerogenic state occurs in both physiological and pathological, and this reprogramming is key in the development of several diseases as different as atherosclerosis or cancer. The results presented in this dissertation indicate that a) ZEB1 expression in macrophages inhibits atherosclerotic plaque formation and b) ZEB1 expression in macrophages promotes ovarian cancer tumor progression while ZEB2 expression inhibits it.

ZEB1 inhibits lipid accumulation in macrophages through increased cholesterol efflux thus protecting mice from atherogenesis. Accordingly, *Zeb1*$^{\Delta Mac}$ mice fed with pro-atherogenic diet have a higher plaque size and higher lipid content compared to *Zeb1*^{WT} counterparts. Mechanistically, ZEB1 is required for the activation of the AMPK-LXRα-ABCA1/G1 pathway, which is critical for cholesterol efflux and anti-inflammatory switch in macrophages. Besides, ZEB1 is a mediator of macrophage activation by ox-LDL through p65.

In regard to ovarian cancer, we show that ZEB1 and ZEB2 in TAMs have an opposite role in ovarian cancer initiation and progression. Expression of ZEB1 in TAMs promotes tumorigenesis and ZEB2 inhibits it. *Zeb1*$^{\Delta Mac}$ TAMs exhibited lower adhesion with tumor cells and increased phagocytosis while *Zeb2*$^{\Delta Mac}$ TAMs have increased PD-1 and promote PD-L1 overexpression in ID8 cells. Moreover, ZEB1 expression in TAMs stimulates stem-like characteristics in ID8 cancer cells while ZEB2 inhibits this phenotype thus promoting enhanced survival in tumor-bearing *Zeb1*$^{\Delta Mac}$ mice and decreased survival in *Zeb2*$^{\Delta Mac}$ counterparts.

These results established ZEB1 as a protector of the cardiovascular system from atherosclerosis development. On the other hand, ZEB1 and ZEB2 are tumor-promoting and tumor-repressor factors in ovarian cancer, respectively, through their regulating of the functions of the TAMs. Altogether, the present dissertation sets ZEB1 and ZEB2 in macrophages as a potential therapeutic target in both pathologies.

RESUMEN

La polarización de los macrófagos de un estado a inflamatorio a uno tolerogénico ocurre tanto en condiciones fisiológicas como patológicas, y esta reprogramación es clave para el desarrollo de múltiples enfermedades tales como la arteriosclerosis o el cáncer. Los resultados presentados en esta tesis indican que a) la expresión de ZEB1 en macrófagos inhibe la formación de la placa arteriosclerótica y b) la expresión de ZEB1 en macrófagos promueve la progresión del cáncer de ovario mientras que la expresión de ZEB2 la inhibe.

ZEB1 inhibe la acumulación de lípidos en macrófagos a través de una mayor salida de colesterol, lo cual, esta protegiendo de la formación de aterosclerosis en ratones. Así, los ratones *Zeb1*$^{\Delta Mac}$ tienen mayor tamaño de la placa y un contenido más alto de lípidos que los *Zeb1*^{WT}. ZEB1 es requerido para la activación de la vía AMPK-LXRα-ABCA1/G1, la cual es crítica para el eflujo de colesterol y la transición de los macrófagos a un fenotipo antinflamatorio. Además, ZEB1 es un mediador de la activación de macrófagos a través de p65.

En cancer de ovario, nosotros mostramos que ZEB1 y ZEB2 en TAMs tienen un papel opuesto en iniciación y progresión del cáncer de ovario. La expresión de ZEB1 en TAMs promueve el desarrollo tumoral y ZEB2 la inhibe. Los TAMs *Zeb1*$^{\Delta Mac}$ muestran un aumento de la capacidad fagocítica y menor adhesión con las células tumorales mientras que los TAMs *Zeb2*$^{\Delta Mac}$ muestran un incremento de PD-1 y promueven la sobreexpresión de PD-L1 en células ID8. Adicionalmente, la expresión de ZEB1 en TAMs estimula la adquisición de características de célula madre en células ID8 y la expresión de ZEB2 la inhibe lo cual podría estar promoviendo un incremento en la supervivencia de los ratones *Zeb1*$^{\Delta Mac}$ y disminuyéndola en los *Zeb2*$^{\Delta Mac}$.

Estos resultados establecen a ZEB1 como un protector del sistema cardiovascular del desarrollo de la arteriosclerosis. Por otro lado, ZEB1 y ZEB2 son, respectivamente, un promotor y un represor de la progresión tumoral en cáncer de ovario a través de la regulación de la función de los TAMs. Los datos presentados en esta Tesis proponen a ZEB1 y ZEB2 en macrófagos como potenciales dianas terapéuticas en ambas patologías.

TABLE OF CONTENTS

ABBREVIATIONS

APOA1	Apolipoproteína A1
CSC	Cancer stem cell
CtBP	C-terminal binding protein
DMEM	Dulbecco's Modified Eagle's Medium
EMT	Epithelial mesenchymal transition
FACS	Fluorescent activated cell sorter
FBS	Fetal bovine serum
GNS	Graphene nanostars
HDAC	Histone deacetylase
HDL	High density lipoprotein
HGSC	High-grade serous carcinoma
H&E	Hematoxylin and eosin
LDL	Low density lipoprotein
miR	microRNA
NAFLD	Non-alcoholic fatty liver disease
NASH	Non-alcoholic steatohepatitis
NP	Nanoparticle
ORO	Oil Red O
PBS	Phosphate buffered saline
PFA	Paraformaldehyde
RNS	Reactive nitrogen species
ROS	Reactive oxygen species
TAM	Tumor-associated macrophages
TIL	Tumor infiltrating lymphocytes
TME	Tumor microenvironment

INTRODUCTION

INTRODUCTION

1. Monocytes and macrophage differentiation

Macrophages are key effectors of innate and adaptive immunity recruiting other immune cells and constitute the first line for host defense being also implicated in organogenesis, homeostasis and growth and tissue repair (Gordon and Martinez, 2010; Murray et al, 2011). Besides these physiological functions, macrophages also participate in different pathological and physiopathological conditions as well as in multiple diseases and pathological syndromes like fibrosis, obesity, autoimmune diseases, atherosclerosis and cancer (Wynn et al, 2013).

Macrophages can be differentiated from peripheral blood monocytes, which, in turn, originate from myeloid precursors at the bone marrow (Van Furth et al., 1972). Myeloid precursors give rise to common myeloid progenitors, macrophages and dendritic cells progenitors and granulocyte-macrophage precursors. Myeloid precursors differentiate into monocytes, macrophages and dendritic cell precursors (Ginhoux and Guilliams, 2016). Peripheral blood monocytes migrate to tissues where they differentiate into macrophages. A second group of macrophages is referred to as “resident macrophages” that are found in the stroma of virtually all tissues and originate from embryonic precursors (yolk-sac or early erythro-myeloid progenitors) and whose population is self-maintained by local proliferation rather than new recruitment (Williams et al, 2018).

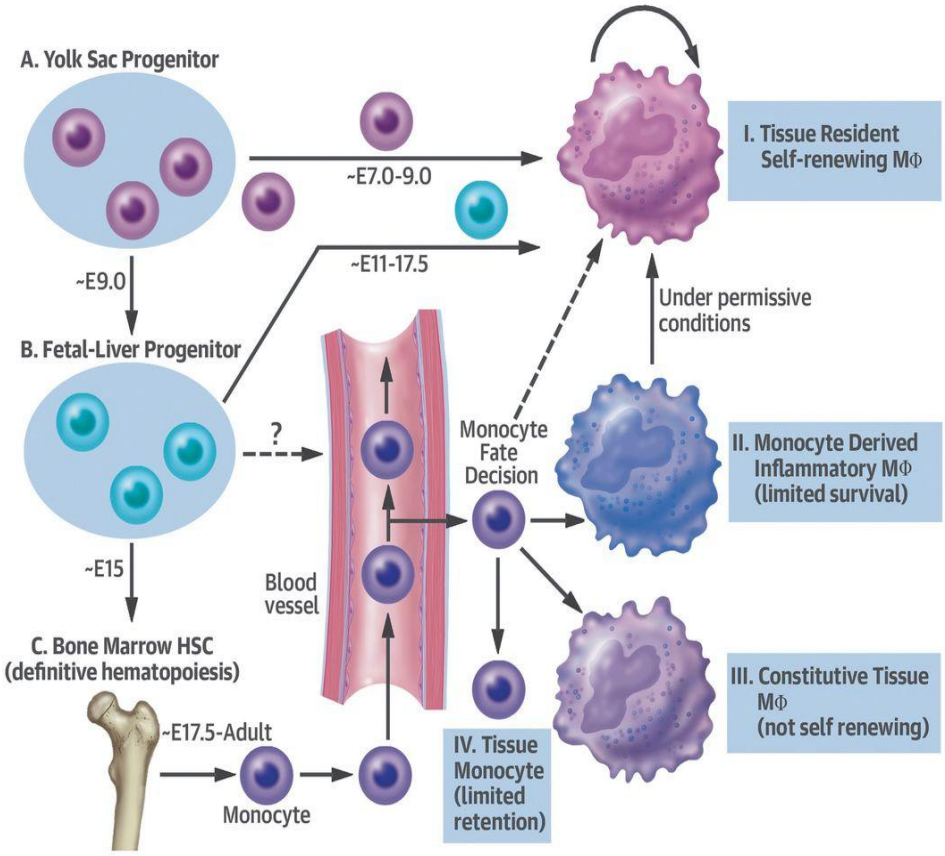

Figure 1. Macrophage developmental origin. (A, B, C) Origins of macrophages. (I, II, III, IV) Types of macrophage populations. Adapted with permission from *Williams et al., 2018*.

Macrophages play an important role in the inflammatory response. The inflammatory response consists of different stages, being initiated by different stimuli and developing an inflammatory response, followed by resolution and repair of affected tissues. Macrophages can participate in all stages of the inflammatory process due to their high plasticity (Chen et al, 2018; Shapouri-Moghaddam et al, 2018; Locati et al., 2020). Macrophages display a wide spectrum of phenotypes depending on the environment or origin.

Depending on their activation status, macrophages can be classified as classically activated/M1 or alternatively activated/M2. However, M1 and M2 are the extremes of these phenotypes only found in vitro polarization while the intermediate phenotypes are the most commonly found in vivo (Sica and Mantovani, 2012; Murray and Wynn, 2014). In vitro, pro-inflammatory/M1 occurs in response to LPS and IFNγ or CSF2 and anti-inflammatory/M2 activation occurs in response to IL4 and IL13 or CSF1 (Varga et al, 2016; Shapouri-Moghaddam et al, 2018). Macrophage activation results in their production and release of different

cytokines. M1 macrophages secrete pro-inflammatory cytokines like IL1β, IL6, IL12 or TNF, as well as reactive oxygen (ROS) and nitrogen species (RNS) and nitric oxide (Arango Duque and Descoteaux, 2014). Consequently, M1 macrophages are mediating the environment for destroying pathogens and cancer cells. These cytokines promote Th1 lymphocytes' response. On the other hand, M2 macrophages secrete anti-inflammatory cytokines like IL10 and TGFβ that promote Th2 lymphocytes response. In contrast to M1 counterparts, M2 macrophages are implicated in resolving inflammation and tissue repair (Van den Bossche et al, 2017).

In mice, the F4/80 antigen (encoded by the *Adgre1* gene) defines different macrophage subsets with resident macrophages expressing high levels of F4/80 while macrophages differentiated from peripheral blood monocytes display low levels of F4/80 (Ghosn et al, 2010; Cassado Ados et al, 2015).

Peripheral blood monocytes can also be distinguished in various functional subsets depending on their cell surface expression markers. Thus, Ly-6C marker allows the separation of monocytes into 2 subsets characterized by different migratory and inflammatory features (Ginhoux and Jung, 2014). Ly-6C^{high} monocytes migrate to inflammatory sites and differentiate mainly to M1 phenotype, thus being referred to as inflammatory monocytes. On the other hand, Ly-6C^{low} monocytes present an M2 phenotype and are denominated non-classical monocytes.

2. The ZEB family of transcription factors

The mammalian ZEB family of transcription factors is constituted by ZEB1 and ZEB2, which regulate developmental and differentiation programs in multiple tissues (Gheldof et al., 2012). In epithelial tumor cells, ZEB1 and ZEB2 drive the so-called epithelial-to-mesenchymal transition (EMT), a cell dedifferentiation reprogramming that is involved in embryogenesis, tissue regeneration, tumor initiation and progression, and radiotherapy and chemotherapy resistance. ZEB1 and ZEB2 present a similar structure that shares 44% of similitude (Postigo and Dean, 2000; Stemmler et al., 2019). Both factors contain two zinc-finger domains, one located at N-terminal and other at C-terminal end, that bind to the regulatory regions of

target genes. ZEB factors can act as transcriptional repressors or activators depending on their binding to other transcription factors and cofactors (Sánchez-Tillo et al., 2011).

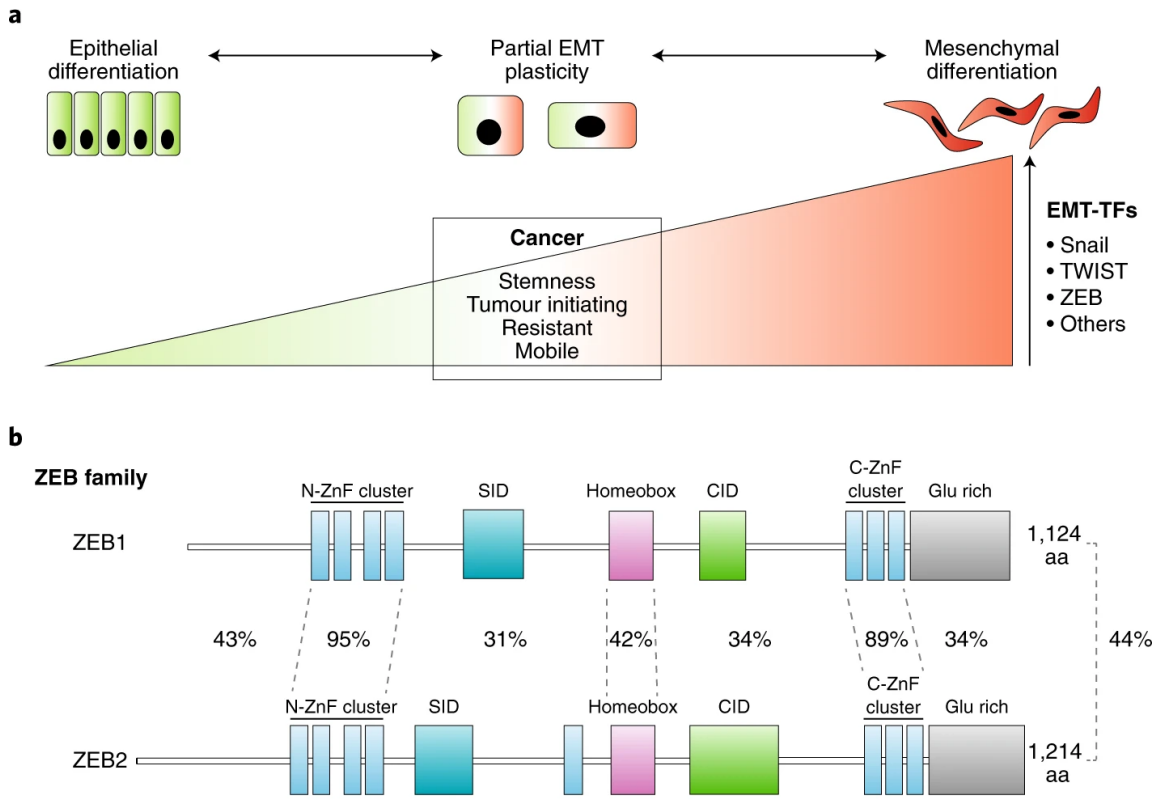

Figure 2. ZEB factors structure and function in EMT. a. ZEB transcription factors are implicated in EMT in cancer cells. b. Schematic representation of the protein structures of ZEB factors. Adapted with permission from *Stemmler et al., 2019*.

Besides, ZEB1 and ZEB2 have a role in the development and differentiation of different cell types, including in the hematopoietic compartment (Goossens et al., 2011; Scott et al., 2019). Both transcription factors are implicated in T cell development in mice (Guan et al., 2018). In the myeloid lineage, ZEB2 regulates dendritic cell development and is implicated in maintaining tissue resident-macrophage identity (Scott et al., 2016; Wu et al., 2016; Scott et al., 2018) and ZEB1 is implicated in peritoneal macrophage maturation and dendritic cell activation in murine models (Cortes et al., 2017; Smita et al., 2018).

ZEB1 plays a role in adipogenesis and is implicated in lipid metabolism. ZEB2 is implicated in Kupffer cell differentiation by regulating NR1H3 (Leussink et al., 2020). ZEB1 regulates adipogenesis by forming a complex with PPARγ and C/EBPß (Gubelmann et al., 2014). ZEB1

linked EMT and lipid metabolism through the regulation of accumulation, mobilization and uptake of lipid that affects adhesion by remodeling the plasma membrane (Mathow et al., 2015; Viswanathan et al., 2017). Also, *Zeb1* deficiency in mice impaired glucose uptake in mice fed with high-fat diet (Saykally et al., 2009). Earlier studies showed that ZEB1 is downregulated in atheromatous plaque lesion compared with plaque-free intima by its hypermethylation (Yamada et al. 2014). However, the role of ZEB1 and ZEB2 in macrophages lipid metabolism and atherosclerosis remains understood.

Accumulating evidence indicates a role for ZEB factors in tumor stroma cells. EMT promotes macrophage infiltration and activates macrophages to Tumor-Associated Macrophages (TAM)-like phenotype (Su et al., 2014). ZEB1 and ZEB2 are not only expressed in tumor cells but are also expressed in stromal cells (Nagaishi et al., 2017). In ovarian cancer, ZEB1 is expressed in TAMs promoting the activation toward pro-tumoral macrophages and tumor progression (Cortes et al., 2017). ZEB1 expression in stromal fibroblasts promotes mammary tumor initiation, progression and metastasis. This is associated, in part, with the inactivation of ZEB1 in stromal fibroblasts decreased macrophage infiltration (Fu et al., 2019). Altogether, these data showed ZEB factors as an important factor that modulate the phenotype of tumor cells through the tumor stroma.

3. Cardiovascular disease

3.1. Metabolic disease and atherosclerosis

Cardiovascular disease is the most prevalent cause of mortality in diabetic patients (Einarson et al, 2018). Insulin resistance is an early symptom of this disease. In metabolic syndrome, hepatic insulin resistance results in continuous glucose production while elevated levels of nutrients induce pancreas beta-cell dysfunction and endoplasmic reticulum stress resulting in β-cell damage and death. This process leads to hyperglycemia and it has been proposed to be influenced by several mechanisms, including inflammatory cytokines, adipokines, non-esterified fatty acid, glucotoxicity, lipotoxicity and others (Muoio and Newgard, 2008). An increase of insulin sensitivity and improved glucose tolerance as a result of exercise, weight loss and drugs reduce cardiovascular risk.

Atherosclerosis is a chronic artery disease that is the major cause of vascular disease worldwide (Herrington et al, 2016). Fatty streak is gradually accumulated in the artery wall and activated endothelial cells to recruit immune cells and develop atheroma plaques. Ruptured plaques cause thrombosis and partial or total occlusion of the vessel. Atherosclerosis can be asymptomatic for many years before being manifested clinically in the form of ischemic stroke, ischemic heart disease and/or peripheral arterial disease. The main underlying risk factors of atherosclerosis include smoking, hypercholesterolemia, hypertension, diabetes mellitus, adiposity and age (Lonardo et al, 2018). Some parameters used for diagnostics of subclinical atherosclerosis are arterial stiffness, carotid artery intima-media thickness, coronary artery calcification, and brachial arterial flow-mediated dilation (Jover et al., 2018; Schmidt et al, 2019).

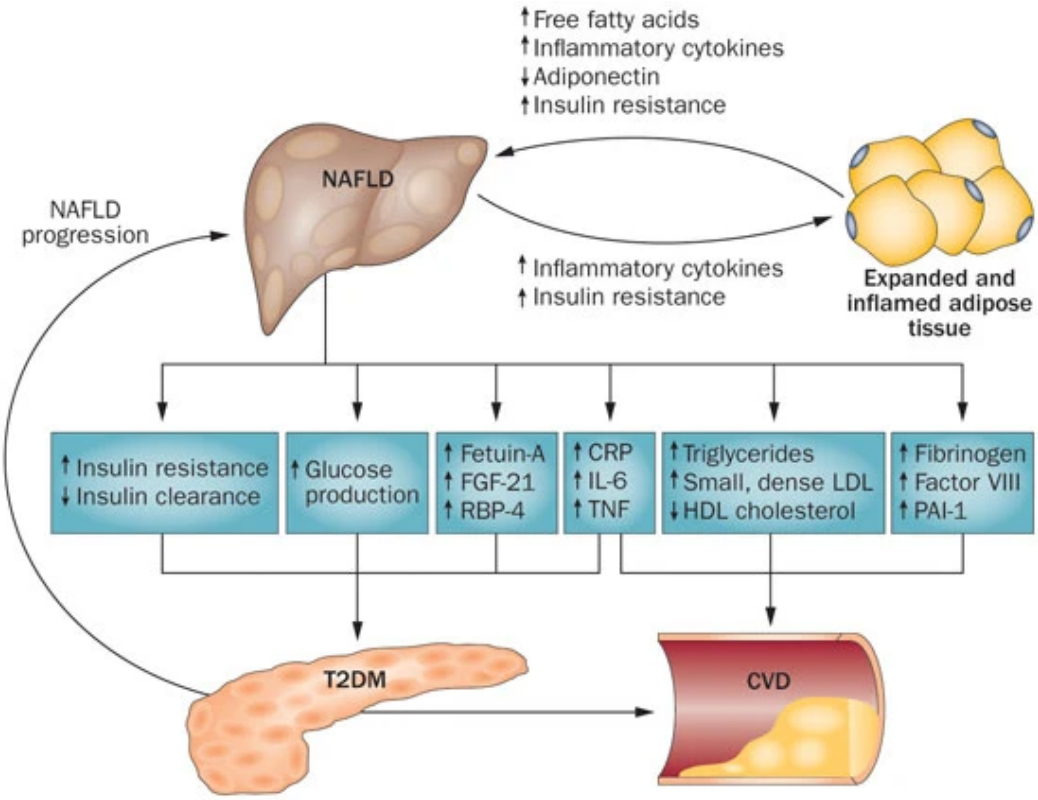

Figure 3. NAFLD contributes to systemic insulin resistance and type II diabetes by increasing glucose production in the liver and producing a systemic release of pro-inflammatory factors. In addition, NAFLD increased cardiovascular risk via atherogenic dyslipidemia, with low levels of HDL cholesterol and increased levels of LDL. Used with permission from *Anstee et al., 2013*.

Blood cholesterol levels originate mainly from the intake of saturated fat, polyunsaturated fat and cholesterol (Schwingshackl and Hoffmann, 2013). However, higher cholesterol levels in blood are produced by reduced energy consumption, genetic or other factors. High LDL serum levels are a risk factor for cardiovascular disease while HDL has an inverse relation (Rader and Hovingh, 2014; Duran et al., 2020; Prats-Uribe et al., 2020). Lowering circulating blood lipids by the use of statins is a current treatment of atherosclerosis. The reduction of LDL cholesterol through the use of these drugs reduces cardiovascular disease. Likewise, a reduction of hypertension using β-blockers and angiotensin-converting enzyme inhibitors are treatment strategies (Rossello et al., 2015).

3.2. Non-alcoholic fatty liver disease

Non-alcoholic fatty liver disease (NAFLD) is an independent risk factor of cardiovascular disease (Bhatia et al., 2012). Early diagnosis of cardiovascular disease in the risk population is necessary to reduce mortality. NAFLD is the most common chronic liver disease affecting around 25% of the total population and is associated with other metabolic diseases like obesity, diabetes mellitus type II, cholesterolemia and hypertension (Fazel et al., 2016). NAFLD is a progressive disease that can produce a wide spectrum of clinical manifestations from steatosis to complications like hepatocytes ballooning and necrosis, fibrosis, cirrhosis and a higher probability of hepatocellular carcinoma. NAFLD can progress toward NASH (nonalcoholic steatohepatitis) where steatosis is accompanied by inflammation and cell damage (Stefan et al., 2019).

Although NASH progression can evolve toward fibrosis, cirrhosis and eventually to hepatocellular carcinoma, the most important cause of mortality by NAFLD is caused by cardiac events (approximately 25%), cirrhosis, hepatocellular carcinoma, kidney disease or extra-hepatic cancer (Mantovani et al., 2020). While, originally, NAFLD was defined as a consequence of the metabolic syndrome, more recently it has been reported that the relation is more complex and experimental evidence demonstrates that there is a bidirectional link and NAFLD may precede and/or promote metabolic syndrome, including hypertension, diabetes type II and cardiovascular disease (Zhou et al, 2018).

Macrophages are implicated in liver disease initiation and progression. Macrophages in liver comprise embryonically-derived Kupffer cells and circulating monocyte-derived macrophages. Liver injury produces, in NAFLD or other liver diseases, KCs depletion or damage. NAFLD triggers the recruitment of monocytes that replenish the pool of hepatic macrophages (Bansal et al., 2020). Under liver injury, KCs and monocyte-derived macrophages secrete inflammatory cytokines and chemokines, including CCL2, IL-1β and TNF-α, that maintain liver inflammation and are implicated in progression to steatosis (van der Heide et al., 2019).

3.3. AMPK signaling in metabolism and inflammation

Atherosclerosis and other metabolic diseases including obesity, diabetes type II, insulin resistance and NAFLD are characterized by chronic low-grade inflammation. Low-grade inflammation reduces AMPK expression in macrophages and other tissues and reduced levels of AMPK are implicated in metabolic diseases (Day et al, 2017). AMPK has functions in multiple physiological and pathological conditions including anti-inflammatory response, lipid metabolism and redox regulation (Jeon, 2016). Inflammation and metabolism are intimately connected in macrophages. Thus, macrophage polarization toward a pro-inflammatory phenotype is supported by glycolysis, while activation toward an anti-inflammatory state is dependent on oxidative metabolism. AMPK is implicated in the switch from pro-inflammatory to anti-inflammatory macrophages (Sag et al, 2008). Accordingly, activators of AMPK (e.g., A-769662, AICAR or GSK621) promote an anti-inflammatory phenotype in macrophages.

In lipid metabolism, AMPK activates fatty acid uptake and beta-oxidation and inhibits de novo synthesis of fatty acid triglycerides and cholesterol. To reduced fatty acid synthesis, AMPK inhibits acetyl-coA carboxylase 1 that catalyzes acetyl-coA to malonyl-coA, a step of fatty acid synthesis, and sterol regulatory element-binding transcription factor 1, that induced lipogenic enzymes expression (Jeon, 2016; Ma et al, 2017). In addition to inhibiting cholesterol synthesis, AMPK activates cholesterol efflux by inducing LXRα, ABCA1 and ABCG1 (Amézaga et al., 2013; Kemmerer et al., 2016; Ma et al., 2017). Also, LXRα activation in macrophages is

implicated in pro- to anti-inflammatory phenotypic switch (Spann et al., 2012; Ito et al., 2015). On the other hand, AMPK activated CPT1α and induces β-oxidation in the mitochondrion (Kemmerer et al., 2015).

3.4. Macrophages in atherosclerosis

Atherosclerosis is an inflammatory and metabolic disease. The inflammatory response is initiated by the accumulation of cholesterol-enriched, apolipoprotein B-containing lipoproteins in the arterial vasculature (Moore et al., 2011). These lipoproteins are susceptible to modifications such as oxidation, acetylation or aggregation and induce the activation of the endothelium. Endothelial activation is driven leukocyte trafficking to the artery wall and the main leukocyte type recruited is monocytes (Tabas and Bornfeldt, 2016; González-Ramos et al., 2019). Peripheral blood monocytes migrate to the artery wall where they are differentiated into macrophages. Macrophages uptake lipoproteins and become lipid-filled known as “foam cells” (Randolph, 2014; Martínez-González and García de Frutos, 2020). Hypercholesterolemia and other cardiovascular risk factors induce the production of monocytes leading to an increased number of circulating monocytes. An impaired resolution of inflammation contributes to atherosclerosis development (Gistera and Hansson, 2017; Arango Duque and Descoteaux, 2019).

In areas of curvature or branching of the artery, endothelial activation is continuous, but the levels of activation are maintained to not lead to an expansion of inflammation (Paulson et al, 2010). Thus, the mononuclear phagocyte cells found in these areas are in a single layer and are responsible for eliminating antigens or pathogens that may be accumulated due to hemodynamic stress. Since these cells are found in areas predisposed to atherosclerosis, it has been hypothesized that they could play a role in the onset of the disease.

Macrophage infiltration and activation in the artery wall produce an inflammatory response leading to secretion of chemoattractant molecules such as the chemokines CCL2 and CCL5 that recruit immune cells generating an unresolved inflammatory process (Moore et al, 2013). Ly-6C^{high} monocytes migrate efficiently to inflammatory sites including atherosclerotic plaque

through chemokine receptors CCR2 and CX3CR1. On the other hand, Ly-6C^{low} monocytes do not express CCR2 but express high levels of CX3CR1. The expression of CCR2, CCR5 y CX3CR1 expression on monocytes is required for plaque progression (Rahman et al, 2017).

Lipoprotein uptake of modified LDL is taken up by several scavenger receptors, including scavenger receptor class A, CD36, SR-BI and LOX1 but lipoprotein uptake can also occur through macropinocytosis and phagocytosis (Tabas and Bornfeldt, 2016). When macrophages take up more cholesterol than they can excrete, the cholesterol is esterified by acyl-coenzyme A:cholesterol acyltransferase (ACAT1) and stored in lipid droplets which results in the foam cell morphology. Cholesterol ester could be hydrolyzed from lipid droplets to generate free fatty acid and cholesterol by neutral cholesteryl ester hydrolase 1 (NCEH1) and lysosomal acid lipase (LAL) (Chistiakov et al, 2017). Macrophages can efflux cholesterol through the ABCA1 and ABCG1 (Moore et al, 2013).

3.5. Use of nanoparticles to modify gene expression in macrophages

The application of nanoparticles to the diagnosis and therapy of diseases has improved many illnesses, including cardiovascular disorders, cancer, neurological disorders or diabetes. Nanoparticles are combined with different compounds with therapeutic effects, such as peptides, proteins and nucleic acids and small-molecule drugs (Davis et al., 2008). Traditional administration of therapeutic compounds has some disadvantages like non-selective targets, poor distribution or undesirable side effects. Nanoparticles have been successfully used in the selective delivery of a wide range of molecules into different types of cells. This approach enhances the concentration of the therapeutic molecules to the diseased site with lower doses and lower side effects (Zhang et al., 2019; Yetisgin et al., 2020). Nanoparticles can be synthesized from various materials like lipids, metals, proteins and synthetic/natural polymers and can be classified into several groups based on the components used for the synthesis (Chenthamara et al., 2019; Sylvestre et al., 2020).

Nanoparticles have been used to deliver safer and more effective chemotherapeutics in cancer, they have been translated into applications for cardiovascular diseases (Flores et al.,

2019). Targeting chronic inflammation, lipid-lowering therapies or resolving defective efferocytosis are some of the efforts to develop novel and more effective treatments for vascular disease.

A type of nanoparticles is graphene nanostars (GNS) consisting of clusters of conical rolls of graphene sheets with cone-shaped tips called nanohorns. These nanohors are linked to form spherical aggregates called nanostars. Like most nanoparticles, GNS are mainly phagocytosed by macrophages. These nanoparticles present high biocompatibility, not inducing pro-inflammatory cytokines and are degraded in a few days (Melgar-Lesmes et al., 2018). Combining GNS with PAMAM-G5 dendrimer allows selective targeting of macrophages and delivery of nucleic acid and has been successfully used in preclinical experiments to treat liver fibrosis.

4. Ovarian cancer

Ovarian carcinomas are classified into different histological subtypes that include serous, endometrioid, clear cell and mucinous carcinomas. The histological subtypes are different epidemiologically, in mutational characteristics, sites of origin and chemotherapy response. Serous types are divided into low-grade serous carcinoma and high-grade serous ovarian carcinoma (HGSC) (Matulonis et al., 2016). HGSC is not only the most common type of ovarian cancer accounting for 80% of all cases, but it is also the most aggressive (Kim et al., 2018). Since ovarian cancer is asymptomatic at early stages, it is often diagnosed when it is already in advanced stages (III-IV) when the 5-year survival rate is approximately only 30% (Cho and Shih, 2009). Patients are commonly treated with platinum-based therapies but resistance to chemotherapy and recurrence of peritoneal metastasis, which is often associated with persistence of cancer stem cells (CSC), can occur after treatment (Zong and Nephew, 2019; Terraneo et al., 2020). In ovarian cancer, especially in serous ovarian cancer, ovarian clear cell carcinomas and malignant ascites, is shown higher PD-L1 levels are associated with poorer prognosis in patients with advanced stages (III-IV) and higher platinum-resistant compare to low PD-L1 expression (Zhu et al., 2017).

Ovarian cancer is characterized by its rapid intraperitoneal spread with the development of ascites (Penet et al., 2018). TAMs are present not only in the primary tumor but also in the ascitic fluid and are associated with enhanced tumor dissemination in the peritoneum and poorer prognosis. Ascites contain spheroids formed by cancer stem cells and macrophages as well as other innate and adaptive immune cells (Nowak and Klink., 2020).

Spheroids are considered metastatic units that can promote dissemination (Al Habyan et al., 2018). Ovarian tumor spheroids are enriched in cells with stem cell-like characteristics harboring high expression of stemness markers like CD44, CD54, CD55 and CD117 (Etzerodt et al., 2020). During metastasis of epithelial ovarian cancer, TAMs promote spheroid formation and constitute a central component of them (Yin et al., 2016). Depletion of TAM by clodronate in mice reduces the size and number of spheroids, also peritoneal implantation was reduced which contributes to prolonging survival time (Yin et al., 2016; Song et al., 2020).

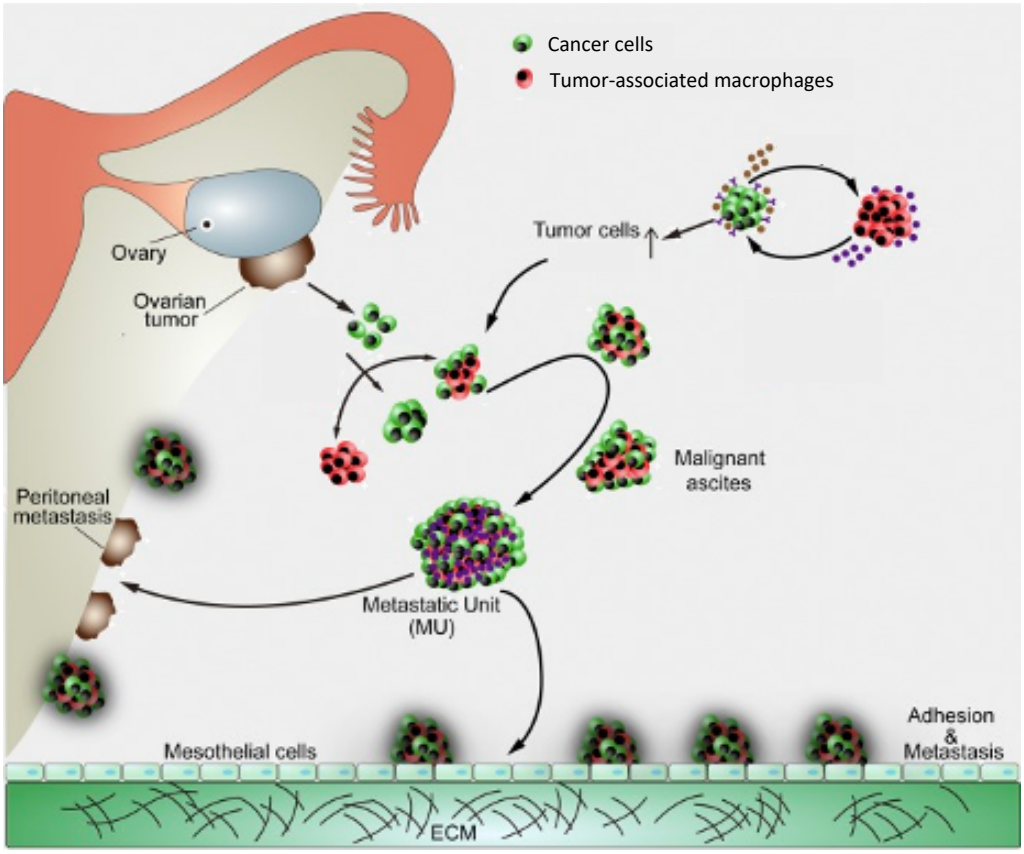

Figure 4. TAMs are implicated in spheroid formation and their role in peritoneal dissemination. Cancer cells and TAMs interact and generate spheroids that have a pivotal role in peritoneal adhesion and invasion. Adapted with permission from Gao et al., 2019.

Cell-cell adhesion between cancer cells and immune cells through adhesion molecules of the integrin receptors and ligands of the immunoglobulin superfamily are crucial to induce immunosuppression. Expression of integrins on tumor cells has been associated with tumor progression and metastasis. Mechanisms of adhesion of cancer cells and TAMs in spheroid formation are not much known. Ovarian cancer cells in spheroids express CD54, a ligand of CD11a/CD18, CD11b/CD18 and CD11c/CD18 integrin receptors on macrophages. Neutralization of CD54 with antibodies reduces spheroid formation in vitro and in vivo mouse models (Yin et al., 2016).

During tumor progression, cancer cells acquire multiple capabilities that include sustaining proliferative signaling, resisting cell death, or avoiding immune destruction. In addition to cancer cells, tumors consist of immune infiltrating cells that form the tumor microenvironment (TME) and this tumor stroma contributes to the acquisition of malignant characteristics (Hanahan and Weinberg, 2011).

Normal tissues control production of growth-promoting signals that are implicated in different steps of the cell cycle and maintain homeostasis of cellular number. However, cancer cells have dysregulated these signals and enable signals that regulate the progression of cell cycle and are implicated in cell survival and energy metabolism. Proliferation also can be maintained by downregulation of pathways that attenuate proliferative signaling (Amit et al., 2007). Cells have a different innate tumor-suppressive mechanism in the programs of proliferation that trigger apoptosis under cell uncontrolled proliferation. However, oncogenic mutations that drive proliferation can uncouple these processes during transformation and tumorigenesis (Lowe et al., 2004).

Senescence constitutes an important tumor suppressor mechanism. Senescent cells exhibit cell-cycle arrest in response to stress, however, they can remain viable for a long period (Collado and Serrano, 2010). Senescent cells have higher activation of senescence-associated (SA)-β-galactosidase, a lysosomal enzyme whose activity is used to assess senescent cells (Wang et al., 2020). Re-education of TAMs to a pro-inflammatory phenotype can induce DNA damage in cancer cells and senescence-associated to tumor inhibition (Di Mitri et al., 2019).

4.1. The tumor microenvironment

Tumor cells escape an anti-tumor response by the immune system through various mechanisms including, tumor-induced immunosuppression, low immunogenicity of tumor cells, tumor surface antigen modulation and recognition of tumor-specific antibodies as autoantigens. This process is important to tumor survival and development. Immune cells in the TME, such as TAMs, myeloid-derived suppressor cells, B cells and regulatory T cells, may contribute to create the immuno-suppressive or tolerogenic environment that protects cancer cells from destruction (Rodríguez-Ubreva et al., 2017; Sarvaria et al., 2017; Fleming et al., 2018; Togashi et al., 2019; Rodriguez-Garcia et al., 2021). Induction of the expression of immunosuppressive molecules or their receptors is implicated in immunosuppression. Some of these molecules included programmed death-ligand 1/programmed death-1 receptor (PD-L1/PD-1), galectin-9/TIM-3, IDO1, LAG-3, and CTLA4 (Chen et al, 2014; Jiang et al, 2019; Labani-Motlagh et al., 2020; Togashi et al., 2019).

PD-L1 and PD-L2 are cell surface molecules expressed on tumor cells that bind to the PD-1 receptor on immune cells (e.g., TILs, TAMs) to inhibit their tumor-suppressor response. Both PD-L1 and PD-L2, inhibit immune responses and do not have any different role. PD-L1 is constitutively expressed in immune cells, such as macrophages, B cells and dendritic cells and its expression is induced in non-hematopoietic cells, like vascular endothelial cells, pancreas and islets cells (Qin et al., 2019). In peripheral tissues, the role of PD-L1 expression is to prevent autoimmune damage (Keir et al., 2006). Also, PD-1 and PD-L1 are expressed in several types of tumor cells and the TME. In TME, PD-1 axis activation in T Lymphocytes results in anti-tumor immunity impairment and immune escape by tumor cells (Jiang et al., 2019).

PD-1 and its ligands are crucial roles in one pathway responsible for the inhibition of T-cell activation (Qin et al., 2019). When T-cells are constantly exposed to an antigen they overexpress PD-1, which is a marker of exhausted T-cells. Also, PD-1 is expressed by a wide variety of immune cells and non-immune cells including B cell, natural killer, T cell, activated monocytes, macrophages, dendritic cells and immature Langerhans cells with a role in the induction of peripheral tolerance and maintenance of the stability and integrity of T-cells (Okazaki and Honjo, 2006).

PD-1 is also expressed in high levels in TAMs and its expression correlates with a decrease in phagocytic capacity. PD-1 inhibition increases partially phagocytosis of tumor cells by TAMs. Analysis of TAMs showed that TAMs expressing PD-1 have an M2-like profile, however, PD-1^{neg} TAMs showed an M1-like profile (Gordon et al, 2017). TAMs can interact with T-cells through PD-1/PD-L1 pathways to inhibit T-cell response against tumor cells.

Macrophages are the major component of the immune cell infiltrate in the TME. Recruitment of myeloid cell into the tumor is developed by chemoattractants, including chemokines and cytokines, particularly CCL2, CCL3, CCL4 and CXCL12 chemokines and CSF1 and VEGFA cytokines (Pathria et al., 2019). TAMs contribute to tumor progression in different ways: purpose nutrients to cancer cells, promoting genetic instability, supporting metastasis and drive adaptative immunity to a protumoral phenotype (Noy and Pollard, 2014; Mantovani et al., 2017). Initially, the characterization of TAM demonstrates that they are close to M2-polarized macrophages by express M2 markers such as CD163, CD206 or IL10. However, transcriptome analysis of TAMs in ovarian and other tumor types indicates that TAMs display a combination of both anti-inflammatory and pro-inflammatory gene signatures (Colvin, 2014, Izar et al., 2020). In human ovarian cancer, a high pro-/anti-inflammatory ratio intratumor is associated with improved survival (Zhang et al., 2014). Approaches to re-educated pro-tumoral TAMs to anti-tumoral TAMs have been shown to reduce tumor progression and improve survival in glioma preclinical models (Pyonteck et al., 2013).

4.2. Metabolism in cancer and stromal cells

Metabolic reprogramming in tumors has been recognized as a hallmark of cancer (Hanahan and Weinberg, 2011). Tumor cells need high amounts of biosynthetic precursors to maintain proliferative rate requirements. Metabolic interaction between tumor cells and TAMs is bidirectional. Cancer cells secrete cytokines that recruit monocyte-derived macrophages to the tumor and favor the polarization toward pro-tumorigenic and immunosuppressive macrophages. Besides, hypoxia and lactate stimulate TAMs to secrete multiple cytokines with metabolic functions on cancer cells (Garcia-Jimenez et al., 2019).

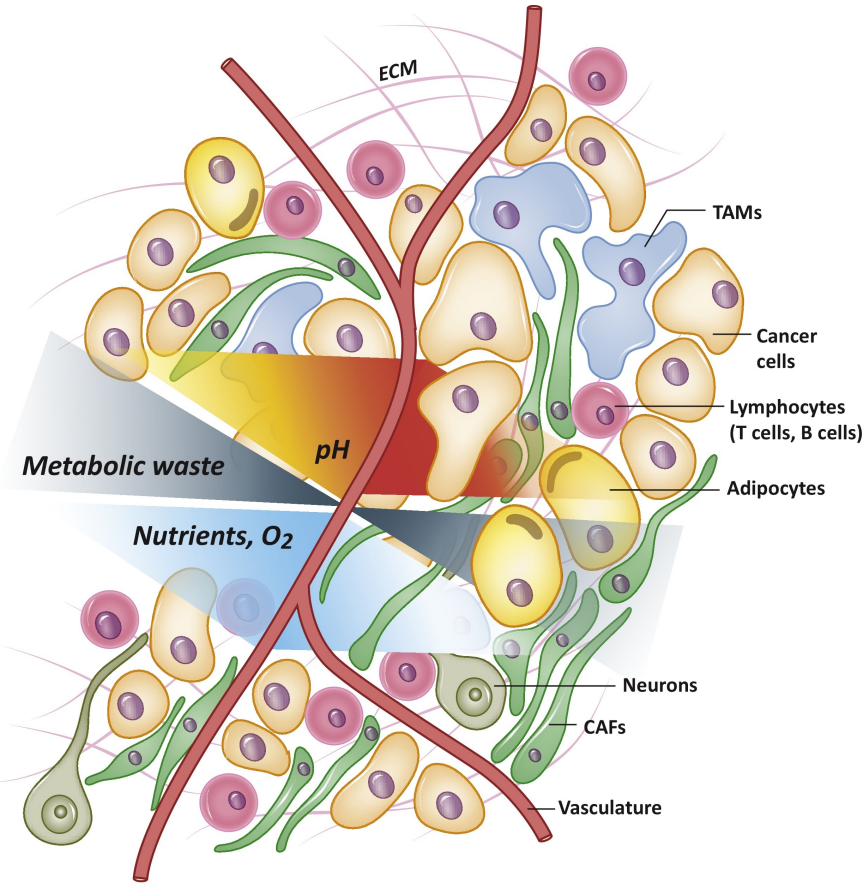

Figure 5. Metabolic heterogeneity in tumor. Variables as heterogeneous cellular populations, nutrient availability, waste and oxygen and pH gradients influence the metabolic properties of tumors. Used with permission from *Lyssiotis and Kimmelman, 2017*.

Two tumor subgroups exist depending on the preference for aerobic glycolysis or oxidative phosphorylation (Gentric et al., 2019; Lahiguera et al., 2020). Tumor cells that have a high glycolytic flux linked to poor vascular supply results in glucose deficiency in the microenvironment. Deficiency of glucose has a high impact on both tumor cells and immune cells of the microenvironment. In macrophages, glucose metabolism is critical to their pro- and anti-inflammatory polarization (Freemerman et al., 2014; Tan et al., 2015; Huang et al., 2016). Tumor cells uptake high amounts of glucose, which is then converted to lactate even in presence of oxygen, producing the acidification of the TME. High levels of lactate levels increase the risk of metastasis, tumor recurrence and death and promote an immunosuppressive phenotype in macrophages, inhibit the secretion of pro-inflammatory cytokines and the migration of monocytes and alter antigen presentation (de la Cruz-Lopez et al., 2019).

Altered lipid metabolism is also exhibited in cancer cells. Uptake or increased synthesis of lipids supports tumor formation and growth (Snaebjornsson et al., 2020). In ovarian cancer, cancer cells use adipocyte-derived lipids for tumor growth and promote metastasis to the omentum (Nieman et al., 2011). Ovarian CSCs have also increased levels of unsaturated lipids by high expression lipid desaturases (Li et al., 2017). In TME, M2-like TAMs reprogram their metabolism toward fatty acid oxidation and increased mitochondrial biogenesis, in line with a lower glycolytic profile.

Amino acids are also an important source of energy supporting cancer and TME cell immunosuppression (Bader et al., 2020). Amino acids are implicated in various metabolic activities like energetic regulation, biosynthetic support, redox balance and epigenetic regulators. Glutamine is widely used to support the Krebs cycle in cancer cells through its conversion to intermediaries of this cycle. Numerous types of cancers are dependent on exogenous non-essential amino acids that can be explained by a loss of expression of an enzyme involved in the synthesis. For instance, in multiple myeloma, ovarian cancer and oligodendroglioma, tumor cells are dependent on glutamine by a loss or downregulation of glutamine synthetase. Also, pro-tumorigenic TAMs are increased uptake of some amino acids like glutamine and arginine (Lyssiotis and Kimmelman, 2017). Glutamine in TAMs is essential in cytokine production, antigen presentation and phagocytosis in murine macrophages in vitro (Biswas, 2015). High consumption of amino acids by tumor cells and TAMs generated a deficiency of these nutrients in the TME that impair T cell activation through an anti-tumoral phenotype.

4.3. Ovarian cancer mouse model

In xenograft cancer models, cells are injected into immunocompromised mice. The use of immunodeficient mice prevent the study of the role of the immune system and the tumor-stroma crosstalk. This disadvantage can be overcome in syngeneic models, which use immunocompetent mice. ID8 model of ovarian cancer is a well-established syngeneic mouse model to study the interaction of tumor and stromal cells in immunocompetent mice (Roby et al., 2000; Hagemann et al., 2006; Etzerodt et al, 2020; Song et al, 2020). ID8 cells are ovarian

cancer surface epithelial cells from C57BL/6 mice. This model reproduces extensive tumors on the peritoneal cavity, ascites development and spheres formation such as it is observed in stage III and IV of human ovarian cancer (Roby et al., 2000). Intraperitoneal injection of ID8 ovarian carcinoma cells into female recipient mice results in their rapid growth and the development of hemorrhagic ascites that contains not only tumor cells but also immune cells particularly TAMs (Hagemann et al, 2006; Yin et al, 2016; Cortes et al, 2017; Goossens et al, 2019). When ID8 cells are isolated from the ascites of mice and are reinoculated into new mice they acquire a higher tumorigenic capacity (Cai et al., 2015; Cortes et al, 2016). Besides, tumor growth in the ID8 model is dependent on the accumulation of TAMs (Hagemann et al, 2008; Rei et al, 2014; Yin et al, 2016).

GENERAL AND SPECIFIC OBJECTIVES

GENERAL AND SPECIFIC OBJECTIVES

The overarching aim of this dissertation is to characterize new potential mechanisms that regulate macrophages function in atherosclerosis and ovarian cancer.

The specific objectives are:

1. To identify new roles and mechanisms of action of ZEB1 as a mediator of lipid metabolism in macrophages during atherosclerosis development.
2. To identify new roles and mechanisms of action of ZEB1 and ZEB2 in TAMs in the initiation and progression of ovarian cancer.

To address these goals, the project made use of a wide range of materials and techniques including human samples, mouse primary cells, conditional knockout mouse models of *Zeb1* and *Zeb2* in macrophages (*Zeb1*$^{\Delta Mac}$; *Zeb2*$^{\Delta Mac}$), the ApoE model of atherosclerosis and the ID8 syngeneic model of ovarian cancer and nanoparticles for in vivo gene delivery in these mouse models.

METHODOLOGY

METHODOLOGY

Human samples

Human samples of atheroma plaques were obtained from patients submitted to programmed endarterectomy. Samples were processed for mRNA extraction. Samples were classified as patients who had suffered a cerebrovascular accident before endarterectomy and patients who had not. Nine carotid arteries from donors of vascular transplants or post-mortem autopsies were used as control samples. The use of human samples was approved by the local Ethics Committee at Hospital Clinic of Barcelona.

Experimental animals and generation of *Zeb1*$^{\Delta Mac}$ and *Zeb1*$^{\Delta Mac}$ mice

Zeb1(+/-) mice were obtained from Dr. Douglas S. Darling (University of Louisville, KY, USA) and Dr. Y. Higashi (Institute for Development Research, Kasugai-shi, Aichi, Japan) (Takagi et al, 1998) and were crossed with *ApoE*(-/-) mice referred as *ApoE*-KO (The Jackson Laboratory; B6.129P2-Apoe^{tm1Unc}/J). The conditional *Zeb1* flox allele mouse (*Zeb1*$^{fl/fl}$, herein referred as *Zeb1*^{WT}) was generated in the joint National Biotechnology Center (CSIC-CNB)/Severo Ochoa's Molecular Biology Center (CSIC-CBMSO) Transgenesis Unit at the Spanish National Research Council (CSIC) and Autonomous University of Madrid (Madrid, Spain). The conditional *Zeb2* flox allele mouse (*Zeb2*$^{fl/fl}$, herein referred as *Zeb2*^{WT}) was generated in the Transgenesis Unit at the Institute of Biomedical Research of Barcelona (IRB) (Barcelona, Spain). Two gRNAs were designed to elicit double-strand breaks (DSBs) flanking exon 6 in the *Zeb1* gene or flanking exon 5-6 in the *Zeb2* gene. Additionally, two ssDNA oligos that contain the LoxP site and a restriction enzyme flanked by two homology arms, which correspond to the sequence surrounding each Cas9 cut site, were designed and purchased from Sigma-Aldrich (Merck KGaA, Darmstadt, Germany). A mixture of transcribe RNA Cas9, two sgRNAs and two ssDNAs was injected into the cytoplasm of B6CBAF2 zygotes, using standard protocols (Behringer et al., 2014). Zygotes that survived were transferred into the oviduct of pseudopregnant foster mothers for development to term. The presence of LoxP sequences was assessed by DNA sequencing. To generate macrophage-specific *Zeb1* and *Zeb2* knockout mice, Zeb1flx/flx or

Zeb2flx/flx were crossed with mice carrying the Cre recombinase selectively in myeloid cells under the control of the endogenous lysozyme 2 (Lyz2, also referred as LysM) promoter. LysMCre (Clausen et al., 1999) (official name: B6.129P2-*Lyz2*$^{tm1(cre)Ifo}$/J) mice were obtained from Jackson Laboratories (Bar Harbor, ME, USA). Macrophage-specific *Zeb1* knockout mice (*Zeb1*$^{floxed/floxed}$ LysMCre/+) were referred as *Zeb1*$^{\Delta Mac}$ and macrophage-specific *Zeb2* Knockout mice (*Zeb2*$^{floxed/floxed}$ LysMCre/+) as *Zeb2*$^{\Delta Mac}$. *Zeb1*$^{floxed/floxed}$ LysMCre+/+ (*Zeb1*^{WT}) and *Zeb2*$^{floxed/floxed}$ LysMCre+/+ (*Zeb2*^{WT}) mice were used as controls. *Zeb1*$^{\Delta Mac}$ and *Zeb2*$^{\Delta Mac}$ mice were also crossed with ApoE(-/-). All animal procedures were approved by Animal Experimentation Ethics Research Committee at the University of Barcelona School of Medicine.

sgRNA oligonucleotides	**Sequence**
sgRNA 5’	5’-TTACAGACACCTCTAACACAAGG-3’
sgRNA 3’	3’-AGTACCAGCAAACCCTTTCTTGG-5’
ssDNA oligonucleotides	**Sequence**
ssDNA #1	5’- agctaagtcccttcaagtgcctggtcactgaggaaagctggggTTACAGACACCTCTAACGCTAGCataacttcgtatagcatacattatacgaagttatACAAGGcttcctcccaaaagggagccgtacagacatgaaaatatttatcaatcaaaggc - 3’
ssDNA #2	3’- aaccaaaggttaacctaactcctaacaaaggagttggcacacgaAGTACCAGCAAACCCTGAATTCataacttcgtataatgtatgctatacgaagttatTTCTTGGctttatggtgaatgggaacatggttgtttaatagtgatcataagcaaagaaga - 5’

Table 1. sgRNA and ssDNA oligonucleotides used in the generation of the *Zeb1*$^{fl/fl}$ mouse.

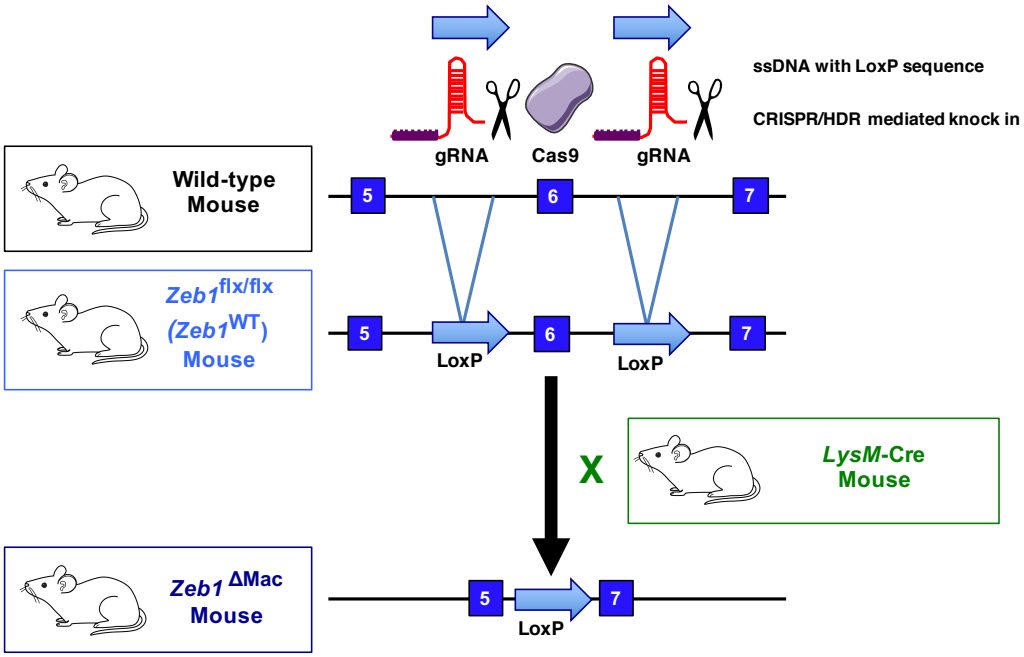

Figure 6. Scheme of transgenic generation of the *Zeb1*$^{\Delta Mac}$ mouse model.

sgRNA oligonucleotides	Sequence
sgRNA 5’	5’- AGCAGATGCATCGGTAGAGAGGG -3’
sgRNA 3’	5’ – GCACAGTCAATTCTCCCAGGAGG - 3’
ssDNA oligonucleotides	**Sequence**
ssDNA #1	5’ – TGAAACACACAAAAAAGGAAATTTAATTTTCTTGAGAAGCCAGACTAAACTTCACCTCCCTCTCTACCGATGgcctgggctagcggatccataacttcgtataatgtatgctatacgaagttatCATCTGCTGCTAAATAAAAGCTTTTGCTATGTTTTT – 3’
ssDNA #2	5’- TTGAAATGACTGAGTAGGGCTAATTCACAGCATCTCTTAAATGTTTCAGCAAAACTGCTCTTTCTATCCTCCTccaggctctagagagctcataacttcgtatagcatacattatacgaagttatGGGAGAATTGACTGTGCAAATTGATATTATGATGTG – 3’

Table 2. sgRNA and ssDNA oligonucleotides used in the generation of the *Zeb2*$^{fl/fl}$ mouse.

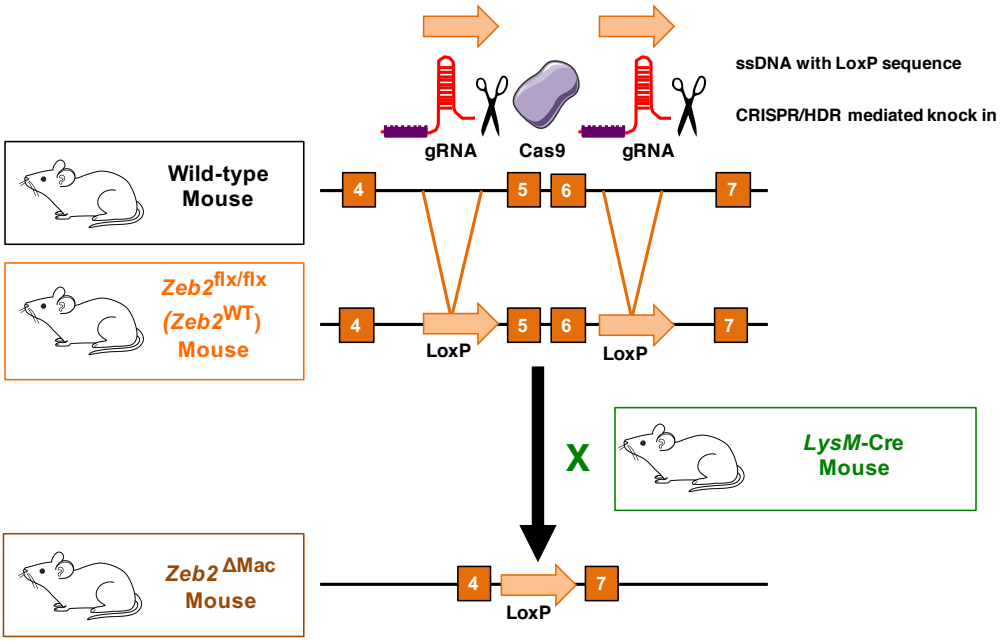

Figure 7. Scheme of transgenic generation of the *Zeb2*$^{\Delta Mac}$ mouse model.

PCR oligonucleotides for genotyping		
Mouse	Forward 5' – 3'	Reverse 5' – 3'
LysM-CRE	ACGAGTGATGAGGTTCGCAAG	CCCACCGTCAGTACGTGAGAT
Zeb1(+/-)	CCAGGAGCCCCAGCACTATTCTCC	TCAGACGGCAAACGACTGTCCTG
Zeb1 flox	GGTCGACAGTCAGTAGCGTT	GCAGAGTTCTACCCAGAACCA
Zeb2 flox	TTCTCTCATTTGTCACGAAACAC	CATTCATAATGCGCCAACAC
ApoE(-/-)	GCCTAGCCGAGGGAGAGCCG	GCCGCCCCGACTGCATCT

Table 3. Primers used in PCR amplification of DNA from mice for genotyping.

Antibodies

Primary antibodies	Source	Clone (Catalog Number)
Fluorescence Associated Cell Sorting (FACS)		
F4/80 APC	BioLegend	BM8 (123116)
F4/80 Alexa Fluor 488	Biolegend	BM8 (123120)
CD11b PE	ImmunoTools	M1/70.15 (22159114)
CD45 PerCP/Cy5.5	BioLegend	30-F11 (103132)

CD206 Alexa Fluor 488	AbD Serotec	MR5D3 (MCA2235A488T)
PD-1 PE	BioLegend	29F.1A12 (135205)
PD-L1 Brilliant Violet 421	BioLegend	10F.9G2 (124315)
CD117 APC	BD Pharmingen	2B8 (553356)
CD55 PE	ImmunoTools	RIKO-3 (22150554)
CD11a PE	ImmunoTools	M17/4 (22850114)
CD54 PE	ImmunoTools	YNI.7.4 (22270544)
Western Blot		
p65	Cell signaling	D14E12 (8242)
p-p65	Santa Cruz Biotechnology	27.Ser 536 (sc-136548)
p-JNK	Santa Cruz Biotechnology	14.Thr183/Tyr185 (sc-293136)
p-p38	Cell signaling	Thr180/Tyr182 (9211)
p38	Sigma-Aldrich	M0800
GAPDH	Cell signaling	14C10 (2118)
Secondary antibodies	Source	Catalog Number
HRP Goat anti-Rabbit	Jackson Immunoresearch	111-035-144
HRP Donkey anti-Mouse	Jackson Immunoresearch	715-545-150

Table 4. Primary and secondary antibodies used.

Cell lines culture

The mouse ovarian cancer cell line ID8 carrying a luciferase reporter was obtained from T. Lawrence (CIML, Marseille, France) (Roby et al., 2000) and cultured in Dulbecco's Modified Eagle Medium (DMEM) (Lonza, Basel, Switzerland), supplemented with 10% FBS (Gibco, Life Technologies), 100 U/mL penicillin and 100 µg/mL streptomycin (Lonza).

Isolation and culture of mouse peritoneal macrophages

Peritoneal macrophages were isolated from 6-8-week-old mice as described (Zhang et al., 2008). Briefly, mice were euthanized and the peritoneal cavity was washed twice with 6 mL of PBS with 3% FBS. Cells from the lavage were centrifuged to 400 x g for 10 min at 4ºC. Then, erythrocytes were osmotically lysed by incubation with Red Blood Cell Lysis Buffer (Sigma-

Aldrich) and the reaction was stopped by adding phosphate-buffered saline (PBS). Peritoneal cells were sorted by detection of CD45, F4/80 and CD11b cell surface expression or plated in RPMI1640 10% FBS and 1% penicillin-streptomycin (Pen/Strep) (Lonza, Basel, Switerland) for 1 h to allow macrophage adherence. Macrophages isolated were then assessed for mRNA expression or used for functional assays.

Cell surface protein expression analysis and cell sorting by flow cytometry (FACS)

Cells were blocked for Fc receptors with mouse gamma globulin for 30 min at 4ºC (Jackson ImmunoResearch Europe). Then, cells were incubated with fluorochrome-labeled antibodies in PBS with 3% FBS at 4ºC for 45 min. Analysis of protein surface expression was assessed in a BD FACSCanto™ III analyzer (BD Biosciences, San Jose, CA, USA) or cells were sorted for specific subpopulations in FACS Aria™ II cell sorter (BD Biosciences) for use in indicates experiments.

Atherosclerosis mouse model

The model of atherosclerosis induction was as described elsewhere (Zhang et al., 1994). Briefly, 8-week mice were fed for 10 weeks in a western diet (21% (wt/wt) fat; 0.21% cholesterol (wt/wt); no sodium cholate, (Ssniff Spezialdiäten GmbH, Soest, Germany). Then, animals were sacrificed and perfused with PBS and hearts and aortic arteries were collected. Aortas were fixed in 4% PFA at 4ºC and hearts were embedded in Tissue-Tek® OCT™ compound (Sakura Finetek, The Netherlands) and stored at 80ºC. For *en face* analysis, aorta was stained with 0.5% Oil Red O solution in methanol ($C_{26}H_{24}N_4O$, ORO; Sigma-Aldrich), a fat-soluble diazol dye that stains neutral lipids in cells, during 1h and lesion area was quantified as previously described (Andrés-Manzano et al., 2015). For crossectional analysis of the lesion area, hearts were cut through the aortic sinus in 7 µm sections, three sections of each mouse were stained with H&E and quantified with Image J software (NIH, Bethesda, MD, USA).

Biochemical analysis of serum

After 10 weeks fed on Western diet, mice fasted overnight and blood was collected at sacrifice and incubated at RT until that is coagulated. Serum was separated by centrifugation at 1500

x g for 10 min in a refrigerated centrifuge. Serum concentration of HDL, LDL, total cholesterol, triglycerides and glucose were measured by enzyme-linked immunosorbent assay (ELISA) using commercial kits.

Determination of blood cell populations

Blood from mice fed on Western diet for 10 weeks was collected in EDTA tubes and immediately measured on a BC-2800Vet automated hematology analyzer (Mindray Bio-Medical Electronics, Shenzhen, P. R. China) for cell blood count.

Aortic root stainings

Hematoxylin and eosin (H&E) staining by equilibrating tissues for 5 min at RT, then, tissues were incubated in hematoxylin for 3 min and followed by washing one in EtOH/LiCl and four in absolute ethanol.

Masson's trichrome staining was performed in the tissue bank of IDIBAPS according to standard protocols. Briefly, 5 µM thickness sections were stained with Hansen's iron hematoxylin for 5 min and washed under running tap water for 5 min. Then, sections were stained with Biebrich scarlet-acid fuchsin for 10 min. After, they were rinsed in water and treated with phosphomolybdic acid for 10 min and transfer sections directly to aniline blue solution for 10 min. Collagen fibers were stained blue.

Lipid content in aorta and liver tissues was assessed by Oil Red O as previously described (Mehlem et al., 2013). Hearts containing aortic root and livers were embedded in Tissue-Tek® OCT™ compound and stored at -80 ºC. Both tissues were cut in sections of 12 µm thickness in a Leica Cryostat (CM 1950) (Leica Biosystems, Heidelberger, Germany). Before staining tissue sections that have been stored at -80 ºC allowed to equilibrate for 5 min at RT. The ORO working solution was prepared from a 0.5 % stock solution (Sigma-Aldrich, St. Louis, MO, USA) in isopropanol and consist of a mixture of 1.5 parts of ORO stock solution to one part of distilled water that was let to stand for 10 min at RT and then filtered to remove precipitates.

Then, sections were incubated for 15 min at RT with ORO working solution. Sections were washed under running tap water.

Images were captured on a bright-field Olympus BX41TF microscope and Cell Sens software (Olympus America Inc., Melville, NY, USA) and quantified with ImageJ software.

LDL isolation and oxidation

Whole human blood from healthy donors in EDTA-coated tubes was obtained from the Catalan Blood and Tissue Bank. Human plasma was separated from blood by centrifugation at 2000 x g for 10 minutes and mixed with KBr to a density of 1.21 g/l. LDL was isolated by ultracentrifugation in a KBr density gradient, as described before (Hamczyk et al., 2018). LDL was dialyzed 48 h in a high retention dialysis tubing (Sigma-Aldrich, St. Louis, MO, USA) against PBS and concentrated with poly-ethylene glycol 20,000 MW (Thermo Fisher Scientific, Waltham, MA, USA). LDL oxidation was carried out by incubation with 5 mmol/L of $CuSO_4$ and incubated for 16 h at 37ºC to fully oxidize LDL in an oxygenated atmosphere. Adding EDTA to a final concentration of 0.24 mM stopped the reaction. Then, LDL solution was dialyzed against 48 h at 4ºC to discard copper excess.

Lipid loading in macrophages

NF-κB inhibitor TPCA-1 was purchased from Sigma-Aldrich (USA) and AMPK activator A-769662 from MedChemExpress (USA). Macrophages were cultured in RPMI 1640 medium containing 10 % FBS. Then, 50ug/mL ox-LDL or/and 1 µM TPCA-1 or 100 µM A-769662 was added and incubated 24 h. Cells were fixed using 4% PFA at RT for 1 hour and neutral lipids were stained with 1 µg/mL Bodipy® 493/503 (4,4-Difluoro-1,3,5,7,8-Pentamethyl-4-Bora-3a,4a-Diaza-s-Indacene) or free cholesterol was stained with 0.05 mg/ml of filipin (Sigma Aldrich) and fluorescence was evaluated in a Leica AF6000 (Leica biosystems, Heidelberger, Germany). Also, cells were processed for RNA or protein extraction.

Synthesis of graphene-dendrimer nanostars

GDNS were generated by Dr. Pedro Melgar (Melgar-Lesmes et al., 2018). Briefly, carbon graphene oxide nanohorns were supplied by Sigma-Aldrich (St. Louis, MO, USA). Stuffer and ZEB1 expression plasmids under LyMCre promoter were obtained from VectorBuilder (Chicago, USA). GNS oxidized were dispersed in DMSO and carbon nanohorns were separated by incubating the dispersion in an ultrasound bath. Then, 100 µL of carbon nanohorns were incubated with 900 µL of 1 mg/mL EDC/NHS containing 30 µL of PAMAM dendrimer 25% v/v for 2 h in the ultrasound bath. After, dispersions were centrifuged at 21000 x g for 10 min, washed three times with DMSO and three times with PBS. Plasmids were incubated with GNS in a 1:10 ratio for 2 h, centrifuged and washed with PBS.

Assay of nanoparticles *in vitro* and *in vivo*

Peritoneal macrophages were isolated and incubated with Stuffer or ZEB1 NPs for three days and untreated or treated with oxLDL on day two for 24 h. Then, cells were fixed and stained with 1ug/mL Bodipy® 493/503 and fluorescence was evaluated in a Zeiss Axiovert 200 inverted microscope (Zeiss, Berkochen, Germany). Mice fed in Western diet were injected with 50 µg/Kg (in a ratio plasmid/DGNS 1:10) of Stuffer or ZEB1 NPs every 4 days for 10 weeks. After the treatment, mice were sacrificed and aorta and peritoneal macrophages were isolated. Aorta was stained with 0.5% Oil Red O solution to plaque area quantification. Peritoneal macrophages were stained with 1 µg/mL Bodipy® 493/503 and fluorescence was assessed by FACS.

Efflux of cholesterol

Peritoneal macrophages were plated on 96-well plates in RPMI 1640 medium and incubated for at least 4h for adherence to the plate and washed twice with PBS. Then, cells were stimulated with 50 µg/mL of oxLDL and labeled with 1 µCi/mL [^{3}H]cholesterol for 24h followed by equilibration in serum-free RPMI 1640 medium containing 1mg/mL of bovine serum albumin (BSA) for 16 h. Cells were washed twice in PBS and incubated with ApoA1 or HDL for 4h. Medium was collected and centrifuged to remove any detached cells and counted for

radioactivity. Cells were washed in PBS and lysed in 0.2M NaOH for 24h and radioactivity was measured in lysates. Cholesterol efflux is expressed as ^{3}H-cholesterol in medium/(^{3}H-cholesterol in medium+^{3}H-cholesterol in cells)x100 and subtracting effluxes of the well without acceptors from those containing the acceptors. All conditions were measured by three technical replicates.

Atto-655-oxLDL uptake assay

Atto-655-oxLDL was used to trace the oxLDL uptake. Peritoneal macrophages were incubated with 50 µg/mL of Atto-655-oxLDL for 2h in low attachment plates with RPMI 1640 and then washed twice with PBS. The mean fluorescence intensity was measured in a BD FACSCanto™ II analyzer after stained with an Alexa Fluor®488-F4/80 antibody to gate macrophages (Table 4).

Determination of ROS production by macrophages

We used 6-carboxy-2',7'-dichlorodihydrofluorescein diacetate, (H2-DCFDA) (C400, Thermo Fisher Scientific), a non-fluorescence molecule that is converted to a green-fluorescent under intracellular oxidation by ROS. Peritoneal macrophages were incubated with 50 µg/mL of oxLDL for 24h in ultra-low attachment plates (Costar®, Corning, New York, NY, USA) in RPMI 1640. Cells were incubated with 5mM CH2-DFCDA for 30min at 37ºC and then stained with Alexa Fluor®488-F4/80 antibody. The mean fluorescent intensity was assessed in a BD FACSCanto™ II analyzer.

ID8 ovarian cancer model and bioluminescence imaging

5 x 10^{6} ID8-luc cells were resuspended in 500 µL of PBS and injected i.p. into 8-week- old *Zeb1*^{WT}, *Zeb1*$^{\Delta Mac}$, *Zeb2*^{WT} and *Zeb2*$^{\Delta Mac}$ female mice and tumor progression was followed by bioluminescent imaging (Evans et al., 2014). At indicated times, mice were injected i.p. with 1.5 mM of CycLuc1 substrate (Calbiochem®, EMD Millipore, Billerica, MA, USA) in 100 µL of PBS and after 10 min mice were anesthetized with 2.5 % of isoflurane. Photon flux signal was measured in a charge-coupled ORCA-2BT imaging system (Hamamatsu Photonics,

Hamamatsu City, Japan). Bioluminescence data were analyzed with Wasabi! Imaging Software (Hamamatsu Photonics). Data were represented as photon flux/sec/cm2 signal emitted from the abdominal cavity. At 5, 9, or 14 weeks, mice were euthanized and cells of the peritoneal cavity were isolated. ID8 tumor cells ($CD45^-$) and tumor associated-macrophages ($CD45^+CD11b^+F4/80^+$) were separated by sorting. ID8 isolated from *Zeb1*^{WT}, *Zeb1*$^{\Delta Mac}$, *Zeb2*^{WT} and *Zeb2*$^{\Delta Mac}$ mice were referred as ID8-ASC^{Zeb1WT}, ID8-ASC$^{Zeb1\Delta Mac}$, ID8-ASC^{Zeb2WT} and ID8-ASC$^{Zeb2\Delta Mac}$, respectively. Cells were analyzed to RNA and ascites to metabolites measure in the Biomedical Diagnostic Center of Hopital Clinic. Also, cells from ascites were analyzed for surface markers by FACS in a BD FACSCanto™ III (Becton Dickinson Biosciences, San Jose, CA, USA). Experiment to evaluate mice survival was performed by injecting ID8-ASC^{Zeb1WT}, ID8-ASC$^{Zeb1\Delta Mac}$, ID8-ASC^{Zeb2WT} and ID8-ASC$^{Zeb2\Delta Mac}$ into new wild-type mice. As ID8 from ascites of mice accelerate tumor progression (Cai et al., 2015), mice survival was assessed for 30 days.

Spheroid formation assay

Ascites from 9 weeks mice were collected and washed with cold PBS. Peritoneal ascites cells were cultured in 6-well ultra-low attachment plates (Corning Life Sciences) in DMEM with 10 % FBS. After 24 h, images of spheroids were captured on an Olympus IX5I (Olympus America Inc., Melville, NY, USA). Also, cells from spheroid were analyzed for surface markers by FACS in a BD FACSCanto™ III (Becton Dickinson Biosciences, San Jose, CA, USA).

In vitro phagocytosis assay

To assessed in vitro phagocytosis of ID8-ASC tumor cells by macrophages, ID8-ASC$^{Zeb1/2WT}$ were stained with 1,25 μg/mL Dil (1,1'-Dioctadecyl-3,3,3',3'-Tetramethylindocarbocyanine perchlorate) and peritoneal macrophages from *Zeb1*^{WT}, *Zeb1*$^{\Delta Mac}$, *Zeb2*^{WT} and *Zeb2*$^{\Delta Mac}$ mice were stained with 5 μM CSFE. Tumor cells and peritoneal cells were co-culture in low attachment plaques (Costar®, Corning, New York, NY, USA) o/n at 37ºC in a 5% CO_2 atmosphere. Then, cells were plated for 30 minutes to isolate macrophage by differential attachment. Double positive cells were counted in a Zeiss Axiovert 200 (Zeiss, Berkochen, Germany) inverted microscope to the quantification of the phagocytic index.

Assessment of cell senescence

ID8-ASC$^{Zeb1/2WT}$, ID8-ASC$^{Zeb1\Delta Mac}$ and ID8-ASC$^{Zeb2\Delta Mac}$ spheroid cells were disaggregated and allowed to attach in a 12-well plate. Cells were fixed before being processed for senescence-associated β-galactosidase (SA β-gal) staining using a commercial kit (Cell Signaling Technology, MA, USA). Briefly, cells were fixed in formaldehyde 3% at RT, washed and incubated overnight at 37ºC with fresh SA β-gal stain solution in CO_2-free conditions. 5 fields per well were captured with an Olympus IX5I (Olympus America Inc., Melville, NY, USA).

Assessment of cell proliferation

To assess proliferation in ID8-ASC$^{Zeb1/2WT}$, ID8-ASC$^{Zeb1\Delta Mac}$ and ID8-ASC$^{Zeb2\Delta Mac}$ cells, Click-iT EdU kit, an EdU uptake assay, (Thermo Fisher) was used. Cells were incubated with 10 µm of EdU for 1 h, washed and fixed with 3,7% formaldehyde for 15 min at 4ºC. Then, cells were permeabilized with 0,5 % Triton X-100 in PBS at RT for 20min. EdU detection was assessed by incubation with Click-iT reaction cocktail at RT for 30 min protected from light. Cells were analyzed in a BD FACSCanto^{TM} II (Becton Dickinson Biosciences, San Jose, CA, USA).

Assessment of cell apoptosis

Apoptosis was assessed by annexin V (ImmunoTools GmbH, Friesoythe, Germany), a Ca^{2+}-dependent phospholipid-binding protein that is bind to anionic phospholipid phosphatidylserine that is exposed in the part of the extracellular membrane during apoptosis. Co-staining with propidium iodide (Thermofisher), a live cell-impermeant stain, was used to exclude dead cells from the analysis. Cells were resuspended in annexin-binding buffer. Then, 5 µL annexin V and 5 µL of PI were added into 100 µL of cell suspension and incubated for 15 min at RT in dark. After incubation, 400 µL of annexin-binding buffer were added and cells were analyzed by flow cytometry.

RNA isolation and quantitative real-time PCR

Total RNA was isolated with Trizol reagent (Life Technologies, Thermo Fisher Scientific, Carlsbad, CA, USA), RNA was resuspended and quantified using NanoDrop™ (Thermo Fisher Scientific), and reverse-transcribed using High-Capacity cDNA Reverse Transcription Kit (Life Technologies). mRNA levels were determined by qRT-PCR Chromo4 (Bio-Rad) or LightCycler 96 (Roche, Basel, Switzerland) using Sybr Green (GoTaq; Promega). Relative gene expression was calculated using the ΔΔCT method and mRNA level was normalized with glyceraldehyde-3-phosphate dehydrogenase (*Gapdh*), Ribosomal Protein S18 (*Rps18*) and Ribosomal Protein L19 (*Rpl19*) as reference genes. DNA primers used in qRT-PCR were purchased from Sigma-Aldrich, and their sequences are listed in Table 5.

qRT-PCR oligonucleotides		
Targeted gene	Forward 5' – 3'	Reverse 5' – 3'
Human genes		
GAPDH	TGCACCACCAACTGCTTAGC	GGCATGGACTGTGGTCATGAG
ZEB1	AGCAGTGAAAGAGAAGGGAATGC	GGTCCTCTTCAGGTGCCTCAG
ZEB2	GAAAAGCAGTTCCCTTCTGC	GCCTTGAGTGCTCGATAAGG
Mouse genes		
Abca1	CAGGGTGGCTCTTCTCATCAAT	GCCGTCTTTCCAGGACAGTATG
Abcg1	TCCGGATTCTTTGTCAGCTT	CAGGACGATGAAATCCAGGT
Cd36	TTTCCTCTGACATTTGCAGGTCTA	AAAGGCATTGGCTGGAAGAA
Cpt1a	CCAGGCTACAGTGGGACATT	GAACTTGCCCATGTCCTTGT
Fabp4	GATGAAATCACCGCAGACG	GCCCTTTCATAAACTCTTGTGG
Fabp5	AGTCTTAAGGATCTCGAAGGGAA	CTCATAGACCCGAGTGCAGGTGG
Gapdh	CGACTTCAACAGCAACTCCCACTCTTCC	TGGGTGGTCCAGGGTTTCTTACTCCTT
Il6	TGGTACTCCAGAAGACCAGAGG	AACGATGATGCACTTGCAGA
Il10	TGTCAAATTCATTCATGGCCT	ATCGATTTCTCCCCTGTGAA
Mrc1	CCATTTATCATTCCCTCAGCAAGC	AAATGTCACTGGGGTTCCATCACT
Nr1h2	GCAGGACCAGCTCCAAGTAG	GGCTCACCAGCTTCATTAGC

Ppargc1a	TTGCTAGCGGTTCTCACAGA	TAAGACCGCTGCATTCATTG
Prkaa1	CTTGACGTGGTGGGAAAAAT	ATAATCAAATAGCTCTCCTCCAGA
Rpl19	GCATCCTCATGGAGCACAT	GCATCCTCATGGAGCACAT
Rps18	GGATGTGAAGGATGGGAAGT	CCCTCTATGGGCTCGAATTT
Scd1	TGGGAAAGTGAGGCGAGCAACTG	AGGGAGGTGCAGTGATGGTGGTG
ScarbI	CTCCCAGACATGCTTCCCATA	CAGATGGATCCTGCTGAAATTCT
Srebf1	GGCCGAGATGTGCGAACT	TTGTTGATGAGCTGGAGCATGT
Tnf	TTTCGATTCCGCTATGTGTG	CCACCACGCTCTTCTGTCTAC
Zeb1	ATTCCCCAAGTGGCATATACA	GAGCTAGTGTCTTGTCTTTCATCC
Zeb2	CGACACGGCCATTATTTACC	TTCTTCTCGTGGCGGTACTT

Table 5. Primers used in qRT-PCR amplification of coding mRNAs.

Assessment of protein expression by Western blot

Peritoneal macrophages were plated, washed with ice-cold PBS, and lysed with radio immunoprecipitation assay (RIPA) buffer (50 mM Tris pH 8.0, 150 mM NaCl, 2mM EDTA, 1% NP-40, 0.5% deoxycholic sodium acid, 0.5% SDS) containing protease inhibitors (1 mg/ml leupeptin, 1 mg/ml pepstatin, 1 mg/ml apoptin, 100 mM PSMF). Protein levels were quantified by using the DC™ Protein Assay kit (Bio-Rad, CA, USA), samples were boiled at 95ºC for 5 min after the addition of WB loading Buffer (0.25 M Tris pH 6.8, 1.2% SDS, 0.06% bromophenol blue, 45% glycerol plus 1% DTT added fresh), and loaded onto 10% polyacrylamide gels. Gels were then transferred onto polyvinylidene difluoride (PVDF) membranes (Immobilon-P; Merck Millipore, USA) which had been previously activated with methanol. Membranes were then blocked for non-specific binding with non-fat diet milk 5% (PanReac-AppliChem, Barcelona, Spain) and immunoblotted overnight at 4ºC with the corresponding primary antibodies (Table 4). The chemiluminescent reaction was detected with Clarity ECL Western Blotting Substrate (Bio-Rad). Quantification of expression with respect to GAPDH in Western blots was assessed with ImageJ software.

Statistical analysis

Statistical analysis of all the data in this dissertation was performed using GraphPad Prism® software for Mac version 8 (GraphPad Software Inc., La Jolla, CA, USA). Statistical significance was assessed with a non-parametric Mann-Whitney U test. Error bars in all figures represent standard errors of means. Statistical significant was set at a $p<0.05$ (*), $p<0.01$ (**) and $p<0.001$ (***).

RESULTS

RESULTS

Chapter I: ZEB factors in atherosclerosis

ZEB1 expression in human atherosclerotic plaque

To investigate whether ZEB1 in macrophages is involved in the development of atherosclerosis, we first analyzed *ZEB1* expression in human aorta macrophages of patients with either stable or ruptured plaque. Our analysis of a published gene expression array (GSE41571) showed that *ZEB1* has a lower expression in patients with ruptured plaque (Figure 8).

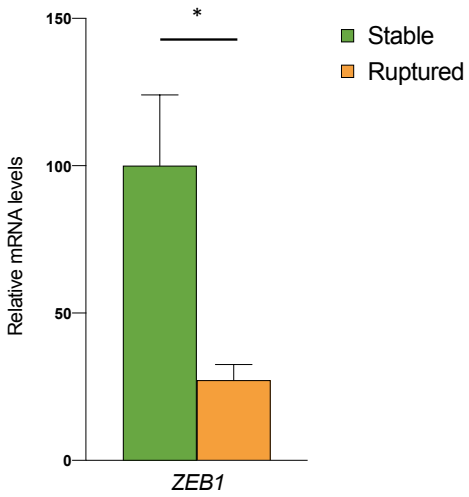

Figure 8. ***ZEB1* expression in macrophages of the atherosclerotic plaque of patients with stable or ruptured plaque**. *ZEB1* mRNA levels in macrophages from 5 patients with stable plaques and 5 patients with ruptured plaques from the gene expression array GSE41571.

To validate these data, we obtained samples from endarterectomies of carotid arteries with atherosclerosis of patients without symptomatology and patients that have suffered a cerebrovascular accident before collecting sample. These samples were compared with control samples with initial o no atherosclerosis. ZEB1 expression was lower in asymptomatic compared to control samples and it was even lower in patients that have suffered a cerebrovascular accident compared with asymptomatic (Figure 9).

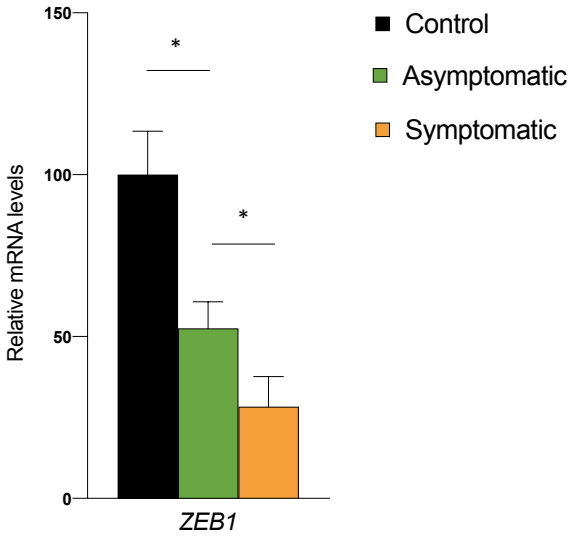

Figure 9. ***ZEB1* decreased in patients with atherosclerotic plaque.** *ZEB1* mRNA levels in atherosclerotic samples from control individuals or asymptomatic and symptomatic patients were assessed by qRT-PCR with respect to *GAPDH* (n=6-10).

Effect of oxLDL on the expression of ZEB factors in mouse macrophages

Lipoproteins and modified lipoproteins are implicated in the formation of foam cells. To investigate whether ZEB expression in macrophages is modulated by oxidized LDL we compared wild-type macrophages in basal conditions and after incubation with ox-LDL. Stimulation of wild-type peritoneal macrophages with ox-LDL resulted in a decrease of *Zeb1* expression (Figure 10).

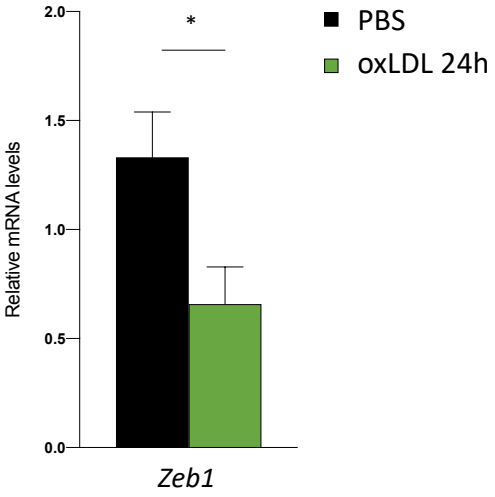

Figure 10. *Zeb1* expression in response to ox-LDL stimulus in peritoneal macrophages *in vitro*. Wild-type peritoneal macrophages were treated with ox-LDL for 24 hours and examined for *Zeb1* mRNA expression by qRT-PCR (n=4).

Zeb1 deficiency promotes atherosclerosis plaque formation in the *ApoE*-KO mouse model

To examine the impact of *Zeb1*-deficiency in atherosclerosis development, we first used *Zeb1* haploinsufficient mice, *Zeb1*(+/-), which express around half of basal ZEB1 protein and mRNA levels in all cell types (Takagi et al., 1998). We crossed *Zeb1*(+/-)—mice-null *Zeb1*(-/-) are embryonic lethal (Takagi et al., 1998)—with *ApoE*-KO, an established model to study atherosclerosis (von Scheidt et al., 2017). *Zeb1*(+/-)/*ApoE*-KO and *Zeb1*(+/+)/*ApoE*-KO mice were fed a western diet for 12 weeks. *Zeb1*(+/-)/*ApoE*-KO mice showed increased body weight as compared with *Zeb1*(+/+)/*ApoE*-KO (Figure 11A). Analysis of the aortic sinus lesion area and quantification of the plaque area relative to aorta area revealed that *Zeb1*(+/-)/*ApoE*-KO mice had a higher plaque size than in *Zeb1*(+/+)/*ApoE*-KO mice (Figure 11B and C).

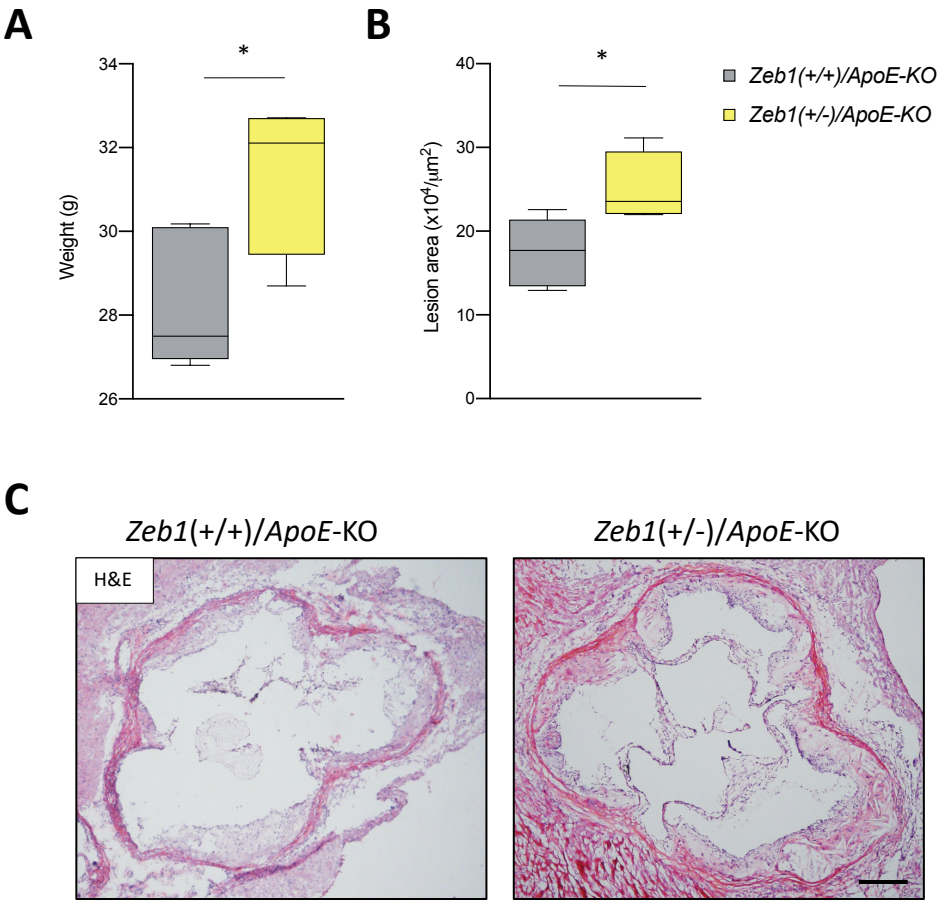

Figure 11. *Zeb1* deficiency promotes atherosclerosis plaque development in *ApoE*-KO mice. (A) Weight of *Zeb1*(+/+)/*ApoE*-KO and *Zeb1*(+/-)/*ApoE*-KO mice subjected to Western diet 12 weeks (n=4-5). (B) Representative images of OCT aortic root sections and quantification of lesion area from *Zeb1*(+/+)/*ApoE*-KO and *Zeb1*(+/-)/*ApoE*-KO mice 12 weeks fed in western diet (n=4-5).

ZEB1 in macrophages is protecting atherosclerosis plaque development in the *ApoE*-KO mouse

To investigate whether ZEB1 expression in macrophages plays a pathogenic role in the formation of atherosclerosis plaque *ApoE*-KO mice were crossed with mice where the expression of *Zeb1* has been specifically deleted in macrophages (*Zeb1*$^{fl/+}$ LysMCre$^{tg/+}$) to generate the experimental models to be used in the study, namely, *Zeb1*^{WT}/*ApoE*-KO and *Zeb1*$^{\Delta Mac}$/*ApoE*-KO. Then, these two models were subjected to Western diet for 10 weeks. Compared to *Zeb1*^{WT}/*ApoE*-KO, *Zeb1*$^{\Delta Mac}$/*ApoE*-KO mice have higher body weight (Figure 12A). Staining with ORO and quantification of plaque area out in the entire aorta showed an increase in *Zeb1*$^{\Delta Mac}$/*ApoE*-KO compared to *Zeb1*^{WT}/*ApoE*-KO mice (Figure 12B). Also, an analysis of atherosclerosis lesion by H&E staining showed an increase of plaque lesion in the aortic root of *Zeb1*$^{\Delta Mac}$/*ApoE*-KO mice (Figure 15).

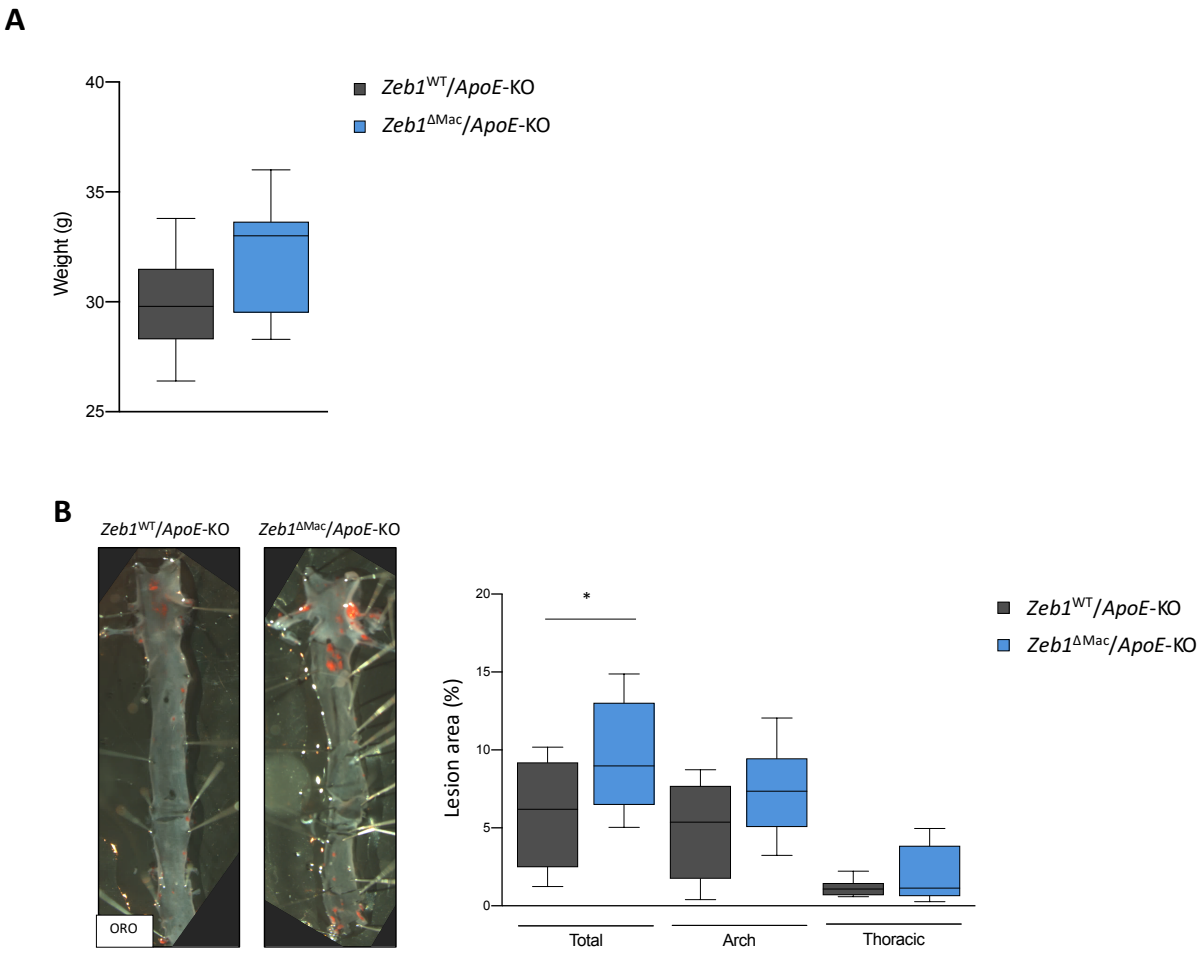

Figure 12. ZEB1 in macrophages is protected against atherosclerosis plaque development in *ApoE*-KO mice. (A) Body weight was obtained at sacrifice of *Zeb1*^{WT}/*ApoE*-KO and *Zeb1*$^{\Delta Mac}$/*ApoE*-KO mice subjected to western diet 10 weeks (n=8-10). (B) Representative images of en face ORO staining of entire aorta and quantification of lesion area of *Zeb1*^{WT}/*ApoE*-KO and *Zeb1*$^{\Delta Mac}$/*ApoE*-KO mice 10 weeks fed in western diet (n=8-10).

Ten weeks into the Western diet feeding protocol, peripheral blood samples were extracted from mice of the two genotypes and the total white blood cell count as well the number of monocytes were quantified but no differences were observed (Figure 13). Also, serum was separated for biochemical parameters analysis.

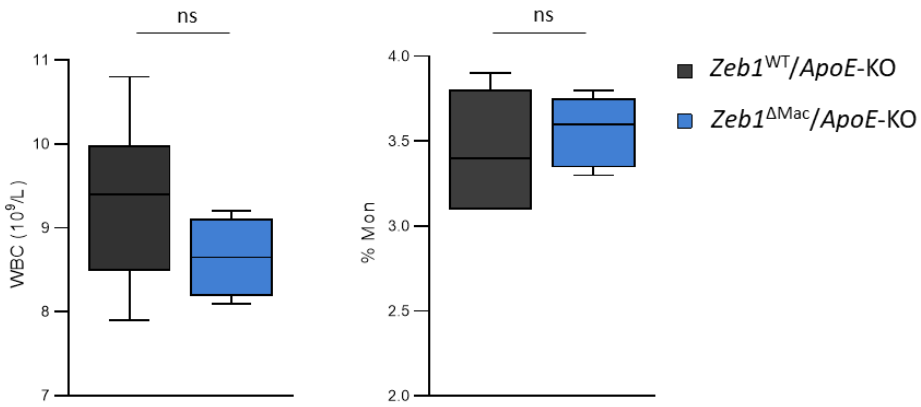

Figure 13. *Zeb1*$^{\Delta Mac}$*/ApoE*-KO mice do not show changes in the number of blood populations compared with *Zeb1*^{WT}*/ApoE*-KO mice. Number of white blood cells (Left) and percentage of monocyte (Right) in blood of mice fed on Western diet 10 weeks (n=4).

The analysis of serum in Figure 14 shows lower levels of HDL and higher levels of LDL in *Zeb1*$^{\Delta Mac}$*/ApoE*-KO compare to *Zeb1*^{WT}*/ApoE*-KO mice, but no differences between both groups were found for cholesterol, triglycerides or glucose levels.

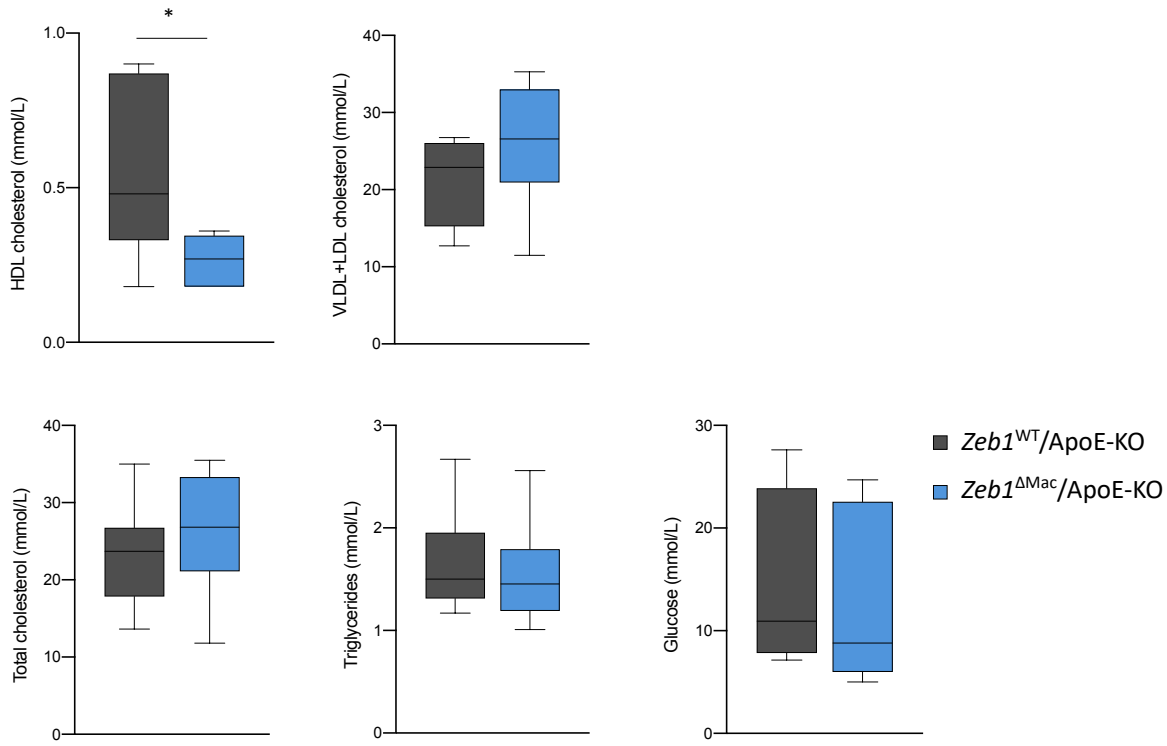

Figure 14. Serum parameters in *Zeb1*$^{\Delta Mac}$*/ApoE*-KO and *Zeb1*^{WT}*/ApoE*-KO mice. HDL cholesterol, VLDL/LDL cholesterol, total cholesterol, triglycerides and glucose were analyzed from serum obtained at sacrifice (n=7-8).

Zeb1$^{\Delta Mac}$ macrophages promote unstable plaque in the *ApoE*-KO mouse

Lipid accumulation preserves vascular inflammation in atherosclerosis (Bäck et al., 2019). Our results in peritoneal macrophages indicated an increase of lipid content in *Zeb1*$^{\Delta Mac}$ macrophages compared to control macrophages. To study whether also there are differences in lipid content in the macrophages of the atherosclerotic plaque of *Zeb1*$^{\Delta Mac}$/*ApoE*-KO mice we stain with ORO. We found an increase in lipid content of *Zeb1*$^{\Delta Mac}$/*ApoE*-KO compared to *Zeb1*^{WT}/*ApoE*-KO mice (Figure 15, Center images).

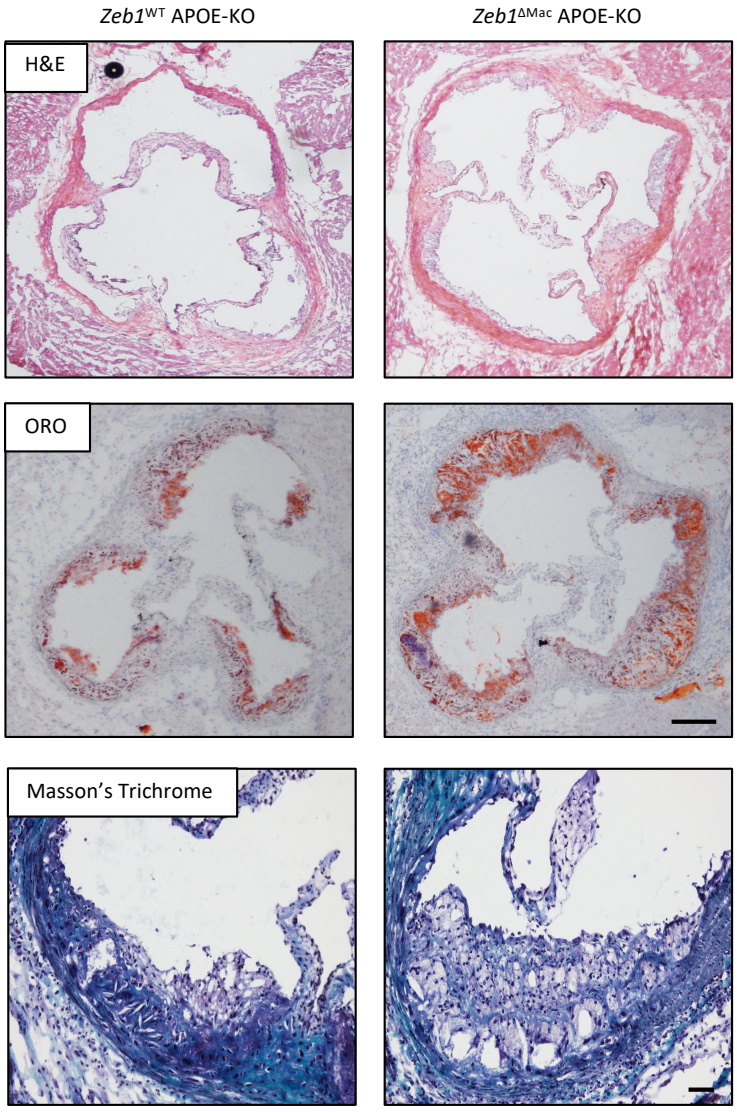

Figure 15. *Zeb1*$^{\Delta Mac}$/*ApoE*-KO mice showed increased pro-atherogenic markers in atherosclerotic plaque compared to *Zeb1*^{WT}/*ApoE*-KO mice. Representative images of aortic root sections stained with H&E (Top images), ORO (Center images) or Masson's Trichrome (Bottom images) of *Zeb1*^{WT}/*ApoE*-KO, *Zeb1*$^{\Delta Mac}$/*ApoE*-KO mice subjected to western diet 10 weeks (n=5-6). Scale bar represents 200 μm (top and center images) or 50 μm (bottom images).

The presence and size of necrosis or fibrosis in the atherosclerotic plaque are markers of risk of plaque rupture (Bentzon et al., 2014). We analyzed the necrotic core by quantifying the area not stained by H&E in stained lesions of the aortic root (Figure 15, Top images). Also, we stained collagen fibers with Masson's Trichrome to analyzed fibrosis and *Zeb1*$^{\Delta Mac}$/*ApoE*-KO mice showed a reduction in collagen stain in plaque lesion (Figure 15, lower images).

ZEB1 expression in macrophages protects the liver from lipid accumulation

A correlation between cardiovascular disease and NAFLD has been established (Anstee et al., 2013). The prevalence of NAFLD increases the risk of cardiovascular events (Targher et al., 2016). Atherosclerosis in *ApoE*-KO mice fed with Westerm diet is accompanied by liver steatosis. Therefore, we also examined liver tissue in mice fed in Western diet for 10 weeks. Compared to *Zeb1*^{WT}/*ApoE*-KO mice, *Zeb1*$^{\Delta Mac}$/*ApoE*-KO mice exhibited enhanced hepatic steatosis, as evidenced by H&E and ORO staining (Figure 16).

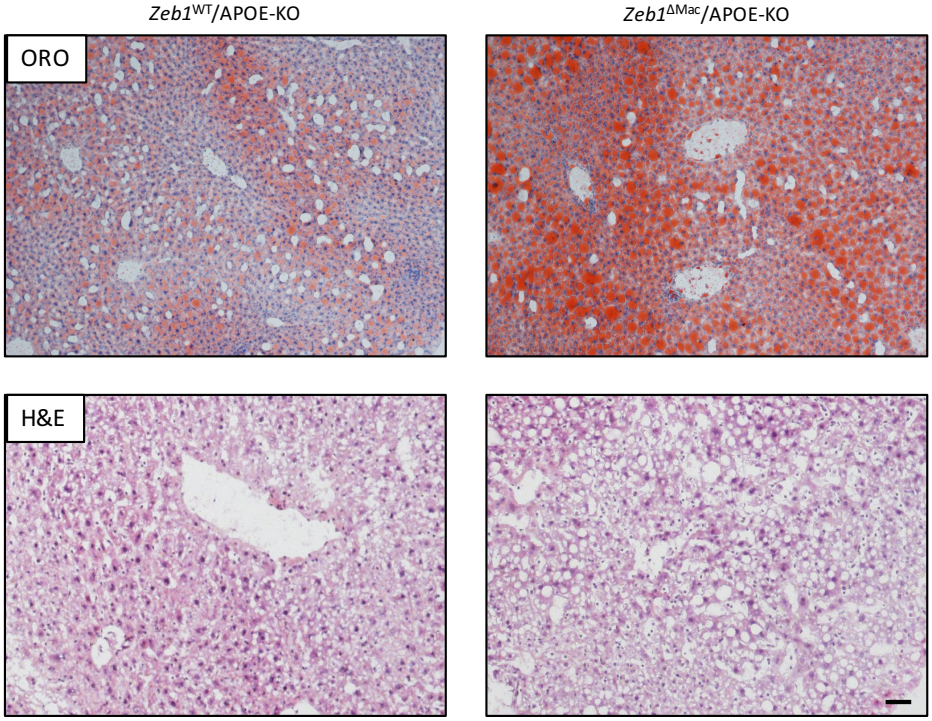

Figure 16. *Zeb1* knockout promotes fatty acid liver disease in *ApoE*-KO mice. Representative images of liver sections stained with ORO or H&E of control and *Zeb1*$^{\Delta Mac}$/*ApoE*-KO (n=3). Scale bar represents 20 μm.

ZEB1 regulates lipid-related genes in peritoneal macrophages

Macrophages are implicated in all stages of atherosclerosis development (Moore et al., 2013). Our group has previously conducted an RNAseq analysis from *Zeb1*(+/+) and *Zeb1*(+/-) peritoneal macrophages (Cortes et al., 2017) from which we have validated several lipid metabolism-related genes and found that several differentially expressed genes between both genotypes (Figure 17).

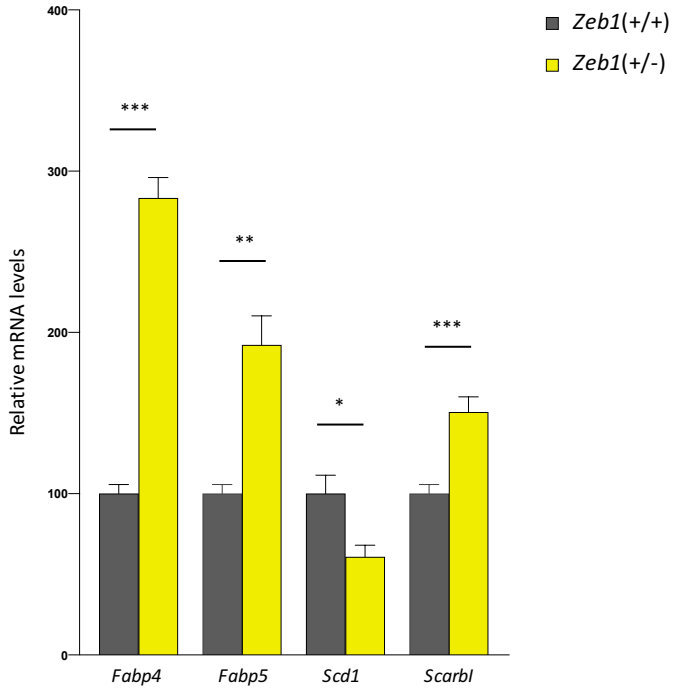

Figure 17. ZEB1 regulates lipid metabolism genes in peritoneal macrophages. mRNA level of *Fabp4*, *Fabp5*, *Scd1* and *ScarbI* were determined by qRT-PCR in peritoneal macrophages from *Zeb1*(+/+) and *Zeb1*(+/-) mice (n=9).

Next, we isolated *Zeb1*(+/-)/*ApoE*-KO and *Zeb1*(+/+)/*ApoE*-KO peritoneal macrophages from mice fed with Western diet for 12 weeks and analyzed gene expression by quantitative analysis of mRNA expression. We investigated whether ZEB1 modulates several archetypal genes involucrated in atherosclerosis. Thus, we analyzed ABCA1, a transporter involved in the efflux of cholesterol and phospholipid, and CD36, a cell receptor involved in the scavenging of ox-LDL. Compared to *Zeb1*(+/+)/*ApoE*-KO macrophages, *Zeb1*(+/-)/*ApoE*-KO macrophages expressed lower levels of *Abca1*, however, no differences were observed in CD36 expression

(Figure 18). *Zeb1*(+/-) macrophages also expressed lower expression than wild-type counterparts of CD206, an M2-like macrophage marker (Figure 18).

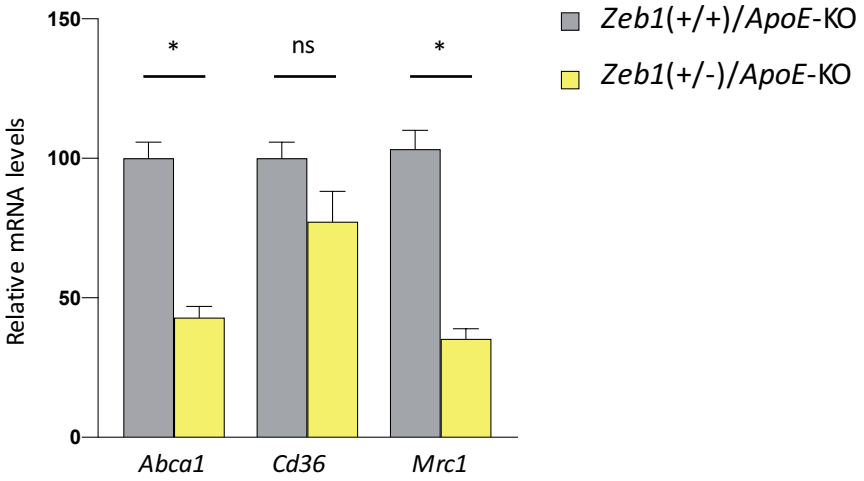

Figure 18. ZEB1 activates *Abca1* and *Mrc1* genes in peritoneal macrophages from *ApoE*-KO mice fed with Western diet. mRNA levels of *Abca1*, *Cd36* and *Mrc1* were determined by qRT-PCR in peritoneal macrophages from Zeb1(+/+)/*ApoE*-KO and Zeb1(+/-)/*ApoE*-KO mice fed in western diet 12 weeks (n=4).

ZEB1 impairs foam cell formation in ox-LDL response

Then, we investigated whether ZEB1 modulates ABCA1 and ABCG1 (two transporters involved in the efflux of cholesterol and phospholipids) and CD36/SCARB3 and SCARB1 (two scavenger receptors) by the used of *Zeb1*$^{\Delta Mac}$ macrophages. Compared to control counterparts, *Abca1* and *Abcg1* expression were downregulated in *Zeb1*$^{\Delta Mac}$ ox-LDL-macrophages but no differences were observed in *Cd36* or *Scarb1* expression (Figure 19).

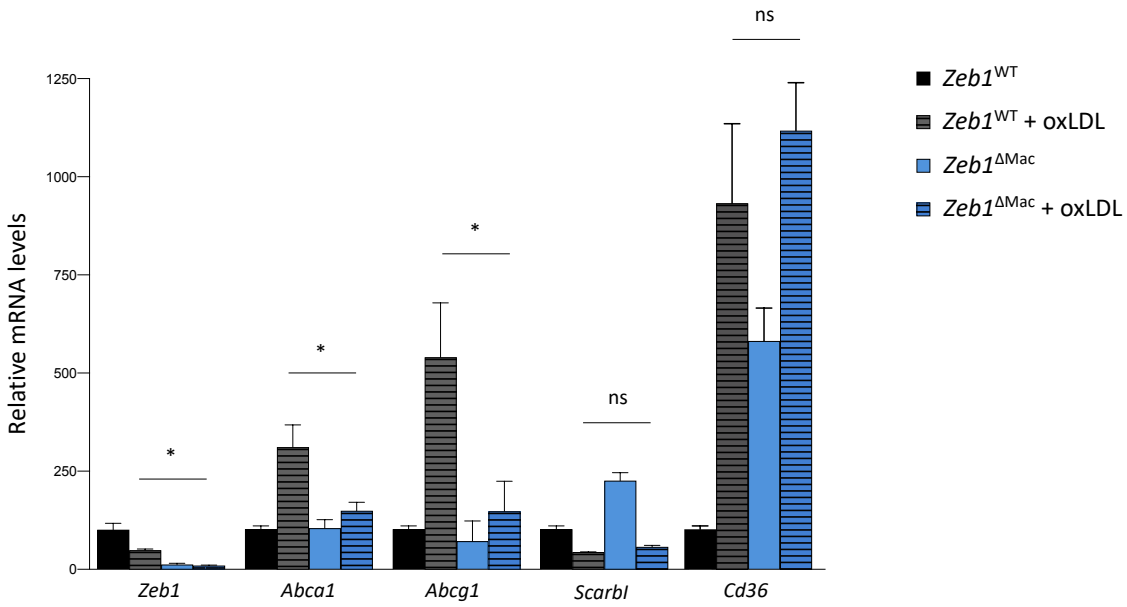

Figure 19. *Zeb1*$^{\Delta Mac}$ macrophages present lower cholesterol efflux-related genes under ox-LDL stimulation compared with *Zeb1*^{WT} macrophages. mRNA level of *Zeb1*, *Abca1, Abcg1, Scarbl* and *Cd36* were determined by qRT-PCR in peritoneal macrophages untreated or treated with 50 µg/mL of oxLDL 24h from *Zeb1*^{WT} and *Zeb1*$^{\Delta Mac}$ mice (n=4-6).

The deletion or knockdown of *Abca1* and *Abcg1* increased lipid content in macrophages (Out et al., 2008). Thus, we investigated whether ZEB1 affected ox-LDL-induced macrophage lipid content and foam cell formation by staining for Bodipy 493/503. Although there was no difference in Bodipy 493/503 staining under basal conditions, interestingly, we observed higher accumulation of lipids in ox-LDL treated *Zeb1*$^{\Delta Mac}$ macrophages than in *Zeb1*^{WT} macrophages (Figure 20A). Furthermore, ox-LDL treatment increased cellular cholesterol content observed by filipin staining in *Zeb1*$^{\Delta Mac}$ macrophages compared to *Zeb1*^{WT} counterparts (Figure 20B).

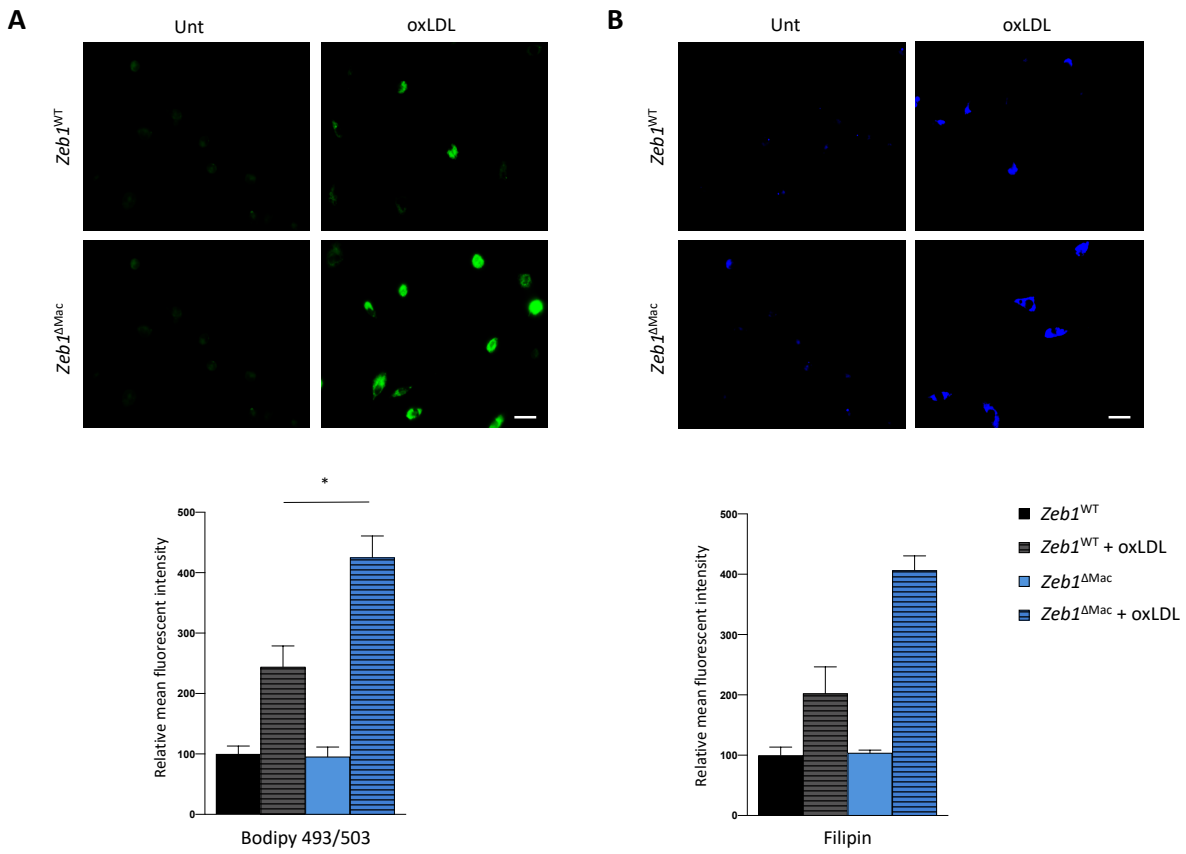

Figure 20. ZEB1 reduced ox-LDL-induced lipid accumulation in macrophages. Representative images and quantification of Bodipy 403/503 (n=6) and filipin (n=3) stained of *Zeb1*^{WT} and *Zeb1*$^{\Delta Mac}$ peritoneal macrophages either untreated or treated with 50µg/mL of ox-LDL for 24h. Scale bar represents 20 µm.

We then analyzed the lipid content in peritoneal macrophages from *Zeb1*^{WT}/*ApoE*-KO and *Zeb1*$^{\Delta Mac}$/*ApoE*-KO mice fed with Western diet for 10 weeks. We found similar results than in oxLDL stimulated macrophages, *Zeb1*$^{\Delta Mac}$/*ApoE*-KO macrophages showed a higher lipid content – as assessed by Bodipy 493/503 staining — than *Zeb1*^{WT}/*ApoE*-KO macrophages (Figure 21).

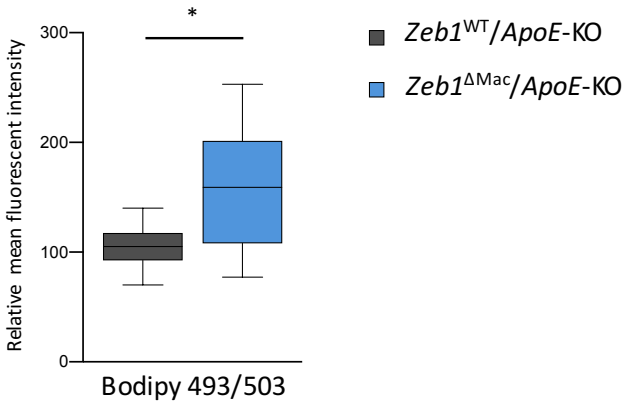

Figure 21. ZEB1 reduced Western diet-induced lipid accumulation in macrophages. Mean fluorescence intensity of Bodipy 493/503 acquired by flow cytometer of *Zeb1*^{WT} and *Zeb1*$^{\Delta Mac}$ peritoneal macrophages of mice fed in Western diet for 10 weeks (n=8).

To exogenously restore ZEB1 expression in macrophages, we generated nanoparticles (NPs) (graphene nanostars) (Melgar et al., 2018) and bound them to an expression vector carrying the *Zeb1* cDNA gene under *Lyz2* promoter and fused to mCherry. Peritoneal macrophages in vitro were treated with NPs with the vector expressing *Zeb1* or a scrambled non-coding sequence referred hereafter to as "stuffer". *Zeb1* expression in *Zeb1*$^{\Delta Mac}$ macrophages decreases lipid content compared with treated with stuffer vector (Figure 22A). *Zeb1*$^{\Delta Mac}$/*ApoE*-KO and *Zeb1*^{WT}/*ApoE*-KO mice on Western diet were treated with both NPs expressing *Zeb1* or stuffer sequence and the same results were found in peritoneal macrophages from these mice (Figure 22B). However, no changes in lipid content were found in *Zeb1*^{WT} macrophages treated with *Zeb1* or stuffer vectors *in vitro* or *in vivo* (Figure 22A and B)

To test whether ZEB1-NPs reduce plaque development, *Zeb1*$^{\Delta Mac}$/*ApoE*-KO and *Zeb1*^{WT}/*ApoE*-KO mice fed on Western diet were injected twice a week with Stuffer-NPs or ZEB1-NPs for 10 weeks. ZEB1-NPs injected mice showed reduced plaque area assessed by "*en face"* ORO staining of aorta compared to Stuffer-NPs treated mice (Figure 22C).

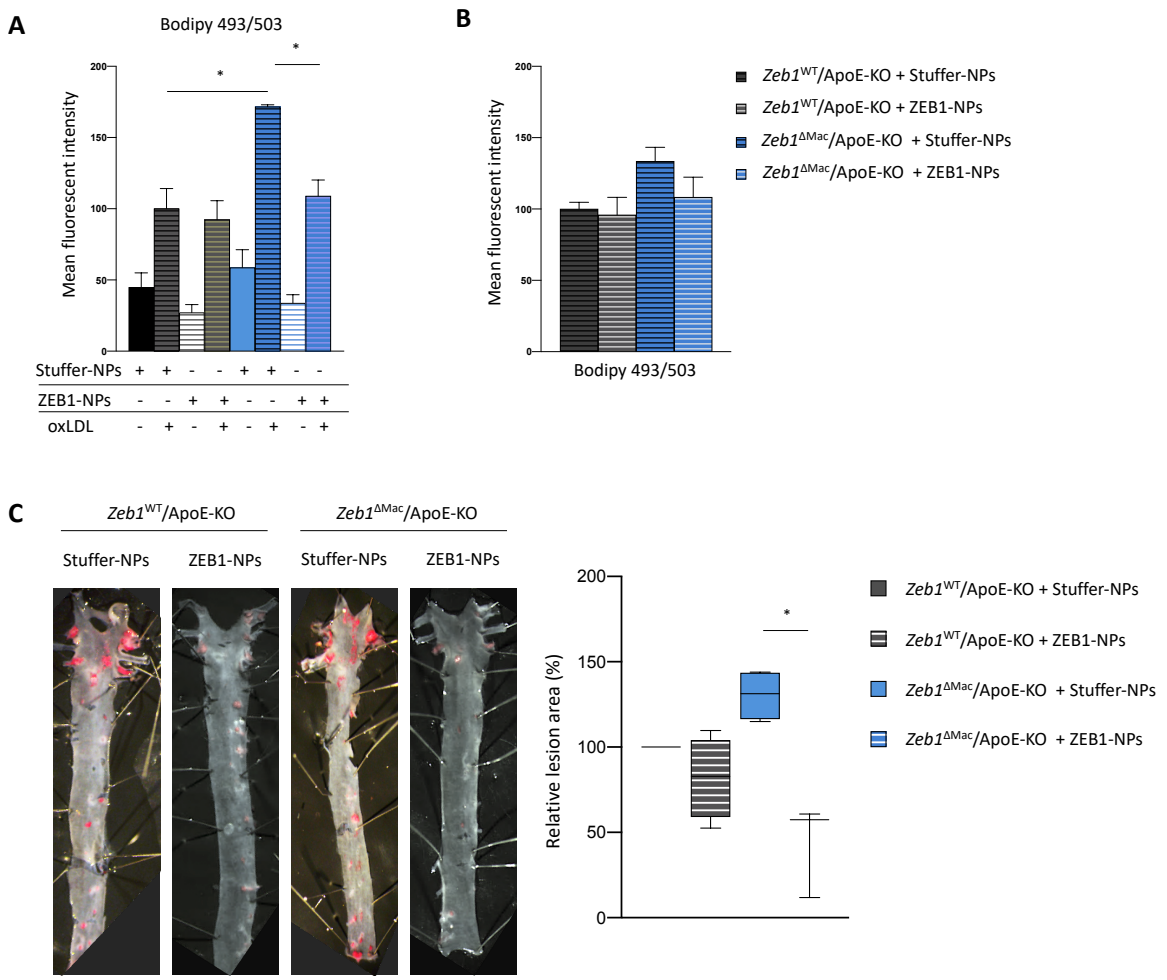

Figure 22. Restore of ZEB1 in *Zeb1*$^{\Delta Mac}$ macrophages decreases lipid accumulation under ox-LDL stimulation and plaque development compared with *Zeb1*$^{\Delta Mac}$ mice treated with stuffer vector. (A) Quantification of lipid content stained with Bodipy 493/503 in *Zeb1*^{WT} and *Zeb1*$^{\Delta Mac}$ peritoneal macrophages treated with 100 ng/mL of stuffer or ZEB1 NPs and untreated or treated for 24h with 50 µg/mL of ox-LDL (n=4). (B) Quantification of mean fluorescent intensity of Bodipy 493/503 in *Zeb1*^{WT}/ApoE-KO and *Zeb1*$^{\Delta Mac}$/ApoE-KO peritoneal macrophages from mice fed on Western diet for 10 weeks and treated with of stuffer-NPs or ZEB1-NPs twice a week (n=4). (C) Representative images of "*en face*" ORO staining of aorta and quantification of lesion area of *Zeb1*^{WT}/ApoE-KO and *Zeb1*$^{\Delta Mac}$/ApoE-KO mice 10 weeks fed in Western diet and treated with 50 µg/kg of stuffer-NPs or ZEB1-NPs twice a week (n=3-4).

Regulation of the influx/efflux of lipids by ZEB1

To assess the molecular mechanisms implicated in the higher lipid accumulation and foam cell formation in *Zeb1*$^{\Delta Mac}$ macrophages, we analyzed whether ZEB1 regulates the uptake of ox-LDL or the efflux of cholesterol.

ox-LDL promotes the transformation of macrophages to foam cells. ox-LDL uptake is taken up by several scavenger receptors and through micropinocytosis and phagocytosis (Tabas and Bornfeldt, 2016). ox-LDL was bound to Atto-655 to trace ox-LDL uptake. FACS analysis showed no significant differences in the uptake of Atto655-oxLDL by *Zeb1*$^{\Delta Mac}$ compared to *Zeb1*^{WT} macrophages (Figure 23).

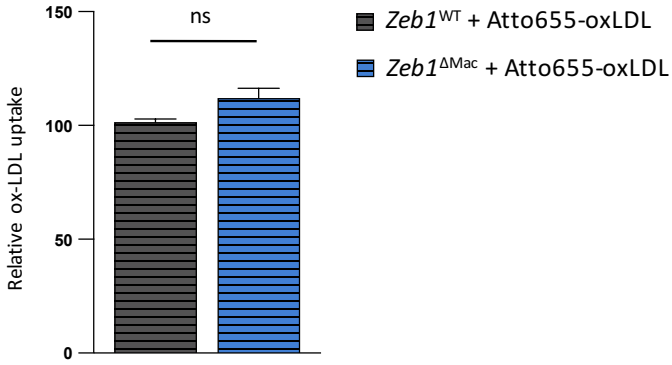

Figure 23. ZEB1 not is implicated in ox-LDL uptake in *in vitro* peritoneal macrophages. *Zeb1*^{WT} and *Zeb1*$^{\Delta Mac}$ peritoneal macrophages were stimulated with 50µg/mL of ox-LDL bound to Atto-655 for 2h and analyzed by flow cytometry (n=6).

Deficient cholesterol efflux by macrophages promotes foam cell formation and atherosclerosis development (Poznyak et al., 2020). ABCA1 and ABCG1 are the most relevant transporters implicated in cholesterol efflux. We hypothesize that lower levels of *Abca1* and *Abcg1* in *Zeb1*$^{\Delta Mac}$ macrophages produce a decrease in efflux associated with the increase in lipid content that we observed. We used ^{3}H-labeled cholesterol and examined its efflux in *Zeb1*^{WT} and *Zeb1*$^{\Delta Mac}$ macrophages. Consistent with changes in mRNA levels, *Zeb1*$^{\Delta Mac}$ macrophages displayed decreased cholesterol efflux to ApoA1 or HDL compared to control macrophages (Figure 24). Altogether, these results suggest that increased foam cell and atherosclerotic plaque formation involves increased lipid accumulation through, at least in part, reduced efflux of cholesterol.

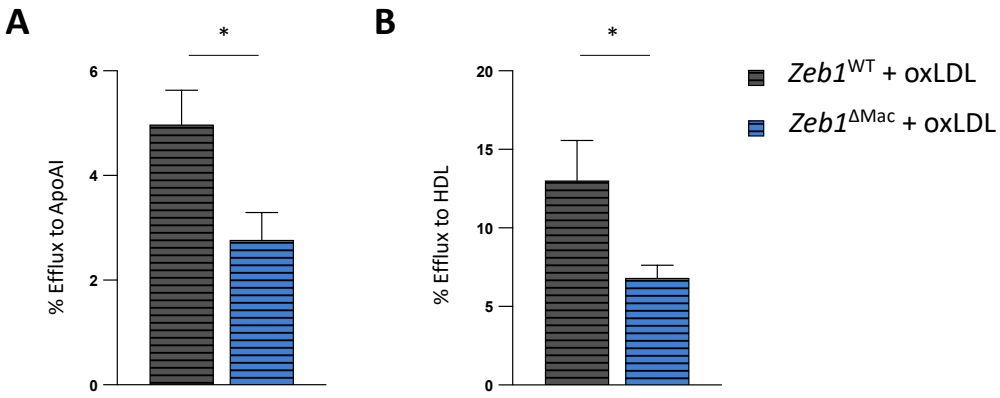

Figure 24. Deletion of ZEB1 promotes foam cell formation by impairing cholesterol efflux. Cholesterol efflux to (A) ApoA1 and (B) HDL in *Zeb1*^{WT} and *Zeb1*$^{\Delta Mac}$ peritoneal macrophages preloaded with ^{3}H-cholesterol and 50µg/mL of ox-LDL (n=6).

ZEB1 reduces foam cell formation through activation of the AMPK-LXRα-ABCA1/G1 axis

To investigate the mechanism by which ZEB1 regulates cholesterol traffic, we examined several genes upstream of ABCA1 and ABCG1. We found that *Prkaa1*, *Nr1h2*, *Srebf1* and *Ppargc1a* expression was lower in oxLDL-stimulated macrophages from *Zeb1*$^{\Delta Mac}$ mice than in *Zeb1*^{WT} counterparts (Figure 25A).

The activation of AMPK in murine BMDM increases cholesterol efflux by inducing LXRα, ABCG1 and ABCA1 expression (Fullerton et al., 2015). We used A-769662, an AMPK activator, to investigate whether the increased cell foam formation in *Zeb1*$^{\Delta Mac}$ macrophages was due to a deficient activation of the AMPK-LXRα-ABCA1/G1 pathway. Indeed, we found that treatment of *Zeb1*$^{\Delta Mac}$ macrophages with A-769662 restored lipid cell content to control levels (Figure 25B).

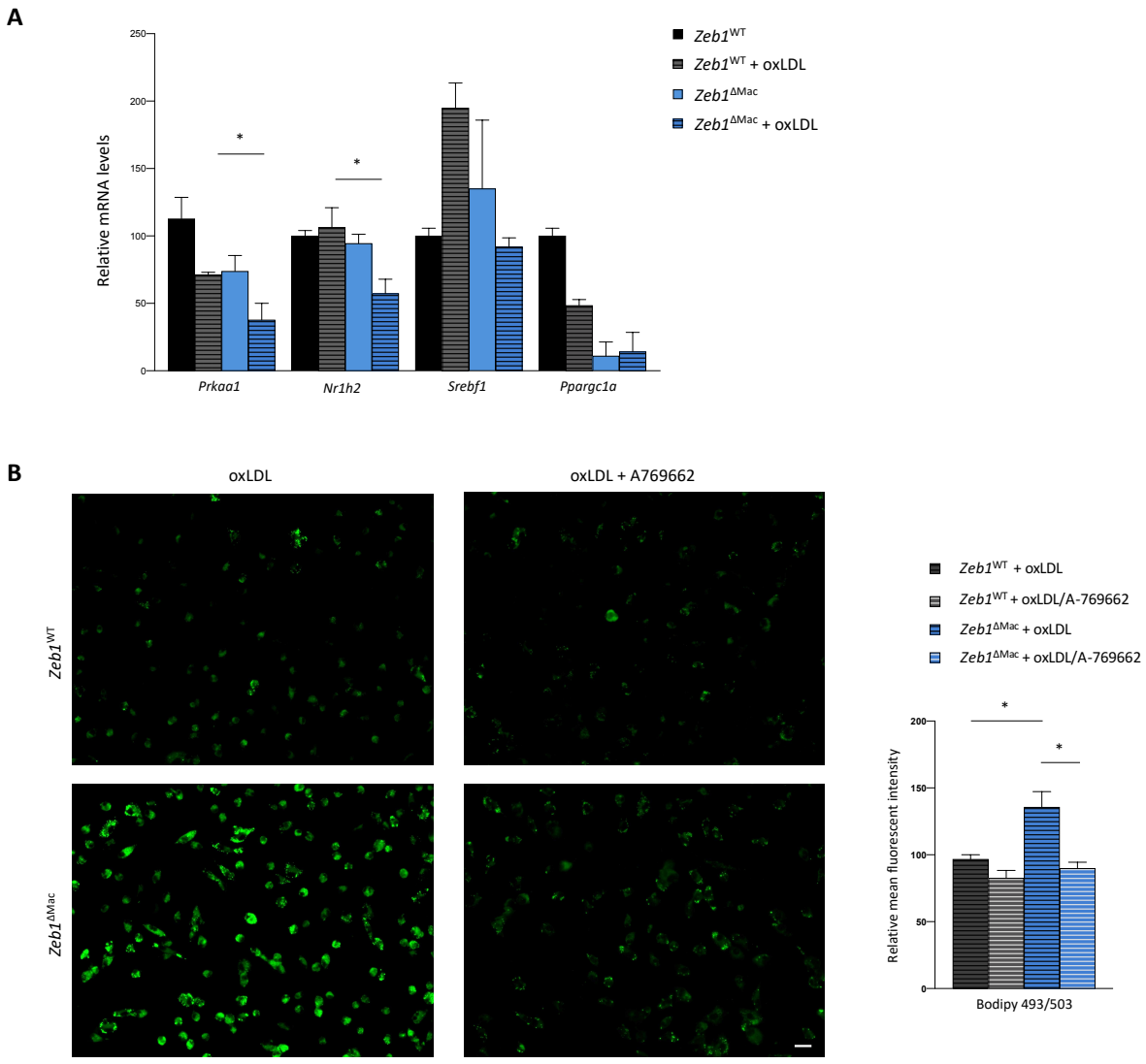

Figure 25. *Zeb1*$^{\Delta Mac}$ macrophages present higher foam cell formation by impairing *Ampk* activation. (A) mRNA levels of *Prkaa1*, *Lxr*, *Srebf1* and *Ppargc1a* in *Zeb1*^{WT} and *Zeb1*$^{\Delta Mac}$ peritoneal macrophages (n=4). (B) Representative images and quantification of *Zeb1*^{WT} and *Zeb1*$^{\Delta Mac}$ peritoneal macrophages treated with 100µM A-769662 and/or 50µg/mL of ox-LDL stained with Bodipy 493/503 (n=4).

ZEB1 in macrophages protects from apoptosis and production of reactive oxygen species

Oxidized lipids trigger the production of ROS by macrophages contributing to apoptosis and subsequent plaque development (Madamanchi et al., 2005). Apoptosis and ROS production in ox-LDL activated peritoneal macrophages were analyzed by staining with annexin V and DFHCE, respectively. *Zeb1*$^{\Delta Mac}$ macrophages displayed an increased number of apoptotic cells (Figure 25A) and ROS production (Figure 25B) compared to *Zeb1*^{WT} peritoneal counterparts.

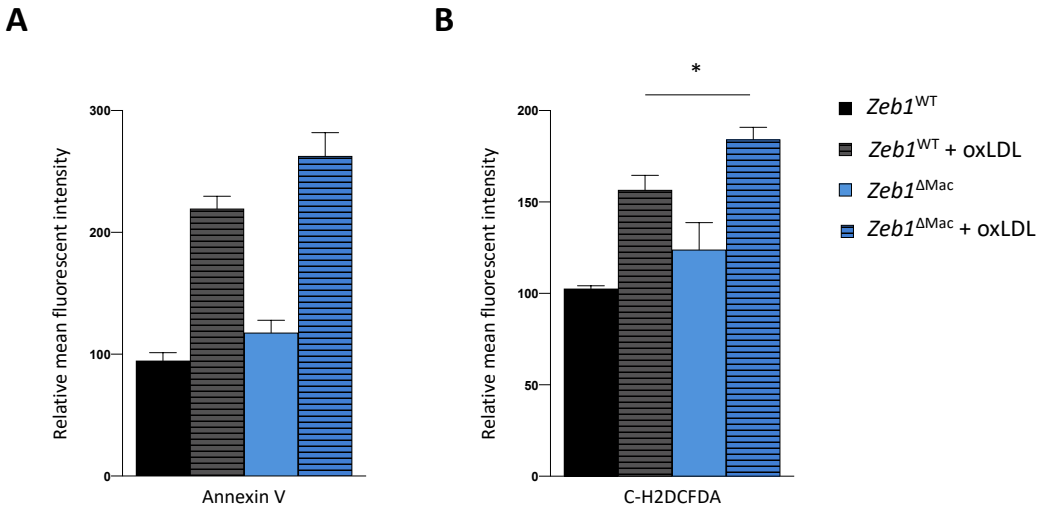

Figure 26. **ZEB1 protects from apoptosis and ROS overproduction.** *Zeb1*^{WT} and *Zeb1*$^{\Delta Mac}$ peritoneal macrophages were untreated or treated with 50µg/mL of ox-LDL for 24h and (A) apoptosis was assessed by annexin V staining or (B) ROS were quantified by staining with H2-DCFDA. Mean fluorescence intensity was evaluated by FACS (n=4).

ZEB1 is required for oxLDL-induced activation of macrophages

Modified lipoproteins activate endothelial and immune cells in the aorta and promote the secretion of chemokines and cytokines. These secreted factors trigger the recruitment of monocytes and their activation toward macrophages involving the activation of several signaling pathways, including p38-MAPK, JNK, and NFkB cascades (Poznyak et al., 2020). We tested whether ZEB1 was implicated in macrophage activation in response to ox-LDL and evaluated different signaling pathways involved. ox-LDL induces p38-MAPK, JNK, and P65 signaling pathways in peritoneal macrophages from *Zeb1*^{WT}, but the activation by ox-LDL of all these pathways is impaired in *Zeb1*$^{\Delta Mac}$ macrophage (Figure 27A), indicating that ZEB1 is required to ox-LDL activation macrophage.

Next, we evaluated the expression of selected inflammatory factors (e.g., *Tnf, Il6*) that are downstream of oxLDL macrophage activation (Luo et al., 2017) by real-time PCR. *Tnf* and *Il6*, were failed to upregulate in *Zeb1*$^{\Delta Mac}$ macrophages in response to ox-LDL (Figure 27B).

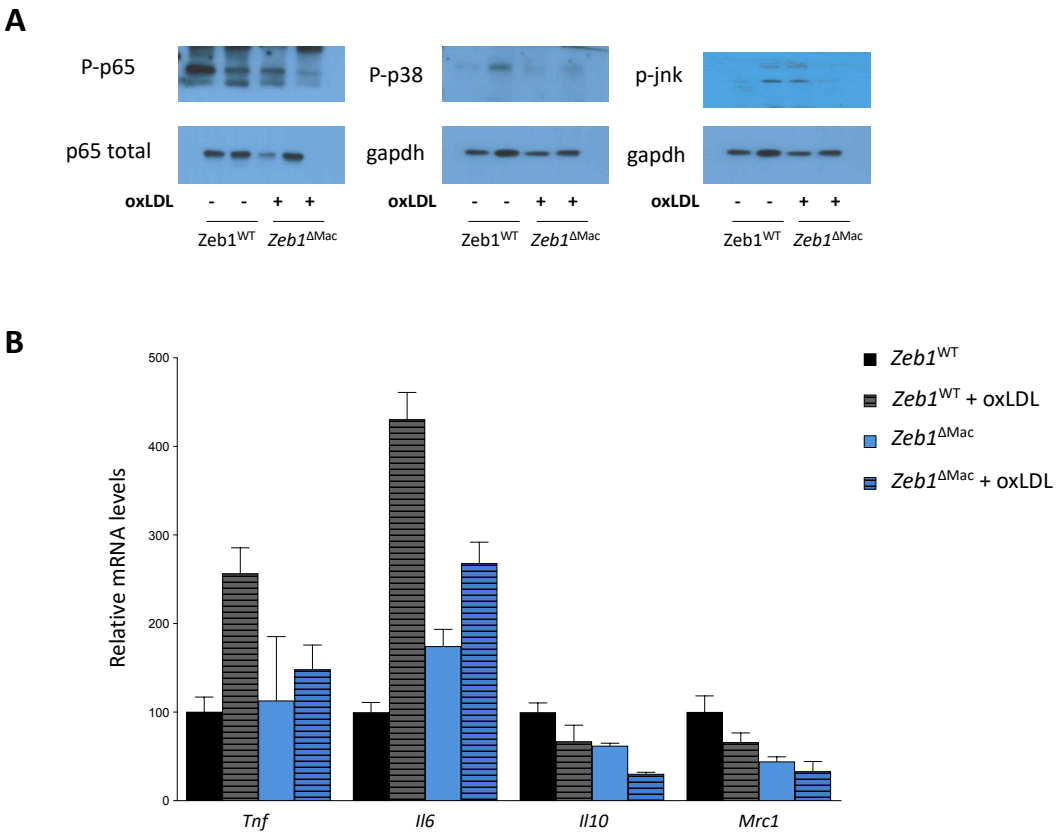

Figure 27. ZEB1 is required for the pro-inflammatory activation of macrophages by oxLDL. (A) Lysates from *Zeb1*^{WT} and *Zeb1*$^{\Delta Mac}$ peritoneal macrophages either untreated or treated for 24h with 50µg/mL of oxLDL were immunoblotted for antibodies against p65, P-p65, P-p38, p-JNK and GAPDH (n=2). (B) mRNA levels of *Tnf*, I*l6*, *Il10* and *Mrc1* were determined by qRT-PCR in control and *Zeb1*$^{\Delta Mac}$ peritoneal macrophages untreated or treated at 24h with 50µg/mL of ox-LDL (n=3).

NF-kB signaling is involved in the activation of macrophages (Liu et al., 2017). To gain further insight into the mechanism responsible for ZEB1 on lipid content in macrophages, we examined whether p65 activation by phosphorylation (P-p65) is involved. To that effect, we used TPCA-1 (2-[(aminocarbonyl)amino]-5-(4-fluorophenyl)-3-thiophenecarboxamide), an IKK inhibitor blocking p65 phosphorylation (Coish et al., 2006), *Zeb1*^{WT} and *Zeb1*$^{\Delta Mac}$ macrophages were treated with TPCA-1 either alone or in combination with ox-LDL. The effectiveness of TPCA-1 was assessed as the downregulation of *Tnf*—itself a target of p65—by real-time PCR. We found that inhibition of P-p65 downregulated *Abca1* and *Abcg1* expression in wild-type macrophages treated with ox-LDL, although levels in *Zeb1*$^{\Delta Mac}$ macrophages did not change (Figure 28).

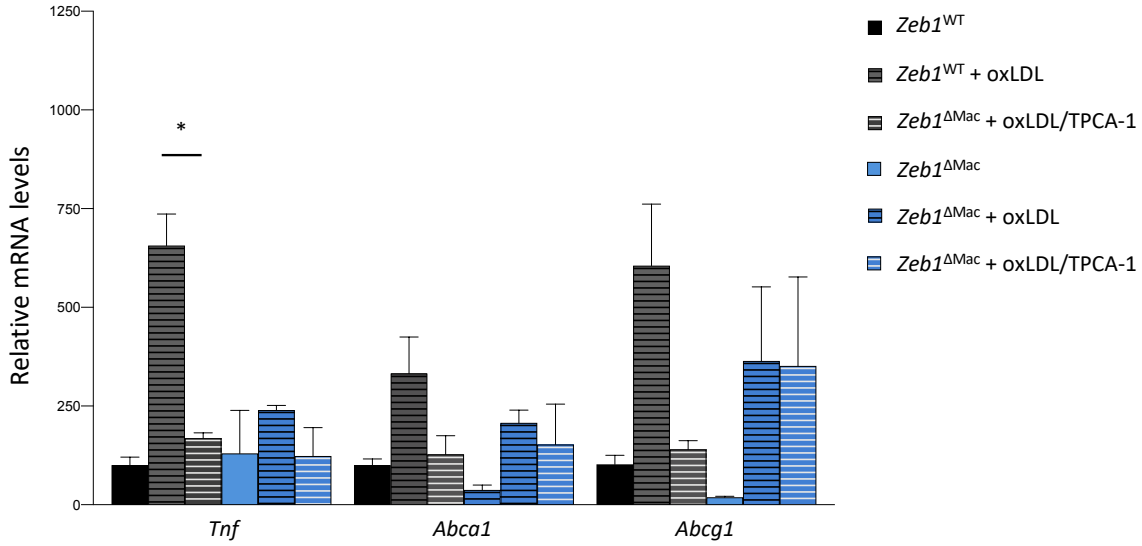

Figure 28. p65 is required for cholesterol transporter overexpression in macrophages ox-LDL response. mRNA levels of *Tnf*, *Abca1* and *Abcg1* were determined by qRT-PCR in *Zeb1*^{WT} and *Zeb1*$^{\Delta Mac}$ peritoneal macrophages either untreated or pre-treated 30 min with TPCA-1 and/or treated 24h with 50µg/mL ox-LDL (n=3).

To investigate whether the downregulation of transporters with TPCA-1 treatment is implicated in lipid content we stained macrophages for Bodipy 493/503. The results showed that TPCA-1 treatment in combination with ox-LDL increased lipid accumulation in *Zeb1*^{WT} macrophages, but no changes were observed in *Zeb1*$^{\Delta Mac}$ macrophages (Figure 29). These results indicate that *Zeb1*$^{\Delta Mac}$ macrophages have higher lipid content, at least in part, by a deficient activation of the p65 pathway.

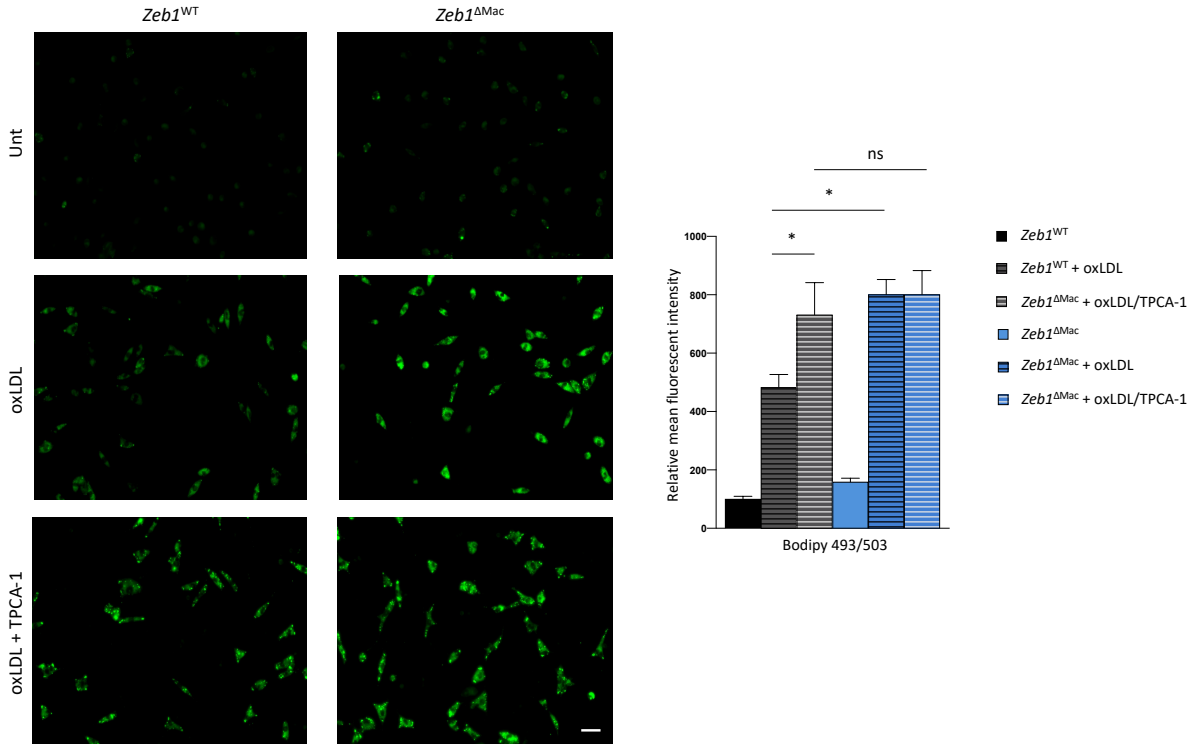

Figure 29. Impair activation of p65 promotes foam cell formation. Representative images (Left) and mean fluorescence intensity quantification (Right) of *Zeb1*^{WT} and *Zeb1*$^{\Delta Mac}$ peritoneal macrophages were untreated, pre-treated 30 min with 1µM TPCA-1 and/or treated at 24h with 50µg/mL of ox-LDL and stained with Bodipy 493/503. Scale bar represents 20 µm.

Chapter II: ZEB factors in tumor-associated macrophages during tumor progression

ZEB factors expression in tumor-associated macrophages and tumor cells

To investigate the role of ZEB factors in the immune response against tumor cells we used the ID8 model of ovarian cancer (Lawrence et al, 2020; Song et al, 2020). TAMs isolated from wild-type mice in which the ID8 cells had been implanted in the peritoneum for 8-14 weeks were compared to peritoneal macrophages isolated from wild-type mice that were not subjected to the protocol. Results showed that *Zeb1* mRNA expression is a significant decrease in TAMs of mice injected 8 weeks or 14 weeks compared to peritoneal macrophages isolated from untreated mice, but *Zeb2* mRNA expression did not show changes in tumor-bearing mice for 8-14 weeks compared to untreated mice not harboring tumor cells (Figure 30A). On the other hand, ID8 cells isolated from wild-type mice showed higher expression of both *Zeb1* and *Zeb2* (Figure 30B).

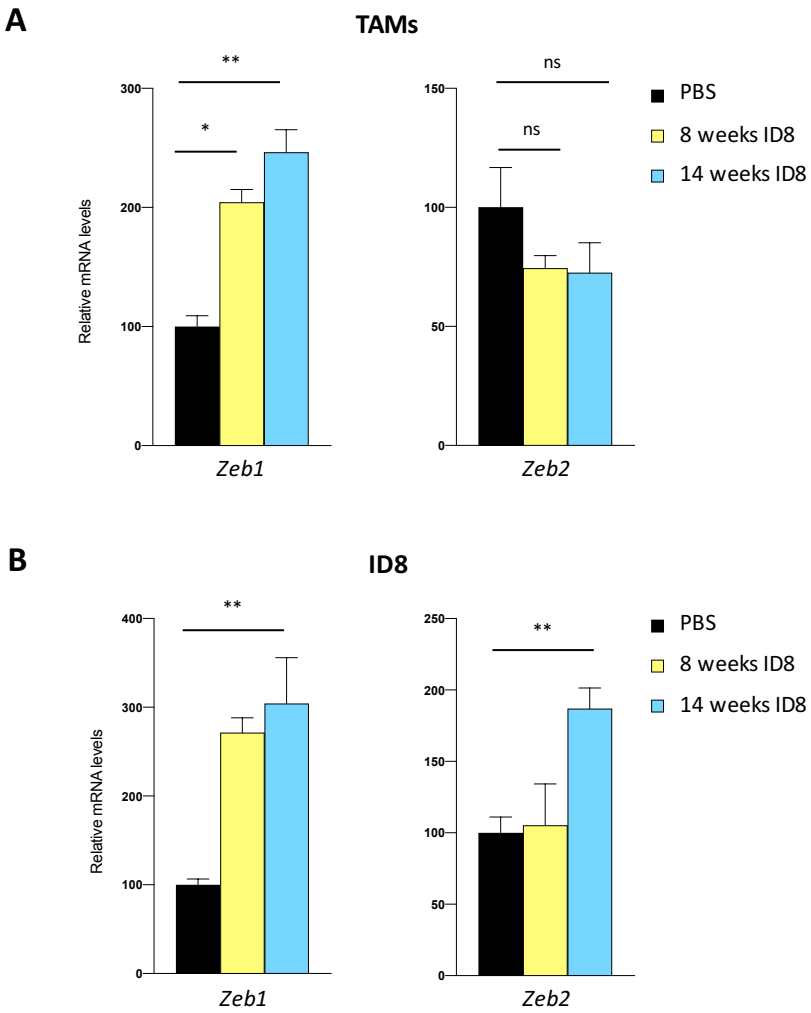

Figure 30. Characterization of *Zeb1* and *Zeb2* expression in TAMs and ID8 cells. (A) ID8 cells or PBS were injected in wild-type mice for 8 or 14 weeks and mRNA levels for *Zeb1* and *Zeb2* were determined by qRT-PCR in (A) TAMs and (B) ID8 cells, using as housekeeping gene *Gapdh* (n=6).

Zeb1 expression in macrophages promotes tumor growth while Zeb2 inhibits it

Tumor growth was followed by bioluminescence imaging in mice injected with ID8-Luc cells for 6 weeks. Results showed lower tumor deposits in *Zeb1*$^{\Delta Mac}$ than in *Zeb1*^{WT}, while *Zeb2*$^{\Delta Mac}$ mice showed higher deposits than *Zeb2*^{WT} mice (Figure 31).

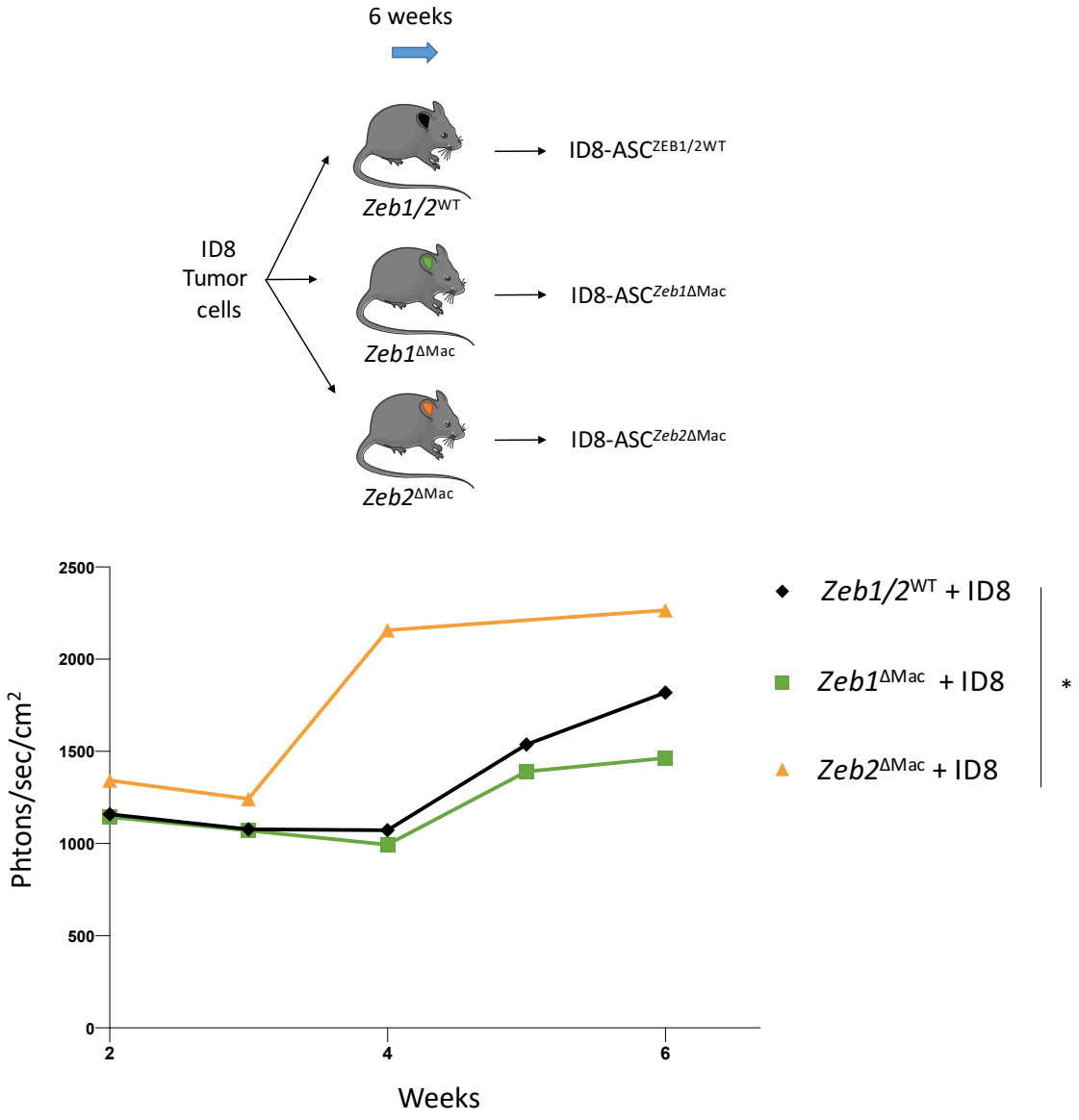

Figure 31. ZEB1 in TAMs promotes ovarian tumor progression and ZEB2 inhibits it. *Zeb1*^{WT}, *Zeb1*$^{\Delta Mac}$, *Zeb2*^{WT} and *Zeb2*$^{\Delta Mac}$ mice were injected with ID8 cells and tumor progression was follow by bioluminescence for 6 weeks (n=4).

ID8 cells were injected during 9 weeks in *Zeb1*^{WT}, *Zeb1*$^{\Delta Mac}$, *Zeb2*^{WT} and *Zeb2*$^{\Delta Mac}$ mice, then we isolated, sorted and ID8-ASC from the different genotypes were reinoculated in wild-type mice and mice survival was monitored over time. Compared to the evolution of mice injected with parental ID8 cells, whose survival usually stands around 12-14 weeks, the survival was reduced to only 3-6 weeks when mice with ID8-ASC. Notably, the survival rate significantly increased in mice injected with ID8RI-ASC$^{Zeb1\Delta Mac}$ compared to control counterparts, however, mice injected with ID8RI-ASC$^{Zeb2\Delta Mac}$ exhibited lower survival than mice injected with ID8RI-ASC^{Zeb2WT} (Figure 32).

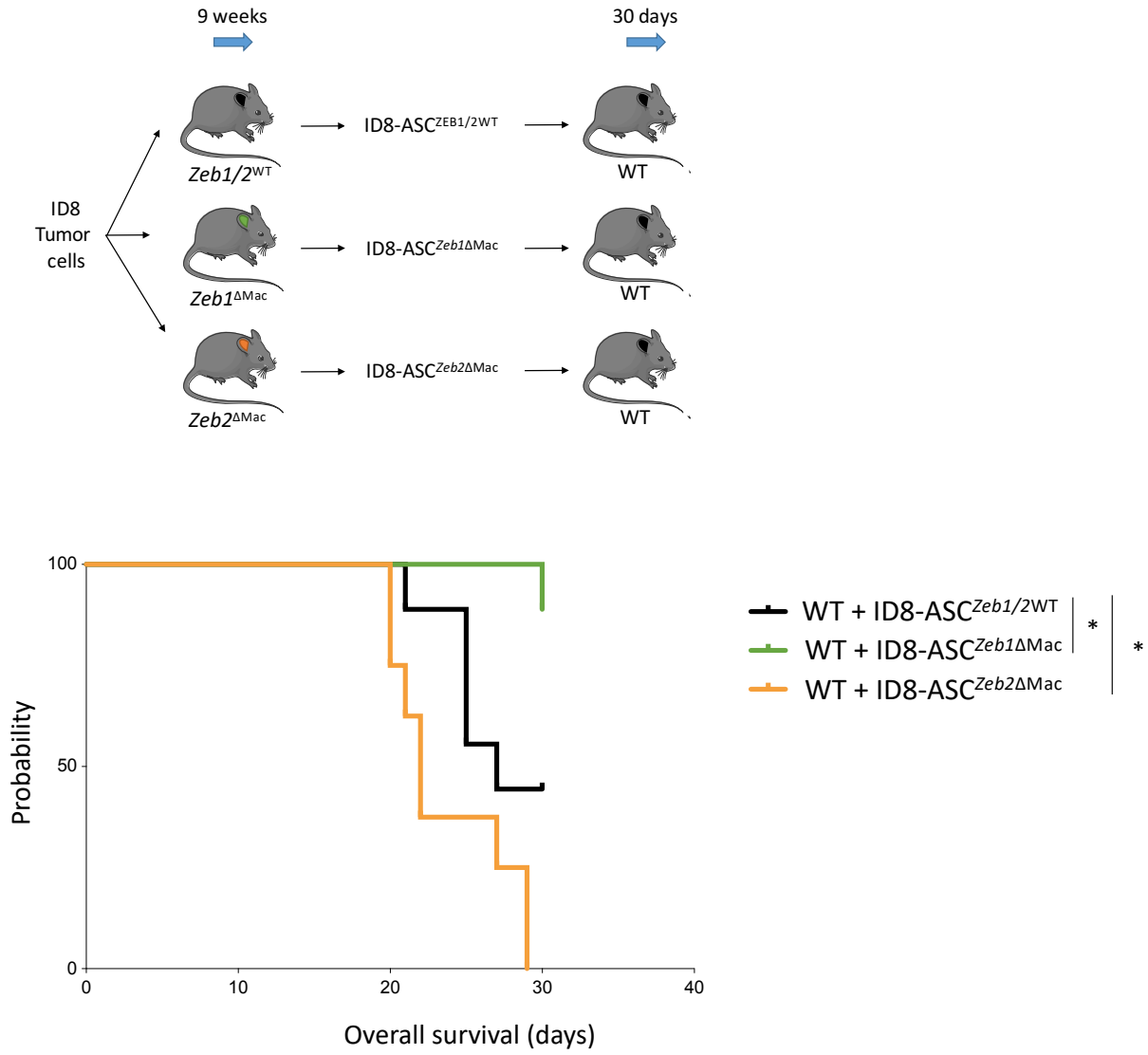

Figure 32. ID8 cells acquire higher tumorigenic potential when they are in contact with *Zeb2*$^{\Delta Mac}$ TAMs but lower when with *Zeb1*$^{\Delta Mac}$ TAMs. *Zeb1*^{WT}, *Zeb1*$^{\Delta Mac}$, *Zeb2*^{WT} and *Zeb2*$^{\Delta Mac}$ mice were injected with ID8 cells and, after 9 weeks ID8 cells were isolated from the different genotypes and inject into new wild-type recipients and their survival was monitored. Kaplan-Meyer plot shows the overall survival of wild-type mice injected with ID8-ASC^{Zeb2WT}, ID8-ASC$^{Zeb1\Delta Mac}$ ID8-ASC^{Zeb2WT}, or ID8-ASC$^{Zeb2\Delta Mac}$ (n=8).

ZEB1 promotes TAM infiltration and ID8 tumor progression, while ZEB2 inhibit them

Abundant evidence generally links immune cell infiltration in tumor stroma with tumor progression, metastasis and treatment resistance (DeNardo et al., 2019). TAMs are implicated in tumor immune evasion directly and indirectly. To analyze whether *Zeb1* and *Zeb2* ablation

in macrophages can be implicated in the infiltration of immune cells in the peritoneum we injected ID8 cells in mice. After 5 weeks, we examined the number of peritoneal TAMs and ID8 cells. We observed that TAMs infiltration and tumor load were lower in *Zeb1*$^{\Delta Mac}$, while *Zeb2*$^{\Delta Mac}$ showed higher content in both cell types compared to control mice (Figure 33A and B). Percentage of cells from *Zeb1*^{WT}, *Zeb1*$^{\Delta Mac}$, *Zeb1*^{WT} and *Zeb2*$^{\Delta Mac}$ tumor-bearing mice were analyzed by flow cytometry. CD206+ TAMs, a marker of a pro-tumoral macrophage phenotype, were lower in *Zeb1*$^{\Delta Mac}$, but no differences were observed in *Zeb2*$^{\Delta Mac}$, than control mice (Figure 33C). A pro-tumoral TAMs phenotype in macrophages is associated with immunosuppression of tumor-infiltrating lymphocytes (TILs) responses and cancer cells have developed mechanisms to reduce TILs infiltration. A higher number of TILs were found in *Zeb1*$^{\Delta Mac}$ and lower in *Zeb2*$^{\Delta Mac}$ mice compared to control mice (Figure 33D).

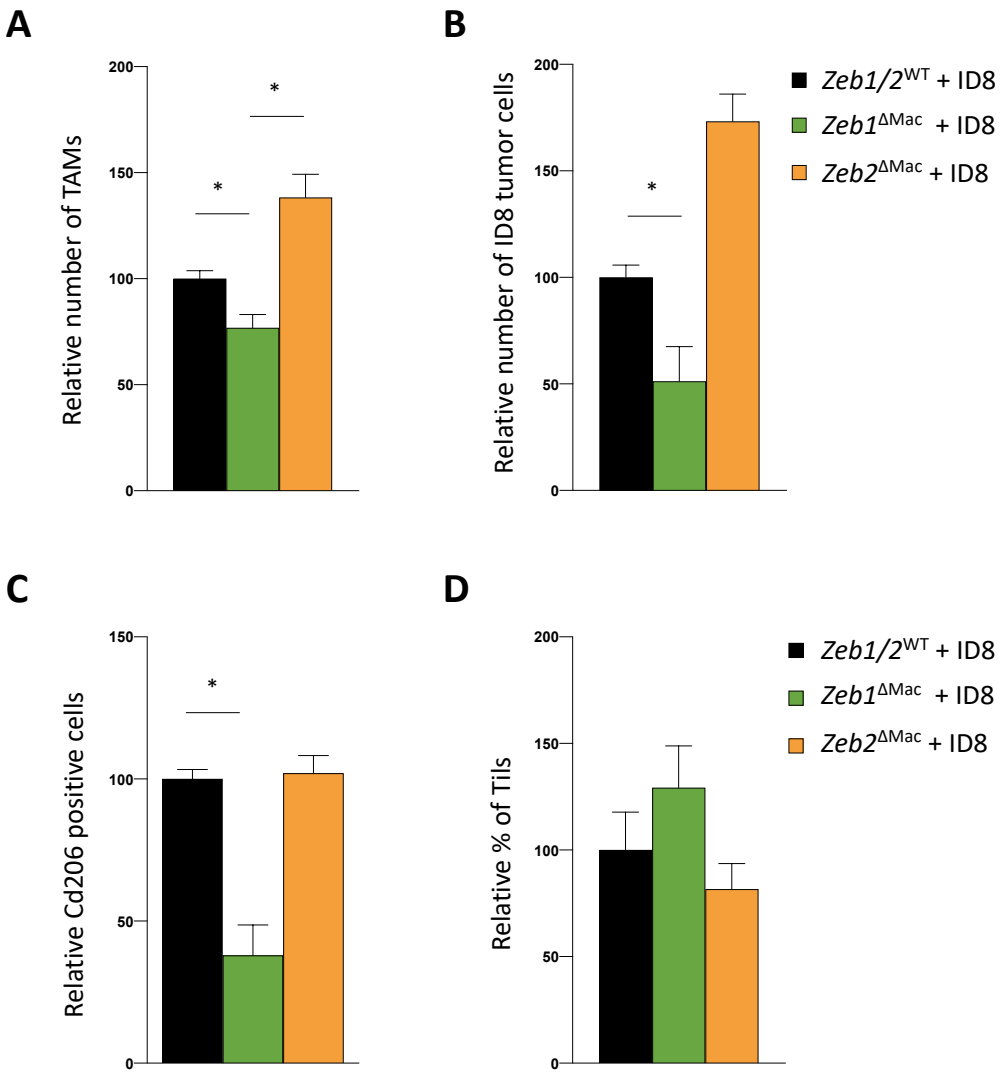

Figure 33. ZEB1 promotes TAM infiltration and ID8 tumor progression, while ZEB2 inhibits it. *Zeb1*^{WT}, *Zeb1*$^{\Delta Mac}$, *Zeb2*^{WT} and *Zeb2*$^{\Delta Mac}$ mice were injected with ID8 cells for 5 weeks, then, peritoneal cells were isolated and (A) ID8 (n=3-4) and (B) TAMs (n=6) cell number were analyzed. Peritoneal exudates were also analyzed by flow cytometry to (C) CD206 positive TAMs and (D) proportion of TILs (n=3).

ZEB1 decreases macrophage phagocytosis of cancer cells

Macrophages are specialized cells that phagocyte foreign agents, apoptotic cells, debris and tumor cells (Gordon et al., 2017; Murray and Wynn, 2011). However, cancer cells develop mechanisms to evade clearance by macrophages. We studied whether tumor progression differences observed in *Zeb1*$^{\Delta Mac}$ and *Zeb2*$^{\Delta Mac}$ mice were mediated in part by changes in the phagocytic capacity. ID8 stained with Dil dye (1,1'-Dioctadecyl-3,3,3',3'-Tetramethylindocarbocyanine Perchlorate ('DiI'; DiIC18(3))) cells were cocultured with the dye 5(6)-carboxyfluorescein N-hydroxysuccinimidyl ester (CFSE)-stained macrophages from *Zeb1*^{WT}, *Zeb1*$^{\Delta Mac}$, *Zeb2*^{WT} or *Zeb2*$^{\Delta Mac}$ mice. After 12 hours, macrophages were plated and the DiI-fluorescence was quantified in CSFE-positive cells. Results showed that macrophages from *Zeb1*$^{\Delta Mac}$ mice have higher phagocytic capacity than *Zeb1*^{WT} and *Zeb2*$^{\Delta Mac}$ macrophages (Figure 34).

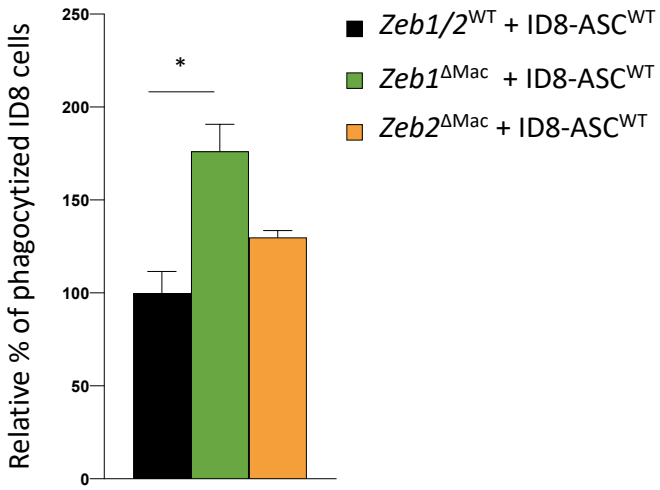

Figure 34. ZEB1 in TAMs inhibits ID8 cell phagocytosis and ZEB2 promotes it. Macrophages from *Zeb1*^{WT}, *Zeb1*$^{\Delta Mac}$, *Zeb2*^{WT} and *Zeb2*$^{\Delta Mac}$ mice were isolated stained with CSFE and cocultured with ID8 cells stained with Dil dye. Phagocytosis of ID8 cells was quantified as CSFE-positive macrophages that were also Dil-positive (n=4).

The expression of PD-1 on TAMs impairs phagocytosis and anti-tumor response (Gordon et al., 2017). Cells from ID8-inoculated *Zeb1*^{WT}, *Zeb1*$^{\Delta Mac}$, *Zeb2*^{WT} and *Zeb2*$^{\Delta Mac}$ mice were isolated from peritoneum at 9 weeks and stained with F4/80, CD45, PD-1 and PD-L1 antibodies to FACS analysis. Analysis of PD-1 expression showed a lower number of positive TAMs in peritoneal cells from *Zeb1*$^{\Delta Mac}$ and higher positive TAMs in *Zeb2*$^{\Delta Mac}$ than in wild-type counterparts (Figure 35A). Likewise, PD-L1 expression in cancer stem cells supports immune evasion (Chen et al., 2014). PD-L1 quantification in CD45^{neg} cells showed a higher number of positive ID8 tumor cells in *Zeb2*$^{\Delta Mac}$ compared to *Zeb2*^{WT} and *Zeb1*$^{\Delta Mac}$ mice (Figure 35B).

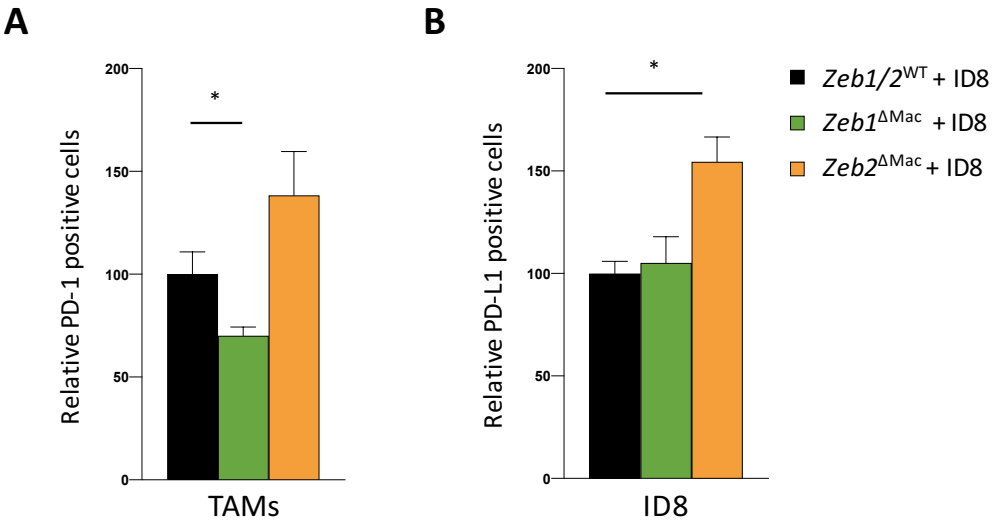

Figure 35. PD-1 is upregulated in *Zeb2*$^{\Delta Mac}$ TAMs that induce PD-L1 in ID8 cells but downregulated in *Zeb1*$^{\Delta Mac}$ TAMs. Peritoneal cells were isolated from tumor-bearing *Zeb1*^{WT}, *Zeb1*$^{\Delta Mac}$, *Zeb2*^{WT} and *Zeb2*$^{\Delta Mac}$ mice and stained with F4/80, CD45, PD-1 and PD-L1 and positive cells were assessed by FACS (n=4).

ZEB factors are regulated tumor spheroid formation

Spheroids in ascites of ovarian cancer patients are key in the dissemination of tumor cells (Al Habyan et al., 2018). We isolated peritoneal cells from *Zeb1*^{WT}, *Zeb1*$^{\Delta Mac}$, *Zeb2*^{WT} and *Zeb2*$^{\Delta Mac}$ mice that were injected for 9 weeks. Cells were plated onto low-attachment dishes and the formation and size of spheroids were analyzed after 24 h. We found a reduced number of spheroids in the ascites of tumor-bearing *Zeb1*$^{\Delta Mac}$ compared to that in tumor-bearing control mice, while the size of spheroids from *Zeb2*$^{\Delta Mac}$ displayed minor differences in their size vis-à-vis control mice however not significative at 9 weeks, but we can not rule out better differences in shorter or longer times of tumor development.

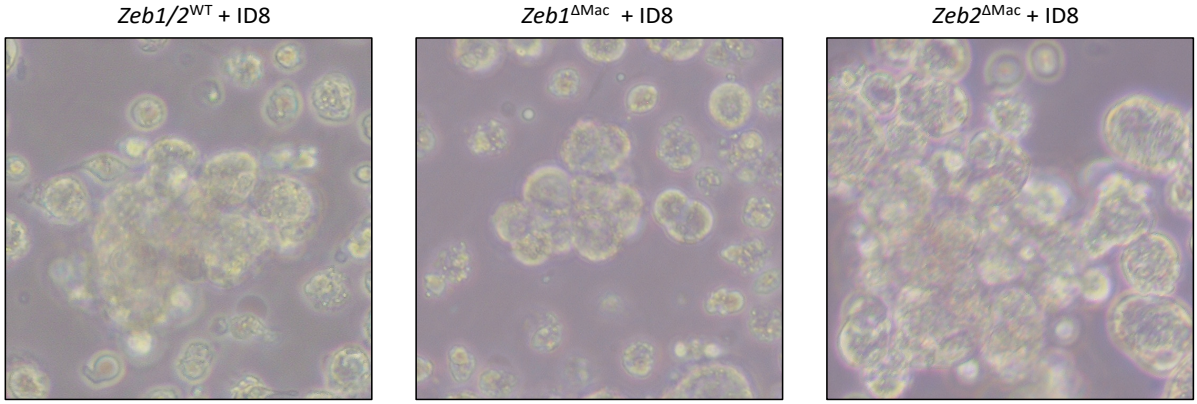

Figure 36. ZEB1 in TAMs promotes spheroid formation. Representative images of heterotypic spheroid formation from ascites cells of *Zeb1*^{WT}, *Zeb1*$^{\Delta Mac}$, *Zeb2*^{WT} and *Zeb2*$^{\Delta Mac}$ mice (n=4).

ZEB1 expression in TAMs drives a CSC signature in ovarian cancer cells and ZEB2 inhibits it

The presence of TAMs in spheroids promotes the formation and acquisition of CSC characteristics by ID8 cells. We measured cell-surface CSC markers by flow cytometry including CD54, CD55 and CD117. ID8ASC$^{Zeb1\Delta Mac}$ showed decreased expression of CD117 and CD55 compared to ID8AS^{WT}. However, the expression of CD117 and CD55 was increased in ID8ASC$^{Zeb2\Delta Mac}$ compared to ID8ASC^{Zeb2WT} (Figure 37A and B). Spheroid formation is promoted by interactions between TAMs and ID8 cells. EGF secretion by TAMs induces expression of CD11b on TAMs and CD54 on tumor cells (Yin et al, 2016). We studied expression of CD54 in ID8 cancer cells and CD11a in TAMs, an integrin that interacts with CD54. Results did not reveal any difference in CD11a expression in *Zeb1*$^{\Delta Mac}$ TAMs with respect to TAMs in *Zeb1*^{WT} mice, but expression was higher in *Zeb2*$^{\Delta Mac}$ TAMs compared to *Zeb2*^{WT} TAMs analyzed by FACS (Figure 37C). On the other hand, CD54 expression in ID8 cells was lower in *Zeb1*$^{\Delta Mac}$ and in *Zeb2*$^{\Delta Mac}$ compared to ID8 from *Zeb1*^{WT} or *Zeb2*^{WT} mice (Figure 37D).

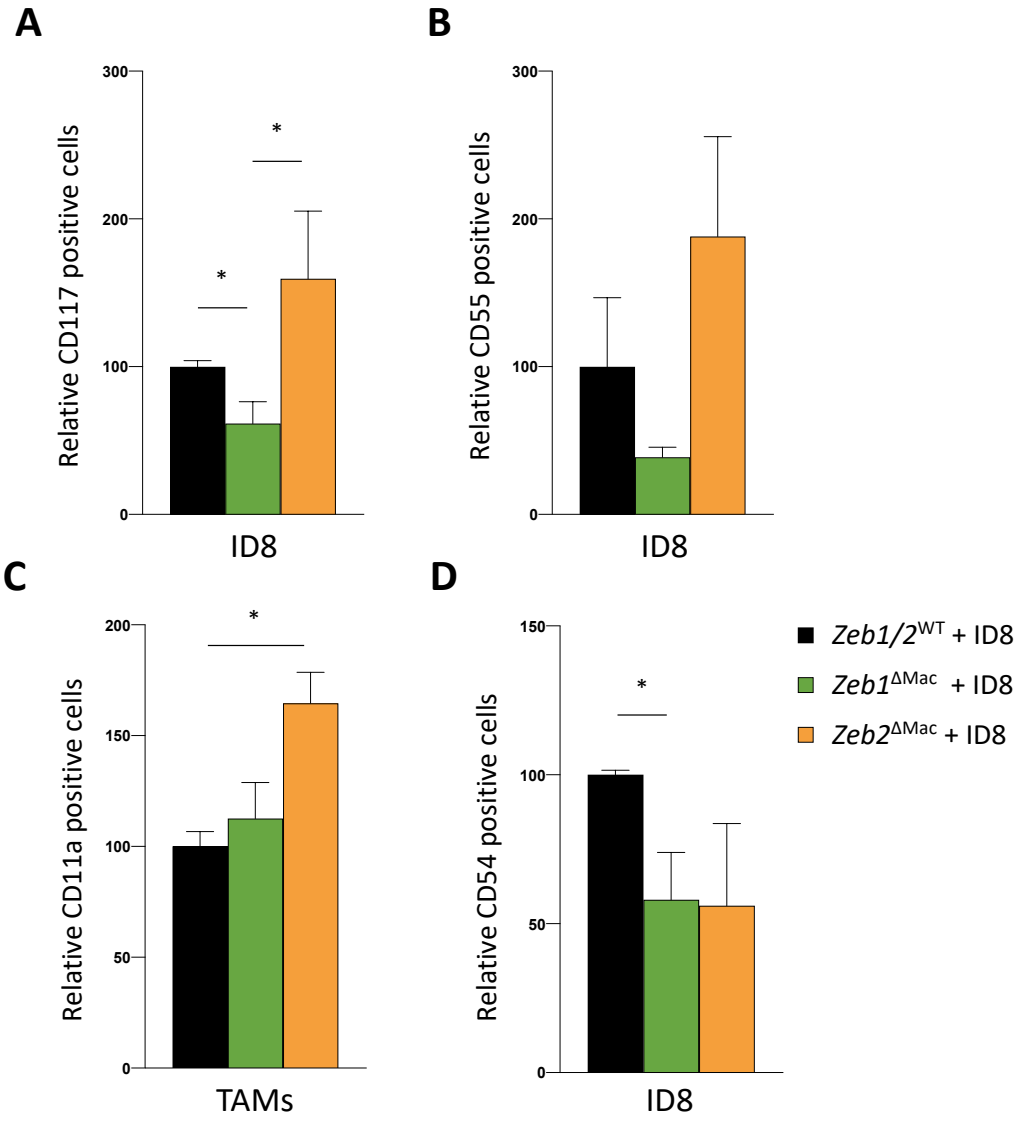

Figure 37. ZEB1 in TAMs increases stemness in ID8 cells and ZEB2 decreases it. ID8 cells were injected in *Zeb1*^{WT}, *Zeb1*$^{\Delta Mac}$, *Zeb2*^{WT} and *Zeb2*$^{\Delta Mac}$ mice, then peritoneal cells were isolated and assessed for (A) CD117, (B) CD55 or (C) CD54 in ID8 cells and for (C) CD11a in TAMs (n=3-4).

ZEB1 in TAMs inhibits ID8 cancer cells senescence

Tumor cells acquire a number of tumor-promoting capabilities during the neoplastic transformation. These include cell death resistance, growth suppressors evading or enabling replicative immortality. Thus, we studied whether ZEB1 or ZEB2 expression in TAMs modulates the cell viability of tumor cells. First, we wonder whether ID8-ASC cells from *Zeb1*^{WT}, *Zeb1*$^{\Delta Mac}$, *Zeb2*^{WT} and *Zeb2*$^{\Delta Mac}$ mice mice proliferated at different rates. The proliferation rate was evaluated by Click-iT Plus EdU stain and FACS analysis. Nevertheless,

we observed no differences in proliferation between ID8RI-ASC^{Zeb1WT} or ID8-ASC^{Zeb2WT} compared with ID8RI-ASC$^{Zeb1\Delta Mac}$ and ID8RI-ASC$^{Zeb2\Delta Mac}$ (Figure 38).

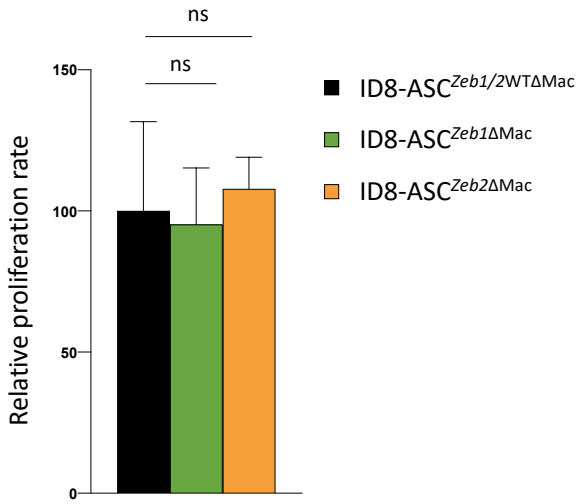

Figure 38. Proliferation rate of ID8 cells is not altered by *Zeb1*$^{\Delta Mac}$ or *Zeb2*$^{\Delta Mac}$ TAMs. ID8-ASC^{Zeb1WT}, ID8-ASC^{Zeb2WT}, ID8-ASC$^{Zeb1\Delta Mac}$ and ID8-ASC$^{Zeb2\Delta Mac}$ were cultured for EdU incorporation and, then, EdU was evaluated by FACS (n=3).

Next, senescence was evaluated by senescence-associated β-galactosidase staining. We observed that ID8 cells from *Zeb1*$^{\Delta Mac}$ presented a higher proportion of senescent cells than ID8 cells from *Zeb1*^{WT}, *Zeb2*^{WT} and *Zeb2*$^{\Delta Mac}$ mice, but no significant differences were observed between these groups (Figure 39).

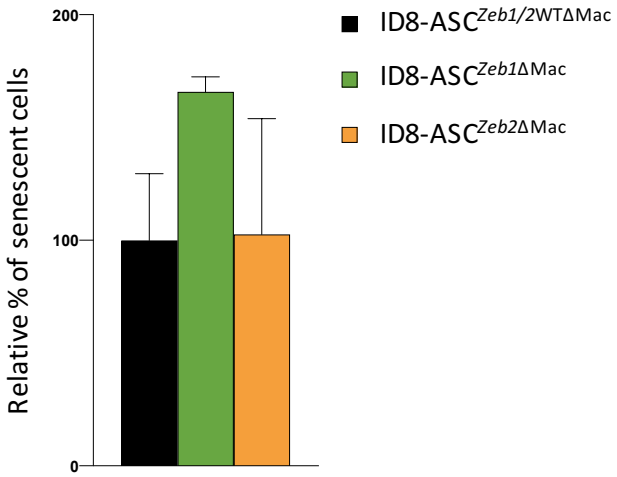

Figure 39. Expression of Zeb1 in TAMs protects ID8 cells from senescence. ID8-ASC^{Zeb1WT}, ID8-ASC^{Zeb2WT}, ID8-ASC$^{Zeb1\Delta Mac}$ and ID8-ASC$^{Zeb2\Delta Mac}$ from spheroids (n=3) were plated and stained for SA with β-gal.

Lastly, the levels of apoptosis were determined by Annexin V staining. Late-stage apoptotic cells and necrotic cells were excluded by staining with propidium iodide. ID8 cells from the

different genotypes were cultured to sphere formation and later disaggregated and stained to FACS analysis. Quantification of Annexin V-positive cells showed no significant differences between ID8-ASC^{Zeb1WT}, ID8-ASC^{Zeb2WT}, ID8-ASC$^{Zeb1\Delta Mac}$ and ID8-ASC$^{Zeb2\Delta Mac}$ (Figure 40).

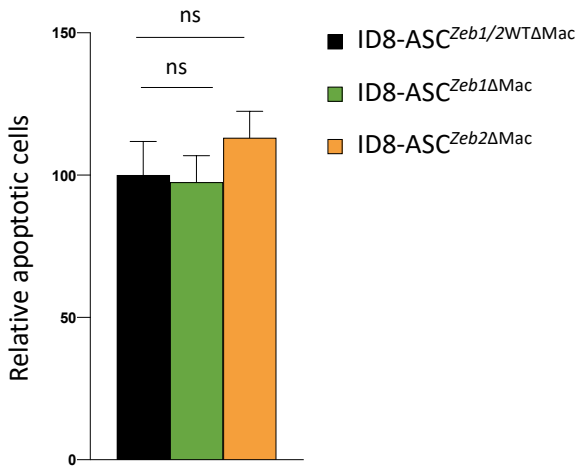

Figure 40. Apoptosis of ID8 cells is not altered by Zeb1 or Zeb2 expression in TAMs. ID8-ASC^{Zeb1WT}, ID8-ASC^{Zeb2WT}, ID8-ASC$^{Zeb1\Delta Mac}$ and ID8-ASC$^{Zeb2\Delta Mac}$ cells were stained with annexin V and propidium iodide and apoptosis were assessed by FACS (n=4).

ZEB factors in TAMs regulate the metabolic activity of ID8 tumor cells

Metabolic reprogramming in tumors promoted cancer progression. Lipid uptake and synthesis enhanced tumor formation and growth (Snaebjornsson et al., 2020). ID8 cells isolated from *Zeb1*$^{\Delta Mac}$, *Zeb2*$^{\Delta Mac}$ and control mice were stained with Bodipy 493/503 to stain for neutral lipids and then analyzed by FACS. Results showed a higher lipid stain in ID8-ASC$^{Zeb2\Delta Mac}$ than in ID8-ASC$^{ZEB1/2WT}$ and ID8-ASC$^{Zeb1\Delta Mac}$ (Figure 41A). Also, cholesterol concentration in ascites was measured. Results showed a higher cholesterol content in ascites from *Zeb1*$^{\Delta Mac}$ than in *Zeb2*$^{\Delta Mac}$ and control mice (Figure 41B).

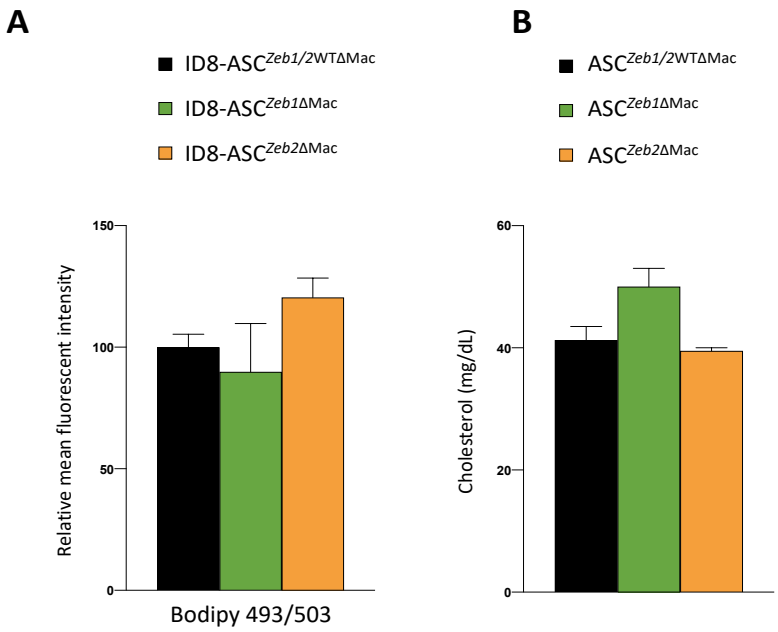

Figure 41. ID8-ASC$^{Zeb2\Delta Mac}$ has higher lipid uptake and ID8-ASC$^{Zeb1\Delta Mac}$ lower than ID8-ASC^{WT} counterparts. (A) ID8-ASC^{Zeb1WT}, ID8-ASC^{Zeb2WT}, ID8-ASC$^{Zeb1\Delta Mac}$ and ID8-ASC$^{Zeb2\Delta Mac}$ cells were stained with Bodipy 493/503 and mean fluorescence intensity was measure by FACS. (B) Ascites from 14 weeks *Zeb1/2*^{WT}, *Zeb1*$^{\Delta Mac}$, and *Zeb2*$^{\Delta Mac}$ tumor-bearing mice were isolated and analyzed for cholesterol quantification.

ID8 cells were injected in *Zeb1*^{WT}, *Zeb1*$^{\Delta Mac}$, *Zeb2*^{WT} and *Zeb2*$^{\Delta Mac}$ mice for 14 weeks to allow the full development of ascites. Ascites were collected and analyzed for different metabolic parameters. The ascites from *Zeb2*$^{\Delta Mac}$–tumor-bearing mice had lower levels of various amino acids, including glutamine that is used to fuel anabolic metabolism by tumor cells and, in consequence, can be depleted (Figure 42A and B).

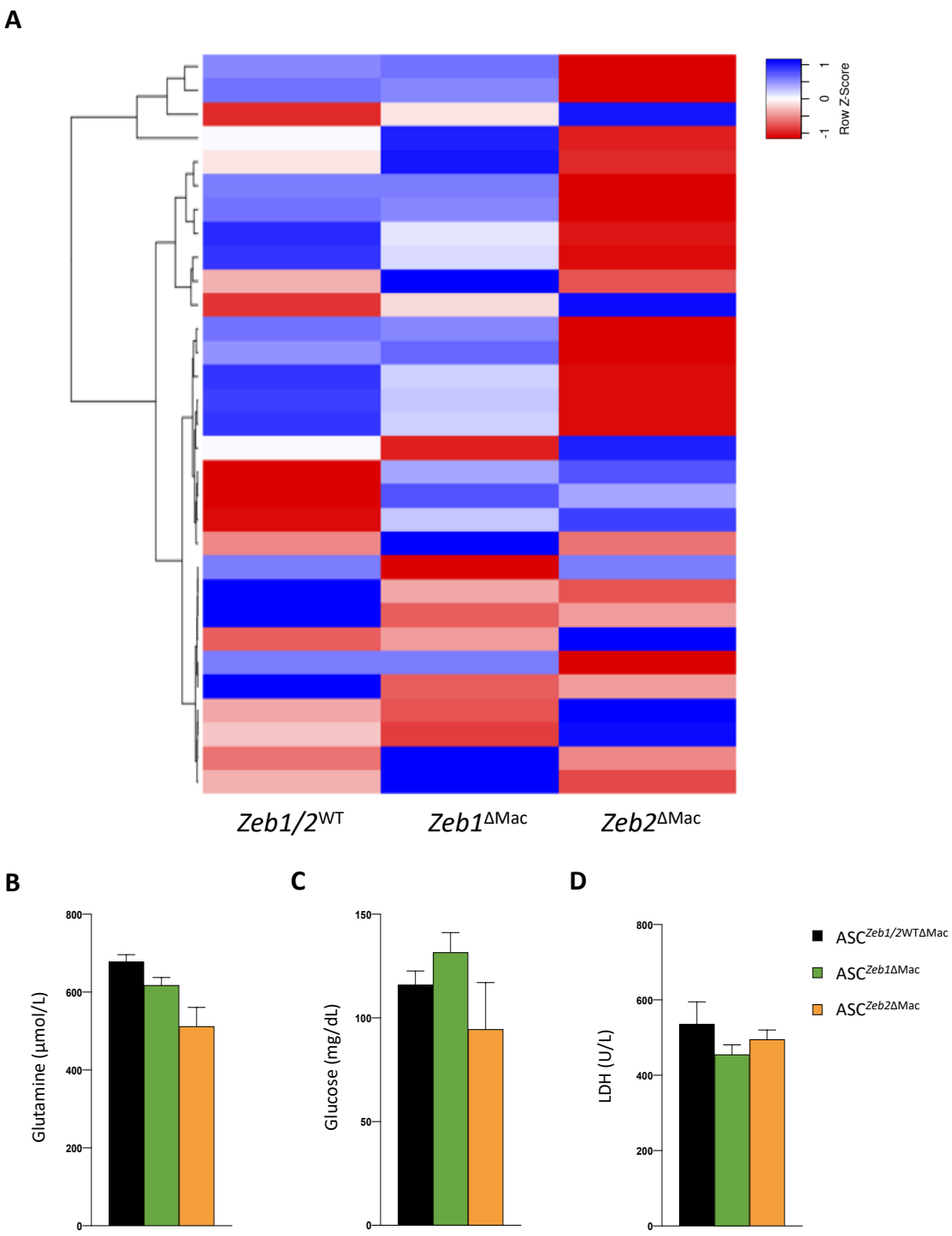

Figure 42. *Zeb2*$^{\Delta Mac}$ mice have a decreased metabolite content in ascites. Ascites from 14 weeks *Zeb1*^{WT}, *Zeb1*$^{\Delta Mac}$, *Zeb2*^{WT} and *Zeb2*$^{\Delta Mac}$ tumor-bearing mice were isolated and analyzed for metabolite quantification. (A) Heat map representation of amino acid quantification and (B) representation of glutamine, glucose and lactate dehydrogenase parameters analyzed in ascites (n=3).

Also, high levels of glycolysis in tumor can trigger glucose limitation. Glucose concentration in ascites of *Zeb1*$^{\Delta Mac}$ was higher than in *Zeb1*^{WT} mice, but no differences were observed in *Zeb2*$^{\Delta Mac}$ compared with control counterparts (Figure 42C). In cancer cells, a high rate of

glucose used in glycolysis is converted to lactate which is excreted. Lactate contributes to extracellular acidification increasing tumor aggressiveness (de la Cruz-Lopez et al., 2019). However, we observed no differences between the ascites from *Zeb1*$^{\Delta Mac}$ neither *Zeb2*$^{\Delta Mac}$ tumor bearing mice in their lactate dehydrogenase concentration compared to control counterparts (Figure 42D). These results suggest that, compared to *Zeb1*^{WT} or *Zeb2*^{WT} mice, tumor cells from the *Zeb2*$^{\Delta Mac}$ mice consume more nutrients, while cancer cells in *Zeb1*$^{\Delta Mac}$ consume less which can be linked to lower and higher tumorigenic capacity of ID8-ASC$^{Zeb1\Delta Mac}$ or ID8-ASC$^{Zeb2\Delta Mac}$, respectively.

In sum, ZEB1 in TAMs in the ID8 mouse model promotes tumor progression by inducing tumorigenic potential of tumor cells, while ZEB2 inhibits it.

DISCUSSION

DISCUSSION

Besides the well-established roles of ZEB factors in cancer cells, mounting evidence indicates that ZEB1 and ZEB2 play multiple roles in immune cells of both myeloid and lymphoid lineages. The results presented in this dissertation indicate that ZEB1 expression in macrophages has an anti-atherogenic role, and set ZEB1 in macrophages as a driver of a pro-tumoral phenotype of TAMs promoting ovarian cancer progression in mice, while ZEB2 have an opposite role and promotes an anti-tumoral phenotype of TAMs.

ZEB1 has an anti-atherogenic role

The first chapter shows that ZEB1 expression in macrophages protects from atherosclerosis development in the *ApoE*-KO mouse model, by inhibiting the formation of foam cells. Also, we characterized ZEB1 as a promoter of cholesterol efflux in macrophages through activation of AMPK-LXRα-ABCA1/G1 axis.

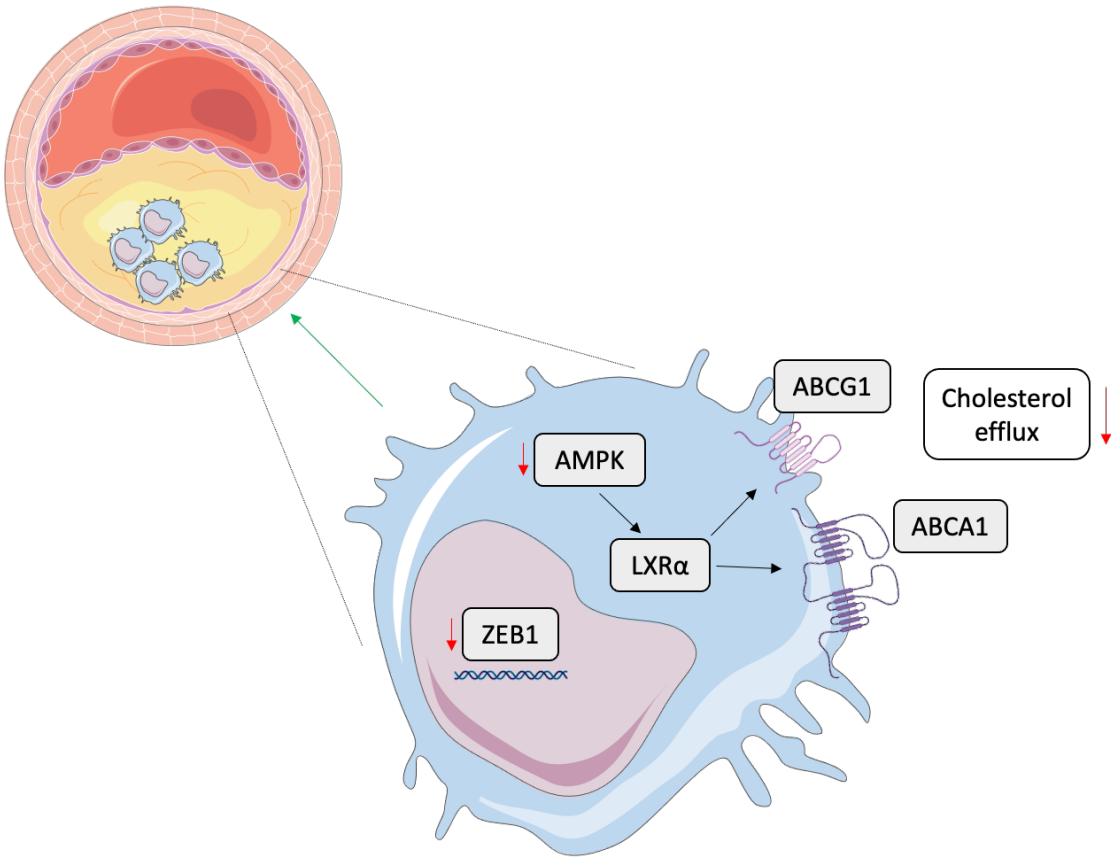

Figure 43. A decrease of ZEB1 expression in macrophages impairs the AMPK-LXRα-ABCA1/G1 axis reducing cholesterol efflux and promoting atherosclerosis development. Created with BioRender.com and Servier medical Art.

ZEB1 plays an important role in lipid metabolism by regulating transcriptionally PPARγ, a regulator of lipid metabolism (Gubelmann et al., 2014). Growing evidence described that ZEB1 regulates accumulation and mobilization of glycosphingolipids to induce an EMT (Mathow et al., 2015). ABCA1 and ABCG1 are the main cholesterol transporters to mediate cholesterol efflux. The deficiency of ABCA1 and ABCG1 promotes foam cell formation and accelerates atherosclerosis by impairing sterol efflux (Yvan-Charvet et al., 2007). ABCA1 and ABCG1 expression increased in macrophages upon treatment with oxLDL, however, *Zeb1*$^{\Delta Mac}$ macrophages have lower levels of both transporters. Overexpression of ZEB1 reduces, while its downregulation increases, cholesterol content in breast cancer cells through recruitment of to CtBP onto the SREBF2 promoter (Zhao et al., 2019). These results are consistent with our findings that macrophages from *Zeb1*$^{\Delta Mac}$ treated with oxLDL have higher lipid content compared to *Zeb1*^{WT}, both treated with oxLDL *in vitro* or fed on Western diet *in vivo*. Uptake of cholesterol by macrophages contributes to lipid accumulation and, on the other hand, cholesterol efflux plays the opposite role (Moore et al., 2013). ABCA1 promotes cholesterol efflux to lipid-poor APOA1 and ABCG1 promotes cholesterol efflux to mature HDL particles (Moore et al., 2013). We found that *Zeb1*$^{\Delta Mac}$ macrophages have deficient cholesterol efflux via both transporters. These results indicate that ZEB1's role in preventing foam cell formation is mediated, at least in part, by promoting macrophage cholesterol efflux through ABCA1 and ABCG1.

Retention of lipids by macrophages in the atherosclerotic plaque exacerbates the disease and makes plaque prone to rupture (Wang et al., 2019). ZEB1 inhibits adipose tissue accumulation and obesity development, an important risk factor for atherosclerosis (Saykally et al., 2009; Kurima et al., 2011), however, the role of ZEB1 in atherosclerosis had not been studied. We found that *Zeb1* haploinsufficiency in all cells in the *Zeb1* (+/-) mice as well as the specific deletion of *Zeb1* macrophages increases atherosclerosis plaque in *ApoE*-KO mice under Western diet. Accordingly, overexpression of ZEB1 leads to increased GUCY1A3 promoter activity which encodes the α1 subunit of the soluble guanylate cyclase and is associated with a protective role in atherosclerotic cardiovascular disease (Kessler et al., 2017). ZEB1

downregulation has been related to elevated levels of miR-33a/b and miR-200 in patients with hypercholesterolemia (D'Agostino et al., 2017; Magenta et al., 2018). LDL modification supports foam cell formation, while HDL promotes cholesterol reverse transport which can contribute to higher lipid accumulation in plaque, being a high LDL/HDL ratio is associated with a higher probability of plaque development (Assmann and GottoJr, 2004; Hao et al., 2014). Analysis of parameters in serum showed that *Zeb1*$^{\Delta Mac}$/*ApoE*-KO mice have lower levels of HDL and higher levels of LDL. This data suggests that HDL and LDL levels in *Zeb1*$^{\Delta Mac}$/*ApoE*-KO mice can impair cholesterol efflux and promote foam cell formation respectively, which can result in increased lesion area and lipid content in the atherosclerotic plaque.

Macrophages loaded with cholesterol are pro-inflammatory while cholesterol efflux decreases the expression of inflammatory factors (Sun et al., 2009; Feig et al., 2011). We found that *Zeb1*$^{\Delta Mac}$ macrophages in addition to increased lipid also have an altered inflammatory state and impaired signaling through pathways downstream oxLDL activation, including p38, JNK, and Nf-kB. Therefore, ZEB1 acts as an upstream regulator to trigger macrophage activation by oxLDL. Although a decrease in cytokines expression and a downregulation of signaling in these pathways are consistent with previous studies from our group in other models that found a defect in the switch from pro- to an anti-inflammatory phenotype in *Zeb1*(+/-) macrophages that is related to an impaired p38 activation (Cortes et al., 2017; Siles et al., 2019). Also, ZEB1 and NF-kB are regulated reciprocally (Chua et al., 2007; Xu et al., 2017). Moreover, NF-kB activation in macrophages has a protective role in atherosclerosis and reduced foam cell formation (Kanters et al., 2003; Ye et al., 2013; Babaev et al., 2016). Accordingly, we observed that inhibition of p65 pathway in *Zeb1*^{WT} macrophages reproduces the phenotype found in *Zeb1*$^{\Delta Mac}$ macrophages with an increase of lipid content and lower expression of ABCA1 and ABCG1. Thus, ZEB1 could be a pivotal regulator of metabolic and inflammatory processes in macrophages. Further, the switch to anti-inflammatory phenotype in macrophages contributes to plaque stabilization by increasing collagen content. ZEB1 regulates collagen deposition in the extracellular matrix by lung cancer cells and vascular smooth muscle cells (Ponticos et al., 2004; Peng et al., 2017). Accordingly, *Zeb1*$^{\Delta Mac}$ mice have higher indicators of unstable plaque, with lower collagen content in atherosclerotic plaque and increased ROS production and apoptosis of macrophages exposed to oxLDL *in vitro*. Consistently, inhibition of ZEB1 induces cell apoptosis by down-regulating

NF-kB in osteosarcoma cells (Xu et al., 2017). Moreover, inhibition of NF-kB or ABCA1 results in an increase of ROS production and apoptosis in macrophages (Yvan-Charvet et al., 2010; Xu et al., 2017; Lingappan, 2018).

Strategies aimed at reducing the accumulation of lipids in macrophages to induce their anti-inflammatory switch can deaccelerate lesion progression and may be a complementary treatment for standard lipid-lowering therapies. In macrophages, AMPK promotes an anti-inflammatory phenotype and reverse cholesterol transport (Day et al., 2017). Activation of AMPK protects against obesity-induced insulin resistance and atherosclerosis (Ma et al., 2017). AMPK activates LXRα results in an increase of cholesterol efflux through activation of the ABCA1 and ABCG1 in macrophages (Rader, 2006; Kemmerer et al., 2016). The activation of AMPK increases the expression of EMT transcription factors in breast cancer cell lines including ZEB1 (Saxena et al., 2018). Nevertheless, the potential regulation of AMPK by ZEB1 had not been studied and we showed here that *Zeb1*$^{\Delta Mac}$ macrophages have reduced expression of the AMPK-LXRα-ABCA1/G1 axis. Pharmacological activation of AMPK in oxLDL treated *Zeb1*$^{\Delta Mac}$ macrophages restore lipid content to control levels. Therefore, we hypothesize that ZEB1 may promote cholesterol efflux and an anti-inflammatory phenotype through the regulation of AMPK-LXRα-ABCA1/G1 axis.

Also, ZEB1 activation could exert a therapeutic effect in atherosclerosis. ZEB1 expression is decreased in macrophages from unstable compared to stable plaques. ZEB1 can be inhibited through the use of CtBP or HDAC inhibitors, specific MirRNA (Meidhof et al., 2015; de Barrios et al., 2017; Ninfali et al., 2018; Title et al., 2018) or activate through stimulation of upstream pathways (Zhang et al., 2019) but specific pharmacological activators or repressors of ZEB1 have not been known currently. Because ZEB1 can be expressed by vascular smooth muscle cells, macrophages, T cells or endothelial cells which are involving in atherosclerosis (Nishimura et al., 2006; Cortes et al., 2017; Guan et al., 2018; Fu et al., 2020), we used a vector with the expression of ZEB1 under Lyz2 (LysM) promoter bind to NPs to only upregulate ZEB1 in macrophages and avoid unexpected or adverse effects. Overexpression of ZEB1 shows decreased lipid accumulation in *Zeb1*$^{\Delta Mac}$ corresponding to *Zeb1*^{WT} macrophages levels and reduced plaque area in *Zeb1*$^{\Delta Mac}$ mice fed on Western diet. That makes pZEB1-GNS a potential

tool for targeting and treatment of macrophages in chronic inflammation areas like the atherosclerotic plaque.

ZEB1 in TAMs promotes tumorigenesis while ZEB2 inhibits it

In the second chapter, we showed that ZEB1 promotes a pro-tumoral phenotype in TAMs, while ZEB2 supports anti-tumoral one.

Lack of ZEB1 in the macrophages of *Zeb1*$^{\Delta Mac}$ mice reduced tumor growth and mortality when injected with ID8 cells, in part due to increased phagocytosis and reduced stemness of ID8 cells. On the other hand, knockout of ZEB2 in macrophages increased tumor progression and mortality in tumor-bearing *Zeb2*$^{\Delta Mac}$ by increasing acquisition of stemness capacity and metabolic adaptation to the microenvironment of ID8 cells.

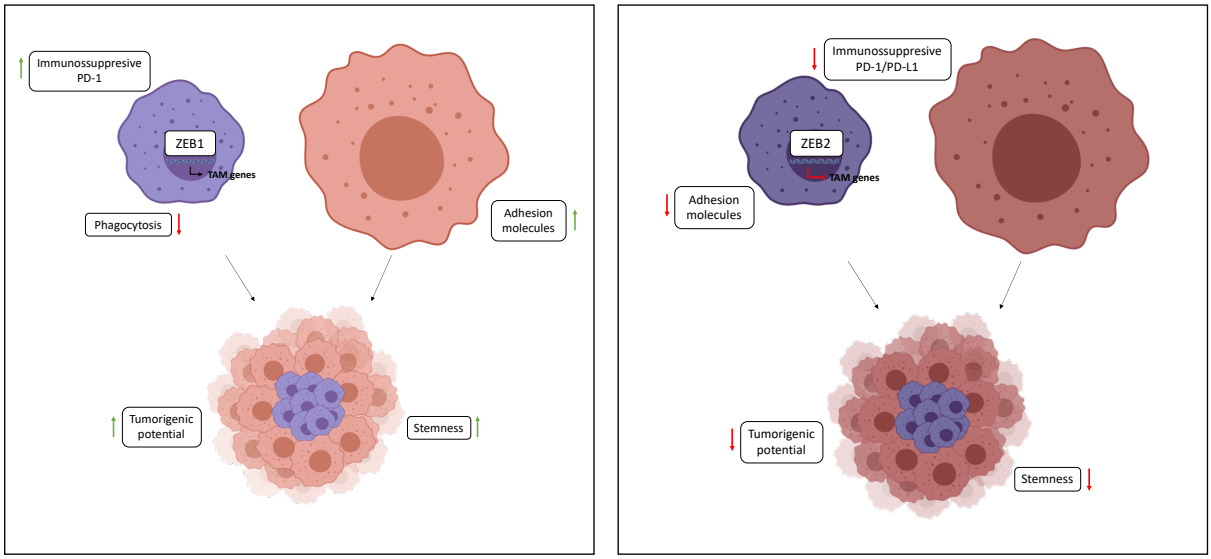

Figure 44. Expression of ZEB1 (left) in TAMs promotes tumorigenic potential and stemness of ID8 cells while ZEB2 inhibits it (right). Created with BioRender.com

Despite their high homology and partly overlapping pattern of expression (Postigo and Dean, 2000), ZEB1 and ZEB2 can have opposing effects in tissue homeostasis, development and tumor biology (Stemmler et al. 2019). For example, loss of ZEB2 is associated with reduced patient survival of patients with melanomas while in a melanoma mouse model ZEB2 inhibits tumor initiation and progression (Caramel et al 2013). However, ZEB1 expression in melanoma can drive tumor initiation and progression and it is associated with poor prognosis

(Stemmler et al., 2019). ZEB factors in a wide range of cancers are implicated in tumor initiation and progression through the regulation of multiple hallmarks such as apoptosis and senescence, tumor invasiveness and metastasis or maintenance of stemness (Qi et al., 2012; Wellner et al., 2009; de Barrios et al., 2017; Dongre and Weinberg, 2019; Zhang et al., 2019). However, the role of ZEB factors in the tumor stroma is still poorly understood. ZEB1 expression in myofibroblasts, macrophages and fibroblasts in TME promote the development of cancer (Cortes et al., 2017; Sangrador et al., 2018; Fu et al., 2019), nevertheless, the role of ZEB2 in tumor stroma has not been studied. We found that ZEB1 is upregulated in macrophages that were exposed to cancer cells compared to macrophages in basal conditions, but no differences were found in ZEB2 expression. ZEB1 and ZEB2 were both upregulated in ID8 cells from mice ascites. Accordingly, ZEB1 is required for pro-tumoral activation of macrophages (Cortes et al., 2017). In addition, contact of ID8 cells with stromal cells in the peritoneum upregulate genes associated with EMT in ascites, including ZEB1 and ZEB2 (Cortes et al., 2017; Etzerodt et al., 2020) which are associated with the acquisition of stem cell properties and predicts poor prognosis (Wellner et al., 2009; Chu et al., 2013; Li et al., 2019).

TAMs are the most abundant immune cell in the TME and play an important role in tumor progression. The extent of infiltration by TAMs in the tumor stroma correlates with a poorer prognosis in tumors of different origins (Morrison, 2016; Ge and Ding, 2020). In line with this, *Zeb1*$^{\Delta Mac}$ mice showed lower TAM infiltration, while *Zeb2*$^{\Delta Mac}$ mice had higher infiltration that is correlated with lower and higher tumor cells in *Zeb1*$^{\Delta Mac}$ and *Zeb2*$^{\Delta Mac}$ mice, respectively. *Zeb1*-deficient macrophages have exhibited a lower expression of CD206 than control counterparts, which is expressed to high levels in pro-tumoral macrophages (Cortes et al., 2017; Siles et al., 2019). Compared to control mice, the proportion of CD206 positive TAMs show not differences in *Zeb2*$^{\Delta Mac}$ mice but is lower in *Zeb1*$^{\Delta Mac}$ mice compared to *Zeb1*^{WT}. Furthermore, TILs were higher in *Zeb1*$^{\Delta Mac}$ and lower in *Zeb2*$^{\Delta Mac}$ mice. TAMs impair activity of TILs while TILs infiltration is often associated with an improved clinical outcome in advanced human ovarian carcinoma (Zhang et al., 2003). Changes in cellular composition of the TME could help to explain, at least in part, lower tumor growth in *Zeb1*$^{\Delta Mac}$ mice and higher in *Zeb2*$^{\Delta Mac}$ mice compared to control mice.

Macrophage polarization modulates the phagocytic capacity, being those with a pro-inflammatory phenotype more efficient at phagocytizing cancer cells than those with an anti-inflammatory phenotype (Martinez and Gordon, 2014). ZEB1 promotes the anti-inflammatory polarization of macrophages and impairs the clearance of cancer cells (Cortes, 2017). PD-1/PD-L1 expression in macrophages hampers their phagocytic capacity and anti-tumor response (Gordon et al., 2017) and anti-PD-1 antibody shifts macrophage polarization to a pro-inflammatory phenotype (Rao et al., 2020). Likewise, the expression of PD-L1 in cancer stem cells supports immune evasion. ZEB2 role has been described in CD8+ T cells where ZEB2 knockout cells increased PD-1 expression and contributed to exhaustion states (Fernandez et al., 2020). ZEB1 induces the expression of PD-L1 in cancer cells leading to T-cell immunosuppression and metastasis (Chen et al., 2014; Dong et al., 2018). PD-L1 has been correlated with ZEB1 and ZEB2 expression and EMT in the invasive front of colon cancer (Martinez-Ciarpaglini et al., 2019). We observed that *Zeb1*$^{\Delta Mac}$ mice have lower PD-1 positive TAMs than *Zeb1/2*^{WT} while *Zeb2*$^{\Delta Mac}$ mice have higher. These results could indicate that CD206^{low}/PD-1^{low} expression promotes a more pro-inflammatory phenotype in *Zeb1*$^{\Delta Mac}$ TAMs and, in contrast, CD206^{high}/PD-1^{high} induce an anti-inflammatory phenotype in *Zeb2*$^{\Delta Mac}$ TAMs. Thus, phagocytosis of ID8 cells was increased in *Zeb1*$^{\Delta Mac}$ but not in *Zeb2*$^{\Delta Mac}$ macrophages. Also, PD-L1 positive cells were higher in ID8-ASC$^{Zeb2\Delta Mac}$ mice than in ID8-ASC^{Zeb2WT} mice indicating that *Zeb2*$^{\Delta Mac}$ macrophages could be promoting immune evasion of ID8 cells. These evidences suggest that ZEB1 may be implicated in tumor progression through impair phagocytosis and induce an immunosuppressive environment by increasing PD-1 expression in macrophages. In turn, ZEB2 could be implicated in tumor progression inhibition mediating a decrease of PD-1 in TAMs and PD-L1 reduction in ID8 cells which could induce an anti-tumoral environment.

PD-L1 also promotes the formation of tumorspheres of ID8 cells formation (Gupta et al., 2016). Pro-tumoral TAMs promote sphere formation through upregulation CD11b on TAMs and CD54 on tumor cells (Yin et al., 2016). Cancer cells in the ascitic fluid show stem cell characteristics (Bapat et al., 2005). The acquisition of cancer cell properties by cancer cells has been associated with promoting cancer progression and metastasis (Kreso and Dick, 2014). TAMs promote cancer stemness in multiple types of cancer such as breast cancer, prostate cancer or ovarian cancer (Yang et al., 2013; Raghavan et al., 2019; Huang et al., 2020).

In addition, the acquisition of stem-like characteristics by cancer cells has been associated with cancer development, progression and resistance to chemotherapy and radiotherapy (Walcher et al., 2020). ZEB1 and ZEB2 expression in tumor cells have been described by promotes cancer stem cell characteristics. We found that ZEB1 in macrophages promotes tumorsphere formation. ID8-ASC$^{Zeb2\Delta Mac}$ cells showed increased and ID8-ASC$^{Zeb1\Delta Mac}$ cells a decreased expression of some stemness markers, like CD55 and CD117, compared to ID8-ASC$^{Zeb1/2WT}$ and opposite results were found in ID8-ASC$^{Zeb2\Delta Mac}$ cells. That suggests that ZEB1 expression in TAMs promotes the tumorigenic potential of ID8 cells, while ZEB2 reduces it. These results are supported by studies of survival where we found that ID8-ASC$^{Zeb1\Delta Mac}$ cells increase survival of wild-type mice, while ID8-ASC$^{Zeb2\Delta Mac}$ cells decrease it.

In sum, our data set ZEB1 in TAMs as a tumor-promoting and ZEB2 as a tumor-repressor in ovarian cancer. Also, ZEB1 in macrophages is protecting from atherosclerosis development. Altogether, these results setting ZEB1 and ZEB2 in macrophages as a potential therapeutic target in cancer and atherosclerosis and other conditions in the context of chronic inflammation.

CONCLUSIONS

CONCLUSIONS

From the results presented in this dissertation, it can be concluded that:

1. ZEB1 is required for the activation of the AMPK signaling pathway in macrophages to suppress lipid accumulation.

2. ZEB1 in macrophages has an anti-atherogenic role in ApoE-KO mice and reduces plaque instability by reducing necrotic area and lipid accumulation.

3. In the context of cancer, ZEB1 expression in macrophages reprograms TAMs towards a pro-tumoral phenotype, while ZEB2 reprograms them toward an anti-tumoral phenotype.

4. ZEB1 expression in TAMs increases the tumorigenic potential of ID8 cells and decreases survival in tumor-bearing mice by inducing stem cell characteristics in cancer cells while ZEB2 expression in TAMs has opposing functions.

BIBLIOGRAPHY

BIBLIOGRAPHY

Al Habyan S, Kalos C, Szymborski J, McCaffrey L. Multicellular detachment generates metastatic spheroids during intra-abdominal dissemination in epithelial ovarian cancer. Oncogene. 2018;37:5127-5135.

Amézaga N, Sanjurjo L, Julve J, Aran G, Pérez-Cabezas B, Bastos-Amador P, Armengol C, Vilella R, Escolà-Gil JC, Blanco-Vaca F, Borràs FE, Valledor AF, Sarrias MR. Human scavenger protein AIM increases foam cell formation and CD36-mediated oxLDL uptake. J Leukoc Biol. 2014;95:509-20.

Amit I, Citri A, Shay T, Lu Y, Katz M, Zhang F, Tarcic G, Siwak D, Lahad J, Jacob-Hirsch J, Amariglio N, Vaisman N, Segal E, Rechavi G, Alon U, Mills GB, Domany E, Yarden Y. A module of negative feedback regulators defines growth factor signaling. Nat Genet. 2007;39:503-12.

Andrés-Manzano MJ, Andrés V, Dorado B. Oil Red O and Hematoxylin and Eosin Staining for Quantification of Atherosclerosis Burden in Mouse Aorta and Aortic Root. Methods Mol Biol. 2015;1339:85-99.

Anstee QM, Targher G, Day CP. Progression of NAFLD to diabetes mellitus, cardiovascular disease or cirrhosis. Nat Rev Gastroenterol Hepatol. 2013;10:330-44.

Arango Duque G, Descoteaux A. Macrophage cytokines: involvement in immunity and infectious diseases. Front Immunol. 2014;5:491.

Arango Duque G, Descoteaux A. Macrophage cytokines: involvement in immunity and infectious diseases. Front Immunol. 2014:5;491.Bäck M, Yurdagul A, Tabas I Öörni K, Kovanen PT. Inflammation and its resolution in atherosclerosis: mediators and therapeutic opportunities. Nat Rev Cardiol. 2019;16:389-406.

Assmann G, GottoJr AM. HDL Cholesterol and Protective Factors in Atherosclerosis. Circulation. 2004;109:III8-14.

Babaev VR, Yeung M, Erbay E, Ding L, Zhang Y, May JM, Fazio S, Hotamisligil GS, Linton MF. Jnk1 Deficiency in Hematopoietic Cells Suppresses Macrophage Apoptosis and Increases Atherosclerosis in Low-Density Lipoprotein Receptor Null Mice. Arterioscler Thromb Vasc Biol. 2016;36:1122-31.

Bäck M, Yurdagul A, Tabas I, Öörni K, Kovanen PT. Inflammation and its resolution in atherosclerosis: mediators and therapeutic opportunities. Nat Rev Cardiol. 2019;16:389-406.

Bader JE, Voss K, Rathmell JC. Targeting Metabolism to Improve the Tumor Microenvironment for Cancer Immunotherapy. Mol Cell. 2020;78:1019-1033.

Bansal R, Mandrekar P, Mohanty SK, Weiskirchen R. Editorial: Macrophages in Liver Disease. Front Immunol. 2020;11:1754.

Bapat SA, Mali AM, Koppikar CB, Kurrey NK. Stem and progenitor-like cells contribute to the aggressive behavior of human epithelial ovarian cancer. Cancer Res. 2005;65:3025-9.

Behringer R, Gertsenstein M, Nagy K, Nagy A. Manipulating the Mouse Embryo: A Laboratory Manual. Cold Spring Harbor, New Cell Res. 2014;Fourth Edition:814.

Bentzon JF, Otsuka F, Virmani R, Falk E. Mechanisms of plaque formation and rupture. Circ Res. 2014;114:1852-66.

Bhatia LS, Curzen NP, Calder PC, Byrne CD. Non-alcoholic fatty liver disease: a new and important cardiovascular risk factor?. Eur Heart J. 2012;33:1190-1200.

Biswas SK. Metabolic Reprogramming of Immune Cells in Cancer Progression. Immunity. 2015;43:435-49.

Cai Q, Yan L, Xu Y. Anoikis resistance is a critical feature of highly aggressive ovarian cancer cells. Oncogene. 2015;34:3315-24.

Caramel J, Papadogeorgakis E, Hill L, Browne GJ, Richard G, Wierinckx A, Saldanha G, Osborne J, Hutchinson P, Tse G, Lachuer J, Puisieux A, Pringle JH, Ansieau S, Tulchinsky E. A switch in the expression of embryonic EMT-inducers drives the development of malignant melanoma. Cancer Cell. 2013;24:466-80.

Cassado Ados A, D'Império Lima MR and Bortoluci KR. Revisiting mouse peritoneal macrophages: heterogeneity, development, and function. Front Immunol. 2015;6:225.

Chen L, Deng H, Cui H, Fang J, Zuo Z, Deng J, Li Y, Wang X and Zhao L. Inflammatory responses and inflammation- associated disease in organs. Oncotarget. 2018;9:7204-7218.

Chen L, Gibbons DL, Goswami S, Cortez MA, Ahn YH, Byers LA, Zhang X, Yi X, Dwyer D, Lin W, Diao L, Wang J, Roybal J, Mayuri Patel 1, Christin Ungewiss 1, David Peng 1, Scott Antonia 6, Melanie Mediavilla-Varela 6, Gordon Robertson 7, Milind Suraokar 1 8, Welsh JW, Erez B, Wistuba II, Chen L, Peng D, Wang S, Ullrich SE, Heymach JV, Kurie JM, Qin FX. Metastasis is regulated via microRNA-200/ZEB1 axis control of tumour cell PD-L1 expression and intratumoral immunosuppression. Nat Commun. 2014;5:5241.

Chenthamara D, Subramaniam S, Ramakrishnan SG, Krishnaswamy S, Essa MM, Lin FH, Qoronfleh MW. Therapeutic efficacy of nanoparticles and routes of administration. Biomater Res. 2019 Nov 21;23:20.

Chistiakov DA, Melnichenko AA, Myasoedova VA, Grechko AV, Orekhov AN. Mechanisms of foam cell formation in atherosclerosis. J Mol Med (Berl). 2017;95:1153-1165.

Cho KR, Shih IeM. Ovarian cancer. Annu Rev Pathol. 2009;4:287-313.

Chu PY, Hu FW, Yu CC, Tsai LL, Yu CH, Wu BC, Chen YW, Huang PI, Lo WL. Epithelial-mesenchymal transition transcription factor ZEB1/ZEB2 co-expression predicts poor prognosis and maintains tumor-initiating properties in head and neck cancer. Oral Oncol. 2013;49:34-41.

Chua HL, Bhat-Nakshatri P, Clare SE, Morimiya A, Badve S, Nakshatri H. NF-kappaB represses E-cadherin expression and enhances epithelial to mesenchymal transition of mammary epithelial cells: potential involvement of ZEB-1 and ZEB-2. Oncogene. 2007;26:711-24.

Clausen BE, Burkhardt C, Reith W, Renkawitz R, Forster I. (1999). Conditional gene targeting in macrophages and granulocytes using LysMcre mice. Transgenic Res. 1999;8:265-77.

Coish P, Wickens PL and Lowinger TB. Small molecule inhibitors of IKK kinase activity. Expert Opin Ther Patens. 2006;16:1-12.

Collado M, Serrano M. Senescence in tumours: evidence from mice and humans. Nat Rev Cancer. 2010;10:51-7.

Colvin EK. Tumor-associated macrophages contribute to tumor progression in ovarian cancer. Front Oncol. 2014;4:137.

Cortes M, Sanchez-Moral L, de Barrios O, Fernández-Aceñero MJ, Martinez-Campanario MC, Esteve-Codina A, Darling DS, Győrffy B, Lawrence T, Dean DC and Postigo A. Tumor-associated macrophages (TAMs) depend on ZEB1 for their cancer-promoting roles. EMBO J. 2017;36:3336-55.

D'Agostino M, Martino F, Sileno S, Barillà F, Beji S, Marchetti L, Gangi FM, Persico L, Picozza M, Montali A, Martino E, Zanoni C, Avitabile D, Parrotto S, Colognesi C, Magenta A. Circulating miR-200c is up-regulated in paediatric patients with familial hypercholesterolaemia and correlates with miR-33a/b levels: implication of a ZEB1-dependent mechanism. Clin Sci (Lond). 2017;131:2397-2408.

Davis ME, Chen ZG, Shin DM. Nanoparticle therapeutics: an emerging treatment modality for cancer. Nat Rev Drug Discov. 2008;7:771-82.

Day EA, Ford RJ, Steinberg GR. AMPK as a Therapeutic Target for Treating Metabolic Diseases. Trends Endocrinol Metab. 2017;28:545-560.

de Barrios O, Győrffy B, Fernández-Aceñero MJ, Sánchez-Tilló E, Sánchez-Moral L, Siles L, Esteve-Arenys A, Roué G, Casal JI, Darling DS, Castells A, Postigo A. ZEB1-induced tumourigenesis requires senescence inhibition via activation of DKK1/mutant p53/Mdm2/CtBP and repression of macroH2A1. Gut. 2017;66:666-682.

De la Cruz-López KG, Castro-Muñoz LJ, Reyes-Hernández DO, García-Carrancá A, Manzo-Merino J. Lactate in the Regulation of Tumor Microenvironment and Therapeutic Approaches. Front Oncol. 2019 Nov 1;9:1143.

DeNardo DG, Ruffell B. Macrophages as regulators of tumour immunity and immunotherapy. Nat Rev Immunol. 2019;19:369-382.

Di Mitri D, Mirenda M, Vasilevska J, Calcinotto A, Delaleu N, Revandkar A, Gil V, Boysen G, Losa M, Mosole S, Pasquini E, D'Antuono R, Masetti M, Zagato E, Chiorino G, Ostano P, Rinaldi A, Gnetti L, Graupera M, Martins Figueiredo Fonseca AR, Pereira Mestre R, Waugh D, Barry S, De Bono J, Alimonti A. Re-education of Tumor-Associated Macrophages by CXCR2 Blockade Drives Senescence and Tumor Inhibition in Advanced Prostate Cancer. Cell Rep. 2019;28:2156-2168.e5.

Dong P, Xiong Y, Yue J, Hanley SJB, Watari H. Tumor-Intrinsic PD-L1 Signaling in Cancer Initiation, Development and Treatment: Beyond Immune Evasion. Front Oncol. 2018;8:386.

Dongre A, Weinberg RA. New insights into the mechanisms of epithelial-mesenchymal transition and implications for cancer. Nat Rev Mol Cell Biol. 2019;20:69-84.

Duran EK, Aday AW, Cook NR, Buring JE, Ridker PM, Pradhan AD. Triglyceride-Rich Lipoprotein Cholesterol, Small Dense LDL Cholesterol, and Incident Cardiovascular Disease. J Am Coll Cardiol. 2020;75:2122-2135.

Einarson TR, Acs A, Ludwig C, Panton UH. Prevalence of cardiovascular disease in type 2 diabetes: a systematic literature review of scientific evidence from across the world in 2007-2017. Cardiovasc Diabetol. 2018;17:83.

Etzerodt A, Moulin M, Doktor TK, Delfini M, Mossadegh-Keller N, Bajenoff M, Sieweke MH, Moestrup SK, Auphan-Anezin N, Lawrence T. Tissue-resident macrophages in omentum promote metastatic spread of ovarian cancer. J Exp Med. 2020;217:e20191869.

Evans MS, Chaurette JP, Adams ST Jr, Reddy GR, Paley MA, Aronin N, Prescher JA, Miller SC. A synthetic luciferin improves bioluminescence imaging in live mice. Nat Methods. 2014;11:393-5.

Fazel Y, Koenig AB, Sayiner M, Goodman ZD, Younossi ZM. Epidemiology and natural history of non-alcoholic fatty liver disease. Metabolism. 2016;65:1017-1025.

Feig JE, Rong JX, Shamir R, Sanson M, Vengrenyuk Y, Liu J, Rayner K, Moore K, Garabedian M, Fisher EA. HDL promotes rapid atherosclerosis regression in mice and alters inflammatory properties of plaque monocyte-derived cells. Proc Natl Acad Sci U S A. 2011;108:7166-71.

Fernandez D, Fernandez NF, Rahman A, Hill C, Shamailova R, Kim-schulze S, Mocco J, Faries P, Merad M, Giannarelli. ZEB2 regulates activation and exhaustion programming of CD8+ T cells in atherosclerosis. Arterioscler Thromb Vasc Biol. 2020;40:A258.

Fleming V, Hu X, Weber R, Nagibin V, Groth C, Altevogt P, Utikal J, Umansky V. Targeting Myeloid-Derived Suppressor Cells to Bypass Tumor-Induced Immunosuppression. Front Immunol. 2018;9:398.

Flores AM, Ye J, Jarr KU, Hosseini-Nassab N, Smith BR, Leeper NJ. Nanoparticle Therapy for Vascular Diseases. Arterioscler Thromb Vasc Biol. 2019;39:635-646.

Freemerman AJ, Johnson AR, Sacks GN, Milner JJ, Kirk EL, Troester MA, Macintyre AN, Goraksha-Hicks P, Rathmell JC, Makowski L. Metabolic reprogramming of macrophages: glucose transporter 1 (GLUT1)-mediated glucose metabolism drives a proinflammatory phenotype. J Biol Chem. 2014;289:7884-96.

Fu R, Han CF, Ni T, Di L, Liu LJ, Lv WC, Bi YR, Jiang N, He Y, Li HM, Wang S, Xie H, Chen BA, Wang XS, Weiss SJ, Lu T, Guo QL and Wu ZQ. A ZEB1/p53 signaling axis in stromal fibroblasts promotes mammary epithelial tumours. Nat Commun. 2019;10:3210.

Fu R, Li Y, Jiang N, Ren BX, Zang CZ, Liu LJ, Lv WC. Li HM, Weiss S, Li ZY, Lu T, Wu ZQ. Inactivation of endothelial ZEB1 impedes tumor progression and sensitizes tumors to conventional therapies. J Clin Invest. 2020;130:1252-1270.

Fullerton MD, Ford RJ, McGregor CP, LeBlond ND, Snider SA, Stypa SA, Day EA, Lhoták Š, Schertzer JD, Austin RC, Kemp BE and Steinberg GR. Salicylate improves macrophage cholesterol homeostasis via activation of Ampk. J Lipid Res. 2015;56:1025-1033.

Gao Q, Yang Z, Xu S, Li X, Yang X, Jin P, Liu Y, Zhou X, Zhang T, Gong C, Wei X, Liu D, Sun C, Chen G, Hu J, Meng L, Zhou J, Sawada K, Fruscio R, Grunt TW, Wischhusen J, Vargas-Hernández VM, Pothuri B, Coleman RL. Heterotypic CAF-tumor spheroids promote early peritoneal metastatis of ovarian cancer. J Exp Med. 2019;216:688-703.

Garcia-Jimenez C and Goding CR. Starvation and pseudo-starvation as drivers of cancer metastasis through translation reprogramming. Cell metabol. 2019;29:254-267.

Ge Z, Ding S. The Crosstalk Between Tumor-Associated Macrophages (TAMs) and Tumor Cells and the Corresponding Targeted Therapy. Front Oncol. 2020;10:590941.

Gentric G, Kieffer Y, Mieulet V, Goundiam O, Bonneau C, Nemati F, Hurbain I, Raposo G, Popova T, Stern MH, Lallemand-Breitenbach V, Müller S, Cañeque T, Rodriguez R, Vincent-Salomon A, de Thé H, Rossignol R, Mechta-Grigoriou F. PML-Regulated Mitochondrial Metabolism Enhances Chemosensitivity in Human Ovarian Cancers. Cell Metab. 2019;29:156-173.e10.

Gheldof A, Hulpiau P, van Roy F, De Craene B and Berx G. Evolutionary functional analysis and molecular regulation of the ZEB transcription factors. Cell Mol Life Sci. 2012;69:2527-2541.

Ghosn EE, Cassado AA, Govoni GR, Fukuhara T, Yang Y, Monack DM, Bortoluci KR, Almeida SR, Herzenberg LA and Herzenberg LA. Two physically, functionally, and developmentally distinct peritoneal macrophage subsets. Proc Natl Acad Sci USA. 2010;107:2568-73.

Ginhoux F and Jung S. Monocytes and macrophages: developmental pathways and tissue homeostasis. Nat Rev Immunol. 2014;14:392-404.

Ginhoux F and Guilliams M. Tissue-resident macrophage ontogeny and homeostasis. Immunity. 2016;44:439-49.

Gisterå A, Hansson GK. The immunology of atherosclerosis. Nat Rev Nephrol. 2017;13:368-380.

González-Ramos S, Paz-García M, Rius C, Del Monte-Monge A, Rodríguez C, Fernández-García V, Andrés V, Martínez-González J, Lasunción MA, Martín-Sanz P, Soehnlein O, Boscá L. Endothelial NOD1 directs myeloid cell recruitment in atherosclerosis through VCAM-1. FASEB J. 2019;33:3912-3921.

Goossens S, Janzen V, Bartunkova S, Yokomizo T, Drogat B, Crisan M, Haigh K, Seuntjens E, Umans L, Riedt T, Bogaert P, Haenebalcke L, Berx G, Dzierzak E, Huylebroeck D and Haigh JJ. The EMT regulator Zeb2/Sip1 is essential for murine embryonic hematopoietic stem/progenitor cell differentiation and mobilization. Blood. 2011;117:5620-30.

Goossens P, Rodriguez-Vita J, Etzerodt A, Masse M, Rastoin O, Gouirand V, Ulas T, Papantonopoulou O, Van Eck M, Auphan-Anezin N, Bebien M, Verthuy C, Vu Manh TP, Turner M, Dalod M, Schultze JL, Lawrence T. Membrane Cholesterol Efflux Drives Tumor-Associated Macrophage Reprogramming and Tumor Progression. Cell Metab. 2019;29:1376-1389.e4.

Gordon S, Martinez FO. Alternative activation of macrophages: mechanism and functions. Immunity. 2010;32:593-604.

Gordon SR, Maute RL, Dulken BW, Hutter G, George BM, McCracken MN, Gupta R, Tsai JM, Sinha R, Corey D, Ring AM, Connolly AJ, Weissman IL. PD-1 expression by tumour-associated macrophages inhibits phagocytosis and tumour immunity. Nature. 2017;545:495-99.

Guan T, Dominguez CX, Amezquita RA, Laidlaw BJ, Cheng J, Henao-Mejia J, Williams A, Flavell RA, Lu J, Kaech SM. ZEB1, ZEB2, and the miR-200 family form a counterregulatory network to regulate CD8+ T cell fates. J Exp Med. 2018;215:1153-68.

Gubelmann C, Schwalie PC, Raghav SK, Röder E, Delessa T, Kiehlmann E, Waszak SM, Corsinotti A, Udin G, Holcombe W, Rudofsky G, Trono D, Wolfrum C and Deplancke B. Identification of the transcription factor ZEB1 as a central component of the adipogenic gene regulatory network. Elife. 2014;3:e03346.

Gupta HB, Clark CA, Yuan B, Sareddy G, Pandeswara S, Padron AS, Hurez V, Conejo-Garcia J, Vadlamudi R, Li R, Curiel TJ. Tumor cell-intrinsic PD-L1 promotes tumor-initiating cell generation and functions in melanoma and ovarian cancer. Signal Transduct Target Ther. 2016;1:16030.

Hagemann T, Wilson J, Burke F, Kulbe H, Li NF, Plüddemann A, Charles K, Gordon S, Balkwill FR. Ovarian cancer cells polarize macrophages toward a tumor-associated phenotype. J Immunol. 2006;176:5023-32.

Hagemann T, Lawrence T, McNeish I, Charles KA, Kulbe H, Thompson RG, Robinson SC, Balkwill FR. "Re-educating" tumor-associated macrophages by targeting NF-kappaB. J Exp Med. 2008;205:1261-8.

Hanahan D, Weinberg RA. Hallmarks of cancer: the next generation. Cell. 2011;144:646-74.

Hao W, Friedman A. The LDL-HDL profile determines the risk of atherosclerosis: a mathematical model. PLoS One. 2014;9:e90497.

Herrington W, Lacey B, Sherliker P, Armitage J and Lewington S. Epidemiology of atherosclerosis and the potential to reduce the global burden of atherothrombotic disease. Circ Res. 2016;118:535-46.

Huang SC, Smith AM, Everts B, Colonna M, Pearce EL, Schilling JD, Pearce EJ. Metabolic Reprogramming Mediated by the mTORC2-IRF4 Signaling Axis Is Essential for Macrophage Alternative Activation. Immunity. 2016;45:817-30.

Huang R, Wang S, Wang N, Zheng Y, Zhou J, Yang B, Wang X, Zhang J, Guo L, Wang S, Chen Z, Wang Z, Xiang S. CCL5 derived from tumor-associated macrophages promotes prostate cancer stem cells and metastasis via activating β-catenin/STAT3 signaling. Cell Death Dis. 2020;11:234.

Izar B, Tirosh I, Stover EH, Wakiro I, Cuoco MS, Alter I, Rodman C, Leeson R, Su MJ, Shah P, Iwanicki M, Walker SR, Kanodia A, Melms JC, Mei S, Lin JR, Porter CBM, Slyper M, Waldman J, Jerby-Arnon L, Ashenberg O, Brinker TJ, Mills C, Rogava M, Vigneau S, Sorger PK, Garraway LA, Konstantinopoulos PA, Liu JF, Matulonis U, Johnson BE, Rozenblatt-Rosen O, Rotem A, Regev A. A single-cell landscape of high-grade serous ovarian cancer. Nat Med. 2020;26:1271-1279.

Ito A, Hong C, Rong X, Zhu X, Tarling EJ, Hedde PN, Gratton E, Parks J, Tontonoz P. LXRs link metabolism to inflammation through Abca1-dependent regulation of membrane composition and TLR signaling. Elife. 2015;4:e08009.

Jeon SM. Regulation and function of AMPK in physiology and diseases. Exp Mol Med. 2016;48:e245.

Jiang X, Wang J, Deng X, Xiong F, Ge J, Xiang B, Wu X, Ma J, Zhou M, Li X, Li Y, Li G, Xiong W, Guo C, Zeng Z. Role of the Tumor Microenvironment in PD-L1/PD-1-mediated Tumor Immune Escape. Mol Cancer. 2019;18:10.

Jover E, Silvente A, Marín F, Martínez-González J, Orriols M, Martinez CM, Puche CM, Valdés M, Rodriguez C, Hernández-Romero D. Inhibition of enzymes involved in collagen cross-linking reduces vascular smooth muscle cell calcification. FASEB J. 2018;32:4459-4469.

Kanters E, Pasparakis M, Gijbels MJ, Vergouwe MN, Partouns-Hendriks I, Fijneman RJ, Clausen BE, Förster I, Kockx MM, Rajewsky K, Kraal G, Hofker MH, de Winther MP. Inhibition of NF-

kappaB activation in macrophages increases atherosclerosis in LDL receptor-deficient mice. J Clin Invest. 2003;112:1176-85.

Keir ME, Liang SC, Guleria I, Latchman YE, Qipo A, Albacker LA, Koulmanda M, Freeman GJ, Sayegh MH, Sharpe AH. Tissue expression of PD-L1 mediates peripheral T cell tolerance. J Exp Med. 2006;203:883-95.

Kemmerer M, Finkernagel F, Cavalcante MF, Abdalla DS, Müller R, Brüne B, Namgaladze D. AMP-Activated protein kinase interacts with the peroxisome proliferator-activated receptor delta to induce genes affecting fatty acid oxidation in human macrophages. PLos One. 2015;10:e0130893.

Kemmerer M, Wittig I, Richter F, Brüne B, Namgaladze D. AMPK activates LXRα and ABCA1 expression in human macrophages. Int J Biochem Cell Biol. 2016;78:1-9.

Kessler T, Wobst J, Wolf B, Eckhold J, Vilne B, Hollstein R, von Ameln S, Dang TA, Sager HB, Rumpf PM, Aherrahrou R, Kastrati A, Björkegren J, Erdmann J, Lusis AJ, Civelek M, Kaiser FJ, Schunkert H. Functional characterization of the GUCY1A3 coronary artery disease risk locus. Circulation. 2017;136:476-489.

Kim J, Park EY, Kim O, Schilder JM, Coffey DM, Cho CH, Bast RC Jr. Cell Origins of High-Grade Serous Ovarian Cancer. Cancers (Basel). 2018;10:433.

Kreso A, Dick JE. Evolution of the cancer stem cell model. Cell Stem Cell. 2014;14:275-91.

Kurima K, Hertzano R, Gavrilova O, Monahan K, Shpargel KB, Nadaraja G, Kawashima Y, Lee KY, Ito T, Higashi Y, Eisenman DJ, Strome SE, Griffith AJ. A noncoding point mutation of Zeb1 causes multiple developmental malformations and obesity in Twirler mice. PLoS Genet. 2011;7:e1002307.

Labani-Motlagh A, Ashja-Mahdavi M, Loskog A. The Tumor Microenvironment: A Milieu Hindering and Obstructing Antitumor Immune Responses. Front Immunol. 2020;11:940.

Lahiguera Á, Hyroššová P, Figueras A, Garzón D, Moreno R, Soto-Cerrato V, McNeish I, Serra V, Lazaro C, Barretina P, Brunet J, Menéndez J, Matias-Guiu X, Vidal A, Villanueva A, Taylor-Harding B, Tanaka H, Orsulic S, Junza A, Yanes O, Muñoz-Pinedo C, Palomero L, Pujana MÀ, Perales JC, Viñals F. Tumors defective in homologous recombination rely on oxidative metabolism: relevance to treatments with PARP inhibitors. EMBO Mol Med. 2020;12:e11217.

Leussink S, Aranda-Pardos I and A-Gonzalez N.Lipid metabolism as a mechanism of immunomodulation in macrophages: the role of liver X receptors. Curr Opin Pharmacol. 2020;53:18-26.

Li J, Condello S, Thomes-Pepin J, Ma X, Xia Y, Hurley TD, Matei D, Cheng JX. Lipid Desaturation Is a Metabolic Marker and Therapeutic Target of Ovarian Cancer Stem Cells. Cell Stem Cell. 2017;20:303-314.e5.

Li N, Babaei-Jadidi R, Lorenzi F, Spencer-Dene B, Clarke P, Domingo E, Tulchinsky E, Vries RGJ, Kerr D, Pan Y, He Y, Bates DO, Tomlinson I, Clevers H, Nateri AS. An FBXW7-ZEB2 axis links EMT and tumour microenvironment to promote colorectal cancer stem cells and chemoresistance. Oncogenesis. 2019;8:13.

Lingappan K. NF-κB in Oxidative Stress. Curr Opin Toxicol. 2018;7:81-86.

Liu T, Zhang L, Joo D, Sun SC. NF-κB signaling in inflammation. Signal Transduct Target Ther. 2017;2:17023–.

Locati M, Curtale G, Mantovani A. Diversity, Mechanisms, and Significance of Macrophage Plasticity. Annu Rev Pathol. 2020;15:123-147.

Lonardo A, Nascimbeni F, Mantovani A and Targher G. Hypertension, diabetes, atherosclerosis and NASH: Cause or consequence?. J Hepatol. 2018;68:335-352.

Lowe SW, Cepero E, Evan G. Intrinsic tumour suppression. Nature. 2004;432:307-15.

Luo Y, Duan H, Qian Y, Feng L, Wu Z, Wang F, Feng J, Yang D, Qin Z, Yan X. Macrophagic CD146 promotes foam cell formation and retention during atherosclerosis. Cell Res. 2017;27:352-372.

Lyssiotis CA, Kimmelman AC. Metabolic Interactions in the Tumor Microenvironment. Trends Cell Biol. 2017;27:863-875.

Ma A, Wang J, Yang L, An Y, Zhu H. AMPK activation enhances the anti-atherogenic effects of high density lipoproteins in apoE-/- mice. J Lipid Res. 2017;58:1536-1547.

Madamanchi NR, Vendrov A, Runge MS. Oxidative stress and vascular disease. Arterioscler Thromb Vasc Biol. 2005;25:29-38.

Magenta A, Sileno S, D'Agostino M, Persiani F, Beji S, Paolini A, Camilli D, Platone A, Capogrossi MC, Furgiuele S. Atherosclerotic plaque instability in carotid arteries: miR-200c as a promising biomarker. Clin Sci (Lond). 2018;132:2423-2436.

Mantovani A, Marchesi F, Malesci A, Laghi L and Allavena P. Tumour-associated macrophages as treatment targets in oncology. Nat Rev Clin Oncol. 2017;14:399-416.

Mantovani A, Scorletti E, Mosca A, Alisi A, Byrne CD and Targher G. Complications, morbidity and mortality of nonalcoholic fatty liver disease. Metabolism. 2020;30:154170.

Martinez FO, Gordon S. The M1 and M2 paradigm of macrophage activation: time for reassessment. F1000Prime Rep. 2014;6:13.

Martinez-Ciarpaglini C, Oltra S, Roselló S, Roda D, Mongort C, Carrasco F, Gonzalez J, Santonja F, Tarazona N, Huerta M, Espí A, Ribas G, Ferrández A, Navarro S, Cervantes A. Low miR200c expression in tumor budding of invasive front predicts worse survival in patients with localized colon cancer and is related to PD-L1 overexpression. Mod Pathol. 2019;32:306-313.

Martínez-González J, García de Frutos P. Cells in Cardiovascular Disease: Using Diversity to Confront Adversity. Cells. 2020;9:2192.c

Mathow D, Chessa F, Rabionet M, Kaden S, Jennemann R, Sandhoff R, Gröne HJ and Feuerborn A. Zeb1 affects epithelial cell adhesion by diverting glycosphingolipid metabolism. EMBO Rep. 2015;16:321-331.

Matulonis UA, Sood AK, Fallowfield L, Howitt BE, Sehouli J, Karlan BY. Ovarian cancer. Nat Rev Dis Primers. 2016;2:16061.

Meidhof S, Brabletz S, Lehmann W, Preca BT, Mock K, Ruh M, Schüler J, Berthold M, Weber A, Burk U, Lübbert M, Puhr M, Culig Z, Wellner U, Keck T, Bronsert P, Küsters S, Hopt UT, Stemmler MP, Brabletz T. ZEB1-associated drug resistance in cancer cells is reversed by the class I HDAC inhibitor mocetinostat. EMBO Mol Med. 2015;7:831-47.

Melgar-Lesmes P, Luquero A, Parra-Robert M, Mora A, Ribera J, Edelman ER, Jiménez W. Graphene-Dendrimer Nanostars for Targeted Macrophage Overexpression of Metalloproteinase 9 and Hepatic Fibrosis Precision Therapy. Nano Lett. 2018;18:5839-5845.

Mehlem A, Hagberg CE, Muhl L, Eriksson U, Falkevall A. Imaging of neutral lipids by oil red O for analyzing the metabolic status in health and disease. Nat Protoc. 2013;8:1149-54.

Moore KJ, Tabas I. Macrophages in the pathogenesis of atherosclerosis. Cell. 2011;145:341-355.

Moore KJ, Sheedy FJ, Fisher EA. Macrophages in atherosclerosis: a dynamic balance. Nat Rev Immunol. 2013;13:709-721.

Morrison C. Immuno-oncologists eye up macrophage targets. Nat Rev Drug Discov. 2016;15:373-4.

Muoio D and Newgard C. Molecular and metabolic mechanisms of insulin resistance and b-cell failure in type 2 diabetes. Nat Rev Mol Cell Biol. 2008;9:193-205.

Murray P, Wynn TA. Protective and pathogenic functions of macrophage subsets. Nat Rev Immunol. 2011;11:723-737.

Murray PJ, Allen JE, Biswas SK, Fisher EA, Gilroy DW, Goerd S, Gordon S, Hamilton JA, Ivashkiv LB, Lawrence T, Locati M, Mantovani A, Martinez FO, Mege JL, Mosser DM, Natoli G, Saeij JP, Schultze JL, Shirey KA, Sica A, Suttles J, Udalova I, van Ginderachter JA, Vogel SN, Wynn TA. Macrophage Activation and Polarization: Nomenclature and Experimental Guidelines. Immunity. 2014;41:14-20.

Nagaishi M, Nakata S, Ono Y, Hirata K, Tanaka Y, Suzuki K, Yokoo H, Hyodo A. Tumoral and stromal expression of Slug, ZEB1, and ZEB2 in brain metastasis. J Clin Neurosci. 2017;46:124-128.

Nieman KM, Kenny HA, Penicka CV, Ladanyi A, Buell-Gutbrod R, Zillhardt MR, Romero IL, Carey MS, Mills GB, Hotamisligil GS, Yamada SD, Peter ME, Gwin K, Lengyel E. Adipocytes promote ovarian cancer metastasis and provide energy for rapid tumor growth. Nat Med. 2011;17:1498-503.

Ninfali C, Siles L, Darling DS, Postigo A. Regulation of muscle atrophy-related genes by the opposing transcriptional activities of ZEB1/CtBP and FOXO3. Nucleic Acids Res. 2018;46:10697-10708.

Nishimura G, Manabe I, Tsushima K, Fujiu K, Oishi Y, Imai Y, Maemura K, Miyagishi M, Higashi Y, Kondoh H, Nagai R. δEF1 Mediates TGF-β Signaling in Vascular Smooth Muscle Cell Differentiation. Dev Cell. 2006;11:93-104.

Nowak M, Klink M. The Role of Tumor-Associated Macrophages in the Progression and Chemoresistance of Ovarian Cancer. Cells. 2020;9:1299.

Noy R, Pollard JW. Tumor-associated macrophages: from mechanisms to therapy. Immunity. 2014;41:49-61.

Okazaki T, Honjo T. The PD-1-PD-L pathway in immunological tolerance. Trends Immunol. 2006 Apr;27(4):195-201.

Out R, Hoekstra M, Habets K, Meurs I, de Waard V, Hildebrand RB, Wang Y, Chimini G, Kuiper J, van Berkel T and van Eck M. Combined deletion of macrophage ABCA1 and ABCG1 leads to massive lipid accumulation in tissue macrophages and distinct atherosclerosis at relatively low plasma cholesterol levels. Arterioscler Thromb Vasc Biol. 2008;28:258-264.

Pathria P, Louis TL and Varner JA. Targeting tumor-associated macrophages in cancer. Trends Immunol. 2019;40:310-327.

Paulson KE, Zhu SN, Chen M, Nurmohamed S, Jongstra-Billen J and Cybulsky MI. Resident intimal dendritic cells accumulated lipid and contribute to the initiation of atherosclerosis. Circ Res. 2010;106:383-390.

Penet MF, Krishnamachary B, Wildes FB, Mironchik Y, Hung CF, Wu TC, Bhujwalla ZM. Ascites Volumes and the Ovarian Cancer Microenvironment. Front Oncol. 2018;8:595.

Peng DH, Ungewiss C, Tong P, Byers LA, Wang J, Canales JR, Villalobos PA, Uraoka N, Mino B, Behrens C, Wistuba II, Han RI, Wanna CA, Fahrenholtz M, Grande-Allen KJ, Creighton CJ, Gibbons DL. ZEB1 induces LOXL2-mediated collagen stabilization and deposition in the extracellular matrix to drive lung cancer invasion and metastasis. Oncogene. 2017;36:1925-1938.

Ponticos M, Partridge T, Black CM, Abraham DJ, Bou-Gharios G. Regulation of collagen type I in vascular smooth muscle cells by competition between Nkx2.5 and deltaEF1/ZEB1. Mol Cell Biol. 2004;24:6151-61.

Postigo AA, Dean DC. Differential expression and function of members of the zfh-1 family of zinc finger/homeodomain repressors. Proc Natl Acad Sci U S A. 2000;97:6391-6.

Poznyak VA, Wu W, Melnichenko AA, Wetzker R, Sukhorukov V, Markin AM, Khotina VA and Orekhov AN. Signaling pathways and key genes involved in regulation of foam cell formation in atherosclerosis. Cells. 2020;9:584.

Prats-Uribe A, Sayols-Baixeras S, Fernández-Sanlés A, Subirana I, Carreras-Torres R, Vilahur G, Civeira F, Marrugat J, Fitó M, Hernáez Á, Elosua R. High-density lipoprotein characteristics and coronary artery disease: a Mendelian randomization study. Metabolism. 2020;112:154351.

Pyonteck SM, Akkari L, Schuhmacher AJ, Bowman RL, Sevenich L, Quail DF, Olson OC, Quick ML, Huse JT, Teijeiro V, Setty M, Leslie CS, Oei Y, Pedraza A, Zhang J, Brennan CW, Sutton JC, Holland EC, Daniel D, Joyce JA. CSF-1R inhibition alters macrophage polarization and blocks glioma progression. Nat Med. 2013;19:1264-72.

Qi L, Sun B, Liu Z, Li H, Gao J, Leng X. Dickkopf-1 inhibits epithelial-mesenchymal transition of colon cancer cells and contributes to colon cancer suppression. Cancer Sci. 2012;103:828-35.

Qin W, Hu L, Zhang X, Jiang S, Li J, Zhang Z, Wang X. The Diverse Function of PD-1/PD-L Pathway Beyond Cancer. Front Immunol. 2019;10:2298.

Raghavan S, Mehta P, Xie Y, Lei YL, Mehta G. Ovarian cancer stem cells and macrophages reciprocally interact through the WNT pathway to promote pro-tumoral and malignant phenotypes in 3D engineered microenvironments. J Immunother Cancer. 2019;7:190.

Rahman K, Vengrenyuk Y, Ramsey SA, Vila NR, Girgis NM, Liu J, Gusarova V, Gromada J, Weinstock A, Moore KJ, Loke P, Fisher EA. Inflammatory Ly6Chi monocytes and their conversion to M2 macrophages drive atherosclerosis regression. J Clin Invest. 2017;127:2904-2915.

Rahman K, Fisher EA. Insights From Pre-Clinical and Clinical Studies on the Role of Innate Inflammation in Atherosclerosis Regression. Front Cardiovasc Med. 2018; 5:32.

Randolph GJ. Mechanisms that regulate macrophage burden in atherosclerosis. Circ Res. 2014;114:1757-1771.

Rader DJ. Molecular regulation of HDL metabolism and function: implications for novel therapies. J Clin Invest. 2006;116:3090-100.

Rader DJ, Hovingh GK. HDL and cardiovascular disease. Lancet. 2014;384:618-625.

Rao G, Latha K, Ott M, Sabbagh A, Marisetty A, Ling X, Zamler D, Doucette TA, Yang Y, Kong LY, Wei J, Fuller GN, Benavides F, Sonabend AM, Long J, Li S, Curran M, Heimberger AB. Anti-PD-1 Induces M1 Polarization in the Glioma Microenvironment and Exerts Therapeutic Efficacy in the Absence of CD8 Cytotoxic T Cells. Clin Cancer Res. 2020;26:4699-4712.

Rei M, Gonçalves-Sousa N, Lança T, Thompson RG, Mensurado S, Balkwill FR, Kulbe H, Pennington DJ, Silva-Santos B. Murine CD27(-) Vγ6(+) γδ T cells producing IL-17A promote ovarian cancer growth via mobilization of protumor small peritoneal macrophages. Proc Natl Acad Sci U S A. 2014;111:E3562-70.

Roby KF, Taylor CC, Sweetwood JP, Cheng Y, Pace JL, Tawfik O, Persons DL, Smith PG, Terranova PF. Development of a syngeneic mouse model for events related to ovarian cancer. Carcinogenesis. 2000;21:585-91.
Rodriguez-Garcia A, Lynn RC, Poussin M, Eiva MA, Shaw LC, O'Connor RS, Minutolo NG, Casado-Medrano V, Lopez G, Matsuyama T, Powell DJ Jr. CAR-T cell-mediated depletion of immunosuppressive tumor-associated macrophages promotes endogenous antitumor immunity and augments adoptive immunotherapy. Nat Commun. 2021;12:877.

Rodríguez-Ubreva J, Català-Moll F, Obermajer N, Álvarez-Errico D, Ramirez RN, Company C, Vento-Tormo R, Moreno-Bueno G, Edwards RP, Mortazavi A, Kalinski P, Ballestar E. Prostaglandin E2 Leads to the Acquisition of DNMT3A-Dependent Tolerogenic Functions in Human Myeloid-Derived Suppressor Cells. Cell Rep. 2017;21:154-167.

Rossello X, Pocock SJ, Julian DG. Long-Term Use of Cardiovascular Drugs: Challenges for Research and for Patient Care. J Am Coll Cardiol. 2015;66:1273-1285.

Sag D, Carling D, Stout RD, Suttles J. Adenosine 5'-monophosphate-activated protein kinase promotes macrophage polarization to an anti-inflammatory functional phenotype. J Immunol. 2008;181:8633-8641.

Sánchez-Tilló E, Siles L, de Barrios O, Cuatrecasas M, Vaquero EC, Castells A, Postigo A. Expanding roles of ZEB factors in tumorigenesis and tumor progression. Am J Cancer Res. 2011;1:897-912.

Sangrador I, Molero X, Campbell F, Franch-Expósito S, Rovira-Rigau M, Samper E, Domínguez-Fraile M, Fillat C, Castells A, Vaquero EC. Zeb1 in Stromal Myofibroblasts Promotes Kras-Driven Development of Pancreatic Cancer. Cancer Res. 2018;78:2624-2637.

Sarvaria A, Madrigal JA, Saudemont A. B cell regulation in cancer and anti-tumor immunity. Cell Mol Immunol. 2017;14:662-674.

Saxena M, Balaji SA, Deshpande N, Ranganathan S, Pillai DM, Hindupur SK, Rangarajan A. AMP-activated protein kinase promotes epithelial-mesenchymal transition in cancer cells through Twist1 upregulation. J Cell Sci. 2018;131:jcs208314.

Saykally JN, Dogan S, Cleary MP and Sanders MM. The ZEB1 transcription factor is a novel repressor of adiposity in female mice. PLoS One. 2009;4:e8460.

Schmidt AM. Diabetes mellitus and cardiovascular disease. Emerging therapeutic approaches. Arterioscler Thromb Vasc Biol. 2019;39:558-568.

Schwingshackl L, Hoffmann G. Comparison of effects of long-term low-fat vs high-fat diets on blood lipid levels in overweight or obese patients: a systematic review and meta-analysis. J Acad Nutr Diet. 2013; 113:1640-1661.

Scott CL, Soen B, Martens L, Skrypek N, Saelens W, Taminau J, Blancke G, Van Isterdael G, Huylebroeck D, Haigh J, Saeys Y, Guilliams M, Lambrecht BN and Berx G. The transcription factor Zeb2 regulates development of conventional and plasmacytoid DCs by repressing Id2. J Exp Med. 2016;213:897-911.

Scott CL, T'Jonck W, Martens L, Todorov H, Sichien D, Soen B, Bonnardel J, De Prijck S, Vandamme N, Cannoodt R, Saelens W, Vanneste B, Toussaint W, De Bleser P, Takahashi N, Vandenabeele P, Henri S, Pridans C, Hume DA, Lambrecht BN, De Baetselier P, Milling SWF, Van Ginderachter JA, Malissen B, Berx G, Beschin A, Saeys Y, Guilliams M. The transcription factor ZEB2 is required to maintain the tissue-specific identities of macrophages. Immunity. 2018;49:312-325.

Scott CL and Omilusik KD. ZEBs: Novel players in immune cell development and function. Trends Immunol. 2019;40:431-446.

Shapouri-Moghaddam A, Mohammadian H, Vazini H, Taghadosi M, Esmaeili SA, Mardani F, Seifi B, Mohammadi A, Afshari JT, Sahebkar A. Macrophage plasticity, polarization, and function in health and disease. J Cell Physiol. 2018;233:6425-6440.

Sica A, Mantovani A. Macrophage plasticity and polarization: in vivo veritas. J Clin Invest. 2012;122:787-95.

Siles L, Ninfali C, Cortés M, Darling DS, Postigo A. ZEB1 protects skeletal muscle from damage and is required for its regeneration. Nat Commun. 2019;10:1364.

Smita S, Ahad A, Ghosh A, Biswas VK, Koga MM, Gupta B, Acha-Orbea H and Raghav SK. Importance of EMT factor ZEB1 in cDC1 "MutuDC Line" mediated induction of Th1 immune response. Front Immunol. 2018;9:2604.

Snaebjornsson MT, Janaki-Raman S, Schulze A. Greasing the Wheels of the Cancer Machine: The Role of Lipid Metabolism in Cancer. Cell Metab. 2020;31:62-76.

Song M, Yeku OO, Rafiq S, Purdon T, Dong X, Zhu L, Zhang T, Wang H, Yu Z, Mai J, Shen H, Nixon B, Li M, Brentjens RJ, Ma X. Tumor derived UBR5 promotes ovarian cancer growth and metastasis through inducing immunosuppressive macrophages. Nat Commun. 2020;11:6298.

Spann NJ, Garmire LX, McDonald JG, Myers DS, Milne SB, Shibata N, Reichart D, Fox JN, Shaked I, Heudobler D, Raetz CR, Wang EW, Kelly SL, Sullards MC, Murphy RC, Merrill AH Jr, Brown HA, Dennis EA, Li AC, Ley K, Tsimikas S, Fahy E, Subramaniam S, Quehenberger O, Russell DW and Glass CK. Regulated accumulation of desmosterol integrates macrophage lipid metabolism and inflammatory responses. Cell. 2012;151:138-152.
Stefan N, Häring HU, Cusi K. Non-alcoholic fatty liver disease: causes, diagnosis, cardiometabolic consequences, and treatment strategies. Lancet Diabetes Endocrinol. 2019;7:313-324.

Stemmler MP, Eccles RL, Brabletz S, Brabletz T. Non-redundant functions of EMT transcription factors. Nat Cell Biol. 2019;21:102-112.

Su S, Liu Q, Chen J, Chen J, Chen F, He C, Huang D, Wu W, Lin L, Huang W, Zhang J, Cui X, Zheng F, Li H, Yao H, Su F, Song E. A positive feedback loop between mesenchymal-like cancer cells and macrophages is essential to breast cancer metastasis. Cancer Cell. 2014;25:605-20.

Sun Y, Ishibashi M, Seimon T, Lee M, Sharma SM, Fitzgerald KA, Samokhin AO, Wang Y, Sayers S, Aikawa M, Jerome WG, Ostrowski MC, Bromme D, Libby P, Tabas IA, Welch CL, Tall AR. Free cholesterol accumulation in macrophage membranes activates Toll-like receptors and p38 mitogen-activated protein kinase and induces cathepsin K. Circ Res. 2009;104:455-65.

Sylvestre M, Crane CA, Pun SH. Progress on Modulating Tumor-Associated Macrophages with Biomaterials. Adv Mater. 2020;32:e1902007.

Tabas I, Bornfeldt KE. Macrophage phenotype and function in different stages of atherosclerosis. Circ Res. 2016;118:653-667.

Takagi T, Moribe H, Kondoh H, Higashi Y. DeltaEF1, a zinc finger and homeodomain transcription factor, is required for skeleton patterning in multiple lineages. Development. 1998;125:21-31.

Tan Z, Xie N, Cui H, Moellering DR, Abraham E, Thannickal VJ, Liu G. Pyruvate dehydrogenase kinase 1 participates in macrophage polarization via regulating glucose metabolism. J Immunol. 2015;194:6082-9.

Targher G, Byrne CD, Lonardo A, Zoppini G and Barbui C. Non-alcoholic fatty liver disease and risk of incident cardiovascular disease: A meta-analysis. J Hepatol. 2016;65:580-600.

Terraneo N, Jacob F, Dubrovska A, Grünberg J. Novel Therapeutic Strategies for Ovarian Cancer Stem Cells. Front Oncol. 2020;10:319.

Title AC, Hong SJ, Pires ND, Hasenöhrl L, Godbersen S, Stokar-Regenscheit N, Bartel DP, Stoffel M. Genetic dissection of the miR-200-Zeb1 axis reveals its importance in tumor differentiation and invasion. Nat Commun. 2018 Nov 7;9:4671.

Togashi Y, Shitara K, Nishikawa H. Regulatory T cells in cancer immunosuppression - implications for anticancer therapy. Nat Rev Clin Oncol. 2019 Jun;16(6):356-371.
Van den Bossche J, O'Neill LA and Menon D. Macrophage immunometabolism: Where are we (going)?. Trends Immunol. 2017:395-406.

van der Heide D, Weiskirchen R, Bansal R. Therapeutic Targeting of Hepatic Macrophages for the Treatment of Liver Diseases. Front Immunol. 2019;10:2852.

Van Furth R, Cohn ZA, Hirsch JG, Humphrey JH, Spector WG, Langevoort HL. The mononuclear phagocytes sytem: a new classification of macrophages, monocytes, and their precursor cells. Bull World Health Organ. 1972;46:845-852.

Varga T, Mounier R, Horvath A, Cuvellier S, Dumont F, Poliska S, Ardjoune H, Juban G, Nagy L and Chazaud B. Tissue-Resident Macrophage Ontogeny and Homeostasis. J Immunol. 2016; 196:4771-4782.

Viswanathan VS, Ryan MJ, Dhruv HD, Gill S, Eichhoff OM, Seashore-Ludlow B, Kaffenberger SD, Eaton JK, Shimada K, Aguirre AJ, Viswanathan SR, Chattopadhyay S, Tamayo P, Yang WS, Rees M, Chen S, Boskovic ZV, Javaid S, Huang C, Wu X, Tseng YY, Roider EM, Gao D, Cleary JM, Wolpin BM, Mesirov JP, Haber DA, Engelman JA, Boehm JS, Kotz JD, Hon CS, Chen Y, Hahn WC, Levesque MP, Doench JG, Berens ME, Shamji AF, Clemons PA, Stockwell BR and Schreiber SL. Dependency of a therapy-resistant state of cancer cells on a lipid peroxidase pathway. Nature. 2017;547:453-457.

Von Scheidt M, Zhao Y, Kurt Z, Pan C, Zeng L, Yang X, Schunkert H and Lusis AJ. Applications and limitations of mouse models for understanding human atherosclerosis. Cell metab. 2017;25:248-261.

Walcher L, Kistenmacher AK, Suo H, Kitte R, Dluczek S, Strauß A, Blaudszun AR, Yevsa T, Fricke S, Kossatz-Boehlert U. Cancer Stem Cells-Origins and Biomarkers: Perspectives for Targeted Personalized Therapies. Front Immunol. 2020;11:1280.

Wang F, Zhang Z, Fang A, Jin Q, Fang D, Liu Y, Wu J, Tan X, Wei Y, Jiang C, Song X. Macrophage Foam Cell-Targeting Immunization Attenuates Atherosclerosis. Front Immunol. 2019;9:3127.

Wang B, Kohli J, Demaria M. Senescent Cells in Cancer Therapy: Friends or Foes? Trends Cancer. 2020;6:838-857.

Wellner U, Schubert J, Burk UC, Schmalhofer O, Zhu F, Sonntag A, Waldvogel B, Vannier C, Darling D, zur Hausen A, Brunton VG, Morton J, Sansom O, Schüler J, Stemmler MP, Herzberger C, Hopt U, Keck T, Brabletz S, Brabletz T. The EMT-activator ZEB1 promotes tumorigenicity by repressing stemness-inhibiting microRNAs. Nat Cell Biol. 2009;11:1487-95.

Williams JW, Giannarelli C, Rahman A, Randolph GJ and Kovacic JC. Macrophage biology, classification and photype in cardiovascular disease: JACC macrophage series (Part I). J Am Coll Cardiol. 2018;72:2166-2180.

Wu X, Briseño CG, Grajales-Reyes GE, Haldar M, Iwata A, Kretzer NM, Kc W, Tussiwand R, Higashi Y, Murphy TL, Murphy KM. Transcription factor Zeb2 regulates commitment to plasmacytoid dendritic cell and monocyte fate. Proc Natl Acad Sci U S A. 2016;113:14775-14780.

Wynn TA, Chawla A, Pollard JW. Macrophage biology in development, homeostasis and disease. Nature. 2013 Apr 25;496:445-55.

Xu XM, Liu W, Cao ZH, Liu MX. Effects of ZEB1 on regulating osteosarcoma cells via NF-κB/iNOS. Eur Rev Med Pharmacol Sci. 2017;21:1184-1190.

Yamada Y, Nishida T, Horibe H, Oguri M, Kato K, Sawabe M. Identification of hypo- and hypermethylated genes related to aterosclerosis by a genome-wide analysis of DNA methylation. Int J Mol Med. 2014;33:1355-1365.

Yang J, Liao D, Chen C, Liu Y, Chuang TH, Xiang R, Markowitz D, Reisfeld RA, Luo Y. Tumor-associated macrophages regulate murine breast cancer stem cells through a novel paracrine EGFR/Stat3/Sox-2 signaling pathway. Stem Cells. 2013;31:248-58.

Ye X, Jiang X, Guo W, Clark K, Gao Z. Overexpression of NF-κB p65 in macrophages ameliorates atherosclerosis in apoE-knockout mice. Am J Physiol Endocrinol Metab. 2013;305:E1375-83.

Yetisgin AA, Cetinel S, Zuvin M, Kosar A, Kutlu O. Therapeutic Nanoparticles and Their Targeted Delivery Applications. Molecules. 2020;25:2193.

Yin M, Li X, Tan S, Zhou HJ, Ji W, Bellone S, Xu X, Zhang H, Santin AD, Lou G, Min W. Tumor-associated macrophages drive spheroid formation during early transcoelomic metastasis of ovarian cancer. J Clin Invest. 2016;126:4157-4173.

Yvan-Charvet L, Ranalletta M, Wang N, Han S, Terasaka N, Li R, Welch C, Tall AR. Combined deficiency of ABCA1 and ABCG1 promotes foam cell accumulation and accelerates atherosclerosis in mice. J Clin Invest. 2007;117:3900-8.

Yvan-Charvet L, Pagler TA, Seimon TA, Thorp E, Welch CL, Witztum JL, Tabas I, Tall AR. ABCA1 and ABCG1 protect against oxidative stress-induced macrophage apoptosis during efferocytosis. Circ Res. 2010;106:1861-1869.

Zhang SH, Reddick RL, Burkey B, Maeda N. Diet-induced atherosclerosis in mice heterozygous and homozygous for apolipoprotein E gene disruption. J Clin Invest. 1994 Sep;94(3):937-45.

Zhang L, Conejo-Garcia JR, Katsaros D, Gimotty PA, Massobrio M, Regnani G, Makrigiannakis A, Gray H, Schlienger K, Liebman MN, Rubin SC, Coukos G. Intratumoral T cells, recurrence, and survival in epithelial ovarian cancer. N Engl J Med. 2003;348:203-13.

Zhang X, Goncalves R, Mosser DM. The isolation and characterization of murine macrophages. Curr Protoc Immunol. 2008;Chapter 14:Unit 14.1.

Zhang M, He Y, Sun X, Li Q, Wang W, Zhao A, et al. A high M1/M2 ratio of tumor-associated macrophages is associated with extended survival in ovarian cancer patients. J Ovarian Res. 2014;7:19.

Zhang Y, Xu L, Li A, Han X. The roles of ZEB1 in tumorigenic progression and epigenetic modifications. Biomed Pharmacother. 2019;110:400-408.

Zhang F, Parayath NN, Ene CI, Stephan SB, Koehne AL, Coon ME, Holland EC, Stephan MT. Genetic programming of macrophages to perform anti-tumor functions using targeted mRNA nanocarriers. Nat Commun. 2019;10:3974.

Zhao Z, Hao D, Wang L, Li J, Meng Y, Li P, Wang Y, Zhang C, Zhou H, Gardner K, Di LJ. CtBP promotes metastasis of breast cancer through repressing cholesterol and activating TGF-β signaling. Oncogene. 2019;38:2076-2091.

Zhou YY, Zhou XD, Wu SJ, Fan DH, Van Poucke S, Chen YP, Fu SW, Zheng MH. Nonalcoholic fatty liver disease contributes to subclinical atherosclerosis: A systematic review and meta-analysis. Hepatol Commun. 2018;2:376-392.

Zhu J, Wen H, Bi R, Wu Y, Wu X. Prognostic value of programmed death-ligand 1 (PD-L1) expression in ovarian clear cell carcinoma. J Gynecol Oncol. 2017;28:e77.

Zong X, Nephew KP. Ovarian Cancer Stem Cells: Role in Metastasis and Opportunity for Therapeutic Targeting. Cancers (Basel). 2019;11:934.